Thesis for the Degree of Master of Science

High Resolution Near-Infrared Spectra of Nearby Quasars

Huynh Anh Le Nguyen

Department of Astronomy and Space Science
Graduate School
Kyung Hee University
Seoul, Korea

February, 2011

High Resolution Near-Infrared Spectra of Nearby Quasars

Huynh Anh Le Nguyen

Department of Astronomy and Space Science
Graduate School
Kyung Hee University
Seoul, Korea

February, 2011

High Resolution Near-Infrared Spectra of Nearby Quasars

by

Huynh Anh Le Nguyen

advised by

Dr. Soojong Pak

Submitted to Department of Astronomy and Space Science and Faculty of the Graduate School of Kyung Hee University in partial fulfillment of the requirement for degree of Master of Science

Dissertation Committee

……………………………………
Dr. Soojong Pak

……………………………………
Dr. Sungsoo Kim

..……………………………………
Dr. Myungshin Im

High Resolution Near-Infrared Spectra of Nearby Quasars

ABSTRACT

We observed three low red shift quasars PG0844+349, PG1226+023, and PG1426+015, using the near-IR high resolution echelle spectrometer, IRCS, at the SUBARU 8.2 m telescope. Using an Adoptive Optics system, the full width at half maximum of the point spread function was about 0.3 arcsec, which can effective separate the quasar spectra from the host galaxy spectra. We also maximize the total exposure time up to several hours per target, and develop data reduction methods to increase the signal-to-noise ratios. The high resolution spectra of nearby quasars and late type template stars in G, K, and M types in H-band are presented. These new spectra unidentified lines will be used to study the physical mechanism of quasars.

Table of Contents

List of Figures

List of Tables

1. INTRODUCTION

1.1 Quasars

Quasars (Quasi Stellar radio Source) are the most distance objects that astronomers can observe in the Universe. Quasars are blue star like objects, extremely luminosity, broad emission lines in their spectra, and reasonable red shift. Researching about quasars gives us information about the early Universe, and the important probes about the history of the Universe. Studying about quasars helps us to understanding about the formation of discrete gas, and first metals. In addition, the evolution and formation for the galaxies, photon ionization equilibrium of the intergalactic medium also find out. Moreover, quasars provide probes of unobserved gas at high red shift. Therefore, the studying and researching about quasars are very meaningful in Astronomy.

1.2 Spectra and purposes of this research

Spectra are the only way can help astronomers research about the Universe. From the spectra, based on the emission lines or absorption lines, we study and research about the properties of the targets as chemical composition, velocity, temperature, motion, etc. Many composite quasars spectra have been created as (Boyle 1989; Cristiani 1989; Francis 1991; Zheng 1995; Brotherton 2000, Glikman 2005; Riffel 2006).

The optical spectra of quasars are similar to the optical spectra of Seyfert 1 galxies. This similar indicate some same properties between quasar and Seyfert 1 galaxies. But, these are also differences between quasars and Seyfert 1 spectra. Quasars are blue objects, extremely luminous, broad lines, and high red-shift. In addition, Seyfert 1 is bright blue nuclear and broad emission lines. Spectrophotometry of Seyfert 1 galaxies and quasars has been created (Malkan & Sargent 1981).

Quasars show continuum emission which comes from the amplified synchrotron radiation of the aligned jets. The continuum emission of quasars follow a roughly power law form, straight, and negative slope. Typical spectra of quasars show two parts as power law form from radio to infrared region, and big blue bump from visual to UV region (Barvainis 1987; Malkan & Sargent 1982).

$$F_{v=}C^{-\alpha}$$

In this formula,

v: frequency
F: flux
α: spectral index
c: constant

or:

$$F_{\lambda} = C'\lambda^{\alpha-2}$$

λ: wavelength

Quasar spectra show very broad emission lines (BEL) in optical band. BEL has wide range of densities and in high ionization states (Hamann \& Ferland 1991). The origins of emission lines have not been much known. In addition, absorption lines are also contaminated in the spectra of quasars. The origin of the absorption lines are thought to be produced from the dust between the quasars and the observers (Trump 2006).

We made the spectra of quasars in H band (1.4-1.82 μm), which rarely studied before. And, we tried to find any useful line from the spectra which can help to understand more about properties of the targets. In this paper, we present the reduction method for data which observed with an near-IR echelle spectrometer. We use IRAF (Images Reduction Analysis Facilites), and made high resolution near-infrared spectra of nearby quasars PG0844+349, PG1226+023, and PG1426+015, as well as the spectra of template stars in G, K, and M types. Chapter 2 presents about the targets and the observations. The data reduction processes is described detail in chapter 3. Chapter 4 presents about the model functions for the quasar PG0844+349. In chapter 5, the results and discussions of the spectra are presented. Section 6 summarizes our results.

2. OBSERVATIONS

The observations were performed at the SUBARU 8.2 m telescope using the IRCS (Tokunaga et al. 1998; Kobayashi et al. 2000) operated with the AO (Adaptive Optics) (Hayano et al. 2008) on 2003 Feb 11 UT and 2004 April 3, 4 UT. We observed three nearby quasars PG0844+349, PG1226+023, and PG1426+015. Table 3 shows the observations logs.

2.1 Telescope and Instrument

Subaru telescope is an optical-infrared 8.2m telescope at 4.200m Summit, Mauna Kea, Hawaii. It is one of the largest telescope and advanced technology in the world. Table 1 shows the specifications and performance about the telescope.

We use IRCS (Infrared Camera and Spectrograph) and A0 (Adaptive Optics) system which can be used as a referent guide star or laser guide star. IRCS has a camera and echelle spectroscopy sections each equipped with Raytheon 1024 x 1024 InSb array with an Aladdin II multiplexer. The pixel scales for spectroscopy were 0.06 arcsec. Cross dispersion echelle of IRCS provide a spectral resolution up to 20000. Table 2 shows the specifications and performance of IRCS.

Table 1

The specifications and performance of the SUBARU telescope

(www.naoj.org/Observing/Telescope/Parameters).

Longitude	+19° 49' 32" N
Latitude	155° 28' 34" W
Altitude	4139 m
Height	22.2 m
Maximum width	27.2 m
Weight	555 t
Effective diameter of primary mirror	8.2 m
Focal length of primary mirror	15 m
Primary focus	F/2.0
Cassegrain focus	F/12.2
Nasmyth foci	F/12.6 (Optical) and F/13.6 (Infrared)

Table 2

The specifications and performance of the IRCS spectrograph *(www.naoj.org/Observing/Instruments/IRCS/parameters)*.

Detector	ALADDIN III 10242 InSb array		
Pixel size	27 um		
Resolution	(slit-length direction) x (slit-width direction)		
Pixel scale			
w/o AO	54.57 mas	x	67.75 mas
w/ AO	54.93 mas	x	68.20 mas
Field of view	3.5-9.4" in slit-length		
Gain	3.8 e-/ADU		
Dark current	0.05 e-/s		
Read noise	68 e- rms		
Saturation level	129 000 e-		
Readout rate (1K x 1K)	0.41 s (standard)		
	0.12 s (fast)		

2.2 Observations

We observed three targets on 2003 Feb 11 UT and 2004 April 3, 4 UT. These are PG0844+349, PG1426+015, and PG1226+023. All of the targets are nearby quasars.

2.2.1 Observation in 2003

In 2003, we observed only PG0844+349 ($z = 0.064$) using the IRCS operated with AO. The slit width was 0.3 arcsec whose spectral resolving power is 10000. The position angle of the slit was 0 deg. The echelle setting of the observations was in H+ band, and the total integration time was about two hours. The observations were done by *Nod-off-slit* mode. We first observed the target, and after that we moved the telescope to the nearby background sky. The sequences of the observations were object→sky→sky→object.

In the observations, we also observed an A0V standard star (HD39357) to correct the telluric absorption lines in the target spectra, and template stars which will be used to model the spectra of host galaxy. We observed two template stars, K2III (HD122675) and M0III (NSV3729). The standard A0V star and the template stars were observed by *Nod-on-slit* mode. The star is taken in two positions *A* and *B*. In the first exposure, the standard star will be place in one position on the slit (position *A*), and after that, we move the telescope a little bit along the slit direction (position *B*).

2.2.2 Observation in 2004

In 2004, we observed three targets PG0844+349, PG1426+015 (z = 0.086), and PG1226+023 (z = 0.158). The slit width was 0.6 arcsec whose spectral resolving power is 5000. The echelle setting of the observations was in *H*- and *H*+ band, and the total integration time was one hours for each target.

The observations were done in *Nod-off-slit* mode. Other instrument settings and the observing modes were same as in 2003. We also observed standard star A0V (HD105388), and eight template stars, G8III (HD64938 and HD148287), K0III (HD55184 and HD155500), K2III (HD52071 and HD146084), K5III (HD154610), and M0III (HD76010).

The data reduction processes were done by using IRAF. This data reduction method will be talked detail in part three of thesis.

Table 3

Log of Observations

Date (UT)	Targets	Echelle setting	Total Exposure
2003 Feb 11	PG0844+349	H+	37 x 180 sec
	HD39357(A0V)	H+	4 x 20 sec
	HD75556(K0III)	H+	4 x 12 sec
	NSV3729(M0III)	H+	4 x 10 sec
2004 April 3	PG0844+349	H-	10 x 300 sec
	PG1226+023	H-	8 x 300 sec
	…	H+	…
	…	H+	…
	PG1426+015	H-	5 x 300 sec
	…	H+	…
	HD55184(K0III)	H+	4 x 6 sec
	…	H-	…
	HD64938(G8III)	H-	4 x 10 sec
	…	H+	…
	HD148287(G8III)	H-	…
	…	H+	…
	HD155500(K0III)	H-	…
	…	H+	…
	HD105388(A0V)	H-	4 x 20 sec
	…	H+	…
2004 April 4	PG0844+349	H+	8 x 300 sec
	PG1426+015	H-	12 x 300 sec
	…	H+	15 x 300 sec
	HD52071(K2III)	H-	4 x 6 sec
	…	H+	…
	HD76010(M0III)	H-	4 x 5 sec
	…	H+	…
	HD154610(K5III)	H-	…
	…	H+	…
	HD146084(K2III)	H+	4 x 10 sec
	…	H-	…

3. DATA REDUCTION

Data reduction processes were done by IRAF (Images Reduction Analysis Facilities) followed by the method in Pyo (2002). In addition, Python language was used in some tasks to get the final spectra of targets. Figure 1 shows the data reduction sequences.

3.1 Pre-processing

Before start to reduce data, we need to do pre-processing which including setting parameters in packages of login.cl of IRAF which following the setting of instrument when we did observation, making dark, flat, and sky frame for correcting spatial distortion and wavelength calibration.

3.1.1 Preparation of data reduction

The data reduction processes were done mainly in the *noao.imred.echelle* and *noao.twodspec.longslit* packages of IRAF. In this step, we need to investigate the aperture width, intensity level, dispersion direction, intervals between apertures, etc. Figure 2 shows the setting parameters in two packages.

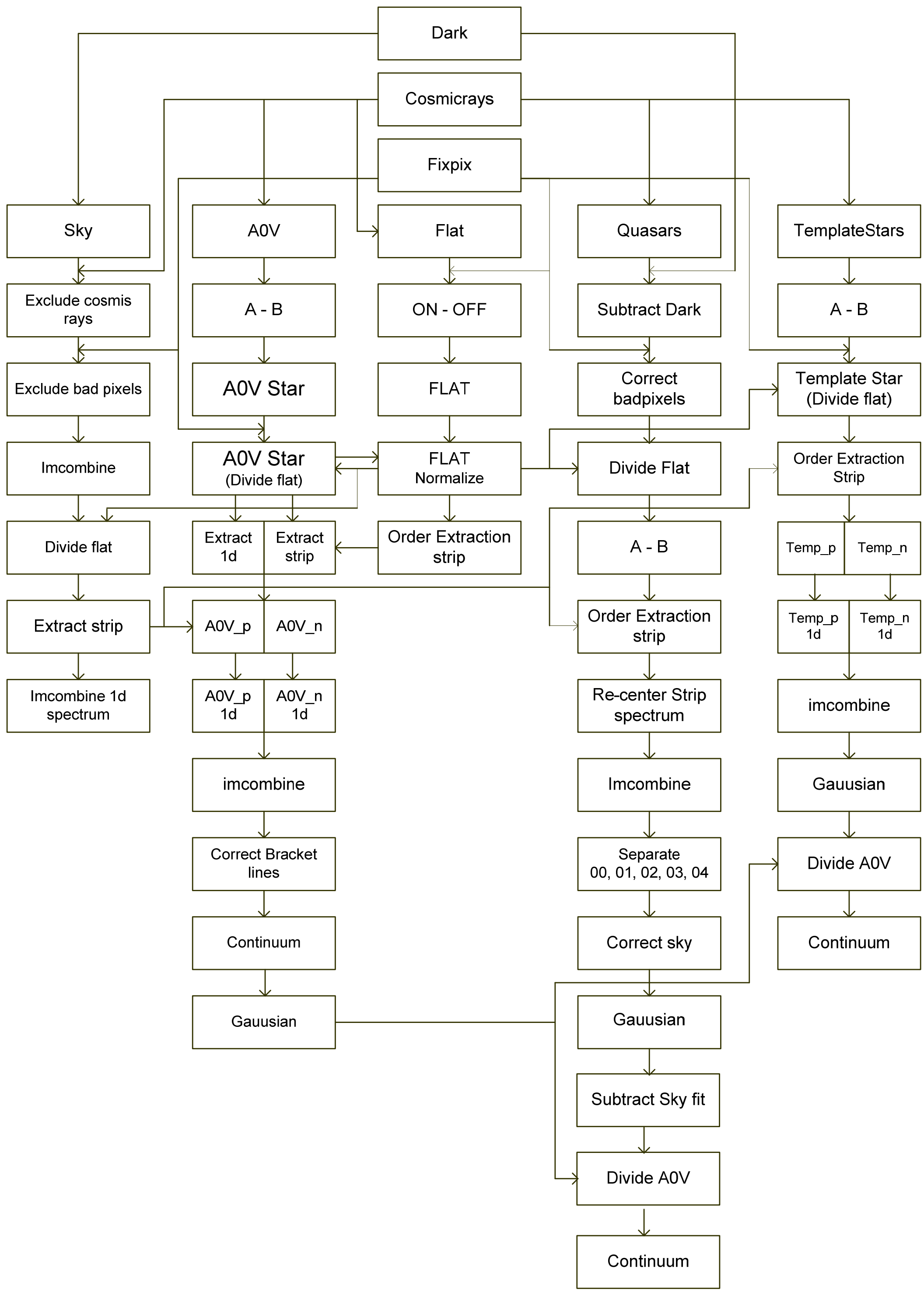

Figure 1. Data reduction sequences.

```
noao.imred.echelle     : Call the echelle package to use
echelle.dispaxis = 1   : Set dispersion axis as X-axis
apedit.width     = 93  : Set aperture width (slit length / pixel scale)
apedit.radius    = 45  : Set radius to calculate the center of the apature
                         (< apedit.width /2)
apfind.minsep    = 75  : Set minimuum seperation between the apatures
apresize.ylevel  = 0.1 : Set intensity level to resize the apature width
apresize.peak    = yes : Set the above ylevel as a fraction of the peak

noao.twodspec.longslit : Call the longslit package to use
longslit.dispaxis = 1  : Set dispersion axis as X-axis)

noao.imred.ccdred      : Call ccdred package to use
noao.imred.crutil      : Call crutil package to use
noao.imred.generic     : Call generic package to use
```

Figure 2. Setting of basic parameters for IRCS echelle spectra during the data reduction processes.

3.1.2 Dark subtraction

Dark frame is obtained in the same integration time as the object frame when the dorm and the primary mirror of the telescope were closed. We use the IMCOMBINE task in IRAF to make a referent dark frame. Figure 3 shows the referent dark frame which we use to subtract the dark current in raw data images.

3.1.3 Correcting cosmic rays and bad pixels

High energy particles or cosmic rays which hit the detector during the integration time create a lot of white point sources in the obtained images. Also, infrared array of the IRCS has bad pixels about 0.7 percents. All raw data images need to be corrected for cosmic rays and bad pixels. These tasks can be done by using the COSMICRAYS and FIXPIX task in IRAF which detect and replace by neighbor pixels.

In COSMICRAYS task, we can set the parameter *threshold* (Detection threshold above the mean of surrounding pixels for cosmic rays) and *fluxratio* (The ratio of the mean neighbor pixel flux to the candidate cosmic ray pixel for rejection). Figure 4 shows an example of cosmic rays correction.

In the FIXPIX task, we use BadPixel070502.fits as a referent image for correcting bad pixels. In addition, in case of using FIXPIX by *.dat file, we can use the IMPLOT task in IRAF to detect for the position of the bad pixels points, then write that position in file.dat. Figure 5 shows the bad pixels image BadPixel070502.fits of echelle section of IRCS. White dots and lines are bad pixels. Figure 6 shows an example of using FIXPIX by file.dat.

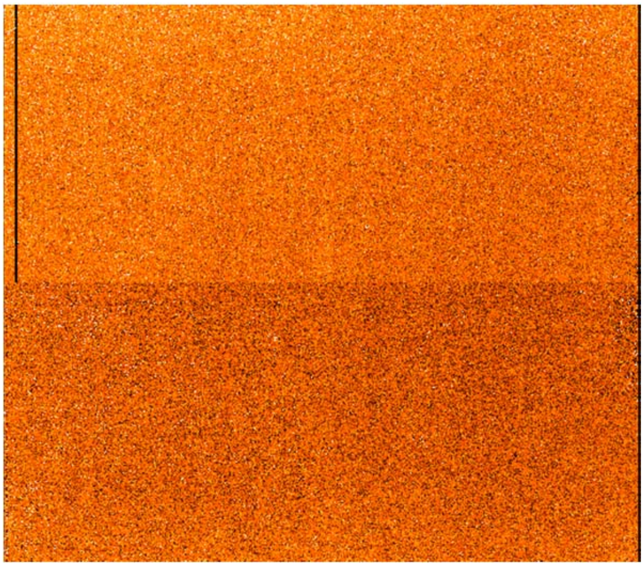

Figure 3. Median dark image. We combined 12 images whose exposure time is 180s each.

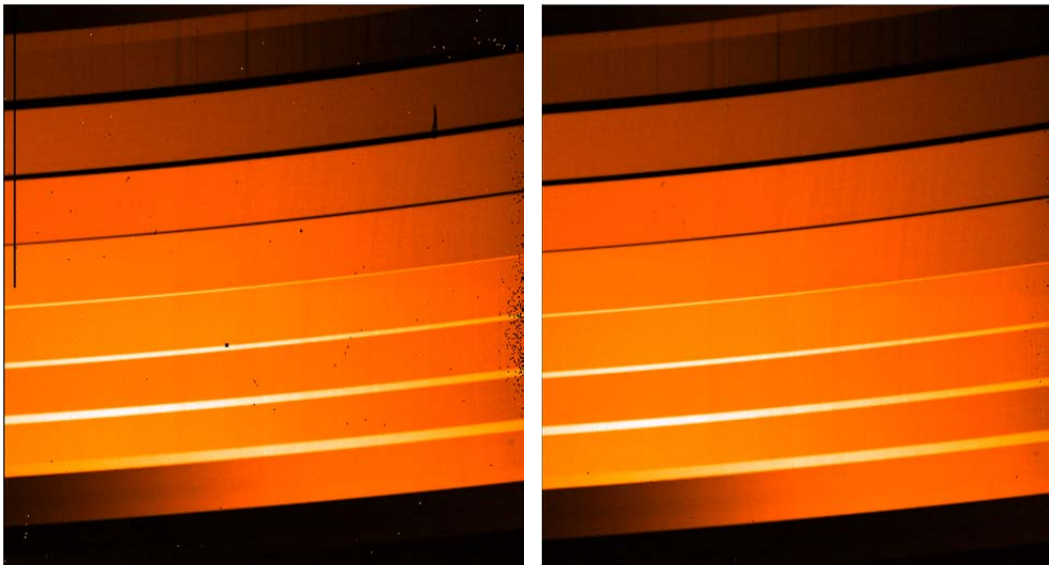

Figure 4. Echellogram flat images correction for cosmic rays and bad pixel. The left image is before correction, and the right image is after correction for cosmic rays and bad pixels.

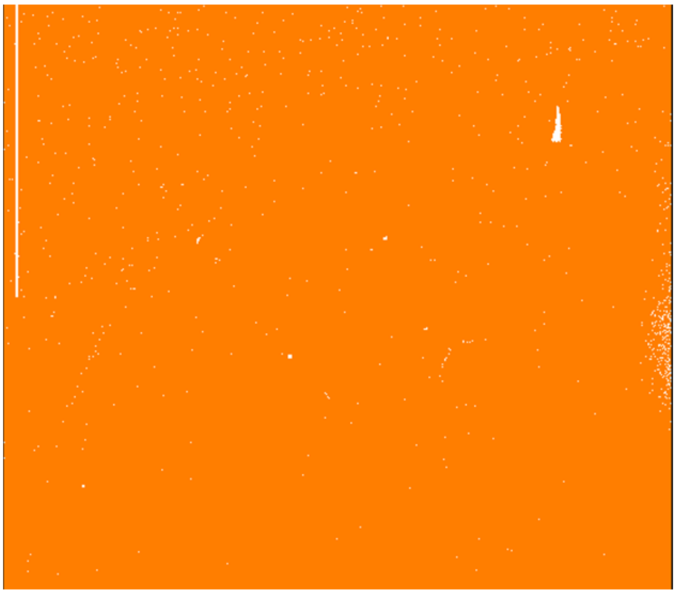

Figure 5. The bad pixels image BadPixel070502.fits of echelle section of IRCS. White dots and lines are bad pixels.

```
cl> epar fixpix
PACKAGE = proto
 TASK = fixpix
images =       A0V_A_t.nfix.0003   List of images to be fixed
masks  =       badpixel.dat  List of bad pixel masks
(linterp=            INDEF)  Mask values for line interpolation
(cinterp=            INDEF)  Mask values for column interpolation
(verbose=              yes) Verbose output?
(pixels =              yes) List pixels?
(mode   =               ql)

FIXPIX: image A0V_A.pfix.0003.fits with mask badpixel3.dat

 676  51 -8.76869  -4.375 675  51 677  51
 676  52 -5.57319 -4.74916 675  52 677  52
```

Figure 6. Using FIXPIX task with file of badpixel.dat. The numbers of bottom show the position and pixel values which replace for the bad pixel points.

3.1.4 Flat fielding

A flat frame is used to correct the pixel-to-pixel variations and non-uniformity of the optics. There are two kinds of flat frames, i.e, *flat-on* and *flat-off*. We took these images when the continuum light sources were turned on and off. *Flat-on* frames must have intensity level with high signal-to-noise ratios. *Flat-off* frames show background thermal emission and dark current.

By using the IMCOMBINE task, we combine all the flat frames to get the flat image. Flat images need to be corrected for cosmic rays and bad pixels, then subtract Flat-off frame from Flat-on frame to get the final flat frame. The final flat frame need to be normalized to make the intensity level to around one. All of the images need to be divided by normalized flat image. Figures 7 and 8 show the flat on and off frame, and the final flat frame. Using this frame, we can also have the order extraction solution for other images. This task will be explained in the processes of standard star.

3.1.5 Extract Apertures

All of frames images can be extracted to each aperture by using APALL task. In this task, we will use flat image as a reference frame. Figure 9 shows an example of spectrum image after APALL task.

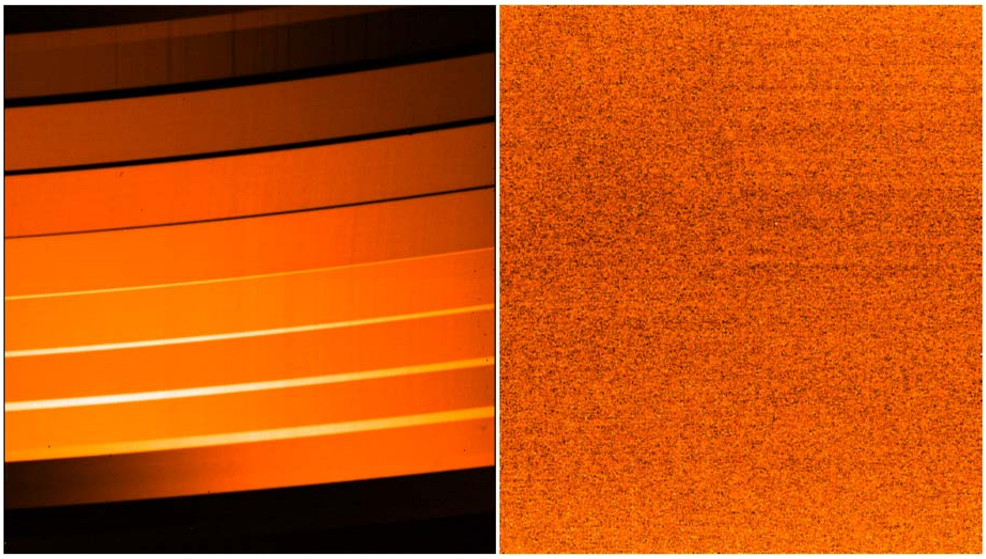

Figure 7. Echellogram H band flat on (left) and flat off (right) images. These images are already corrected for cosmic rays and bad pixels.

Figure 8. Echellogram final H band flat image. After subtraction flat off from flat on, and correction for cosmic rays and bad pixels.

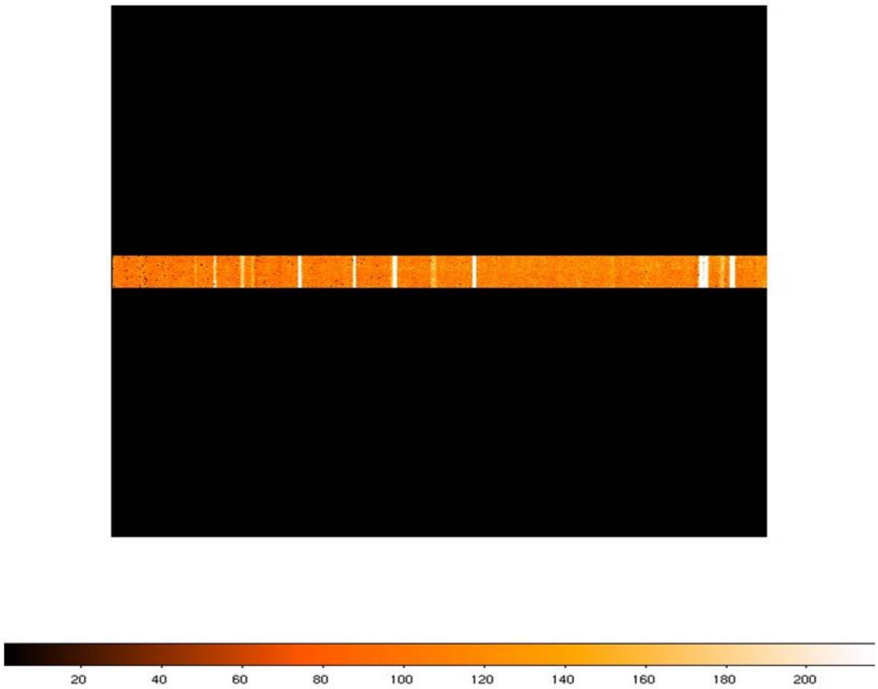

Figure 9. One aperture of sky frame after APALL task.

3.2 Sky, Wavelength calibration and distortion correction

3.2.1 Sky frames

The sky background emissions need to be subtracted from the object images. The sky frames are taken from the sky near the target because the sky background varies with time. The sky frames can be observed by sequences as *object→sky→sky→object*. Figures 10 and 11 show the sky frame taken from the data after pre-processing process in *H*+ and *H*- settings. The sky frames will be used to correct for the sky background in raw images data.

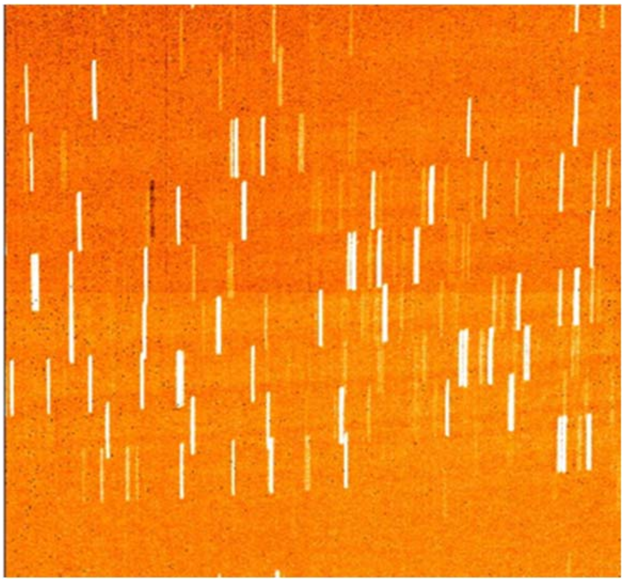

Figure 10. Echellogram sky image in H + band.

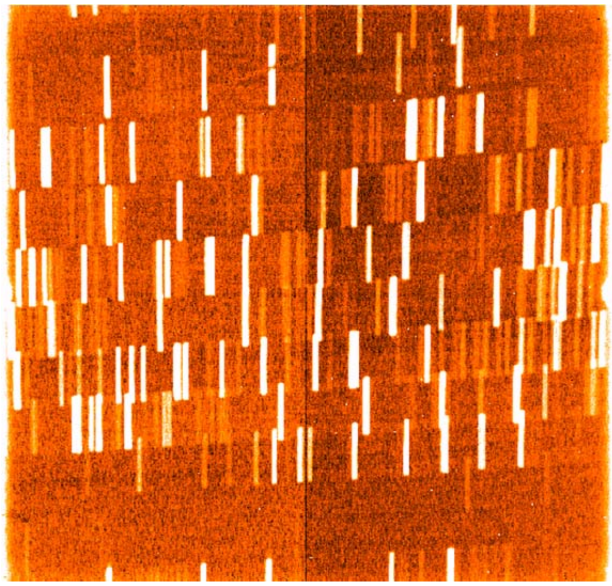

Figure 11. Echellogram sky image in H - band.

3.2.2 Wavelength calibration and distortion correction

We use OH night sky emission lines as a reference for wavelength calibration (Rousselot et al. 2000). These processes are separated into two parts. The first step can be obtained the relationship between pixel numbers and wavelength along the dispersion direction which is called dispersion solution. The second step is to convert the non-uniform wavelength interval per pixel to the equal wavelength interval, and to redistribute the pixel values along the wavelength which is called *linearize.*

Geometric distortions in the spectral images also need to be corrected. Figure 12 shows the curvature and inclination of slit images and monochromatic lines in the spectra. The geometric distortions in the spectra vary with wavelength or pixel numbers along the dispersion axis. The relations between distortions and pixel numbers can be obtained from the comparison lines which are called *distortion solution*.

By using the IRAF package *noao.twodspec.longslit*, we can make wavelength calibration and distortion solution for the data by the tasks like IDENTIFY, REIDENTIFY, FITCOORD, and TRANSFORM.

To determine the dispersion solution, we use the IDENTIFY task in IRAF. This task is used to identify the comparison lines in the one dimension spectra images. We used the REIDENTIFY task in IRAF to determine the *distortion solution.* This task trace the line images and measure their positions along the spatial dispersion axis of the comparison lines which identified by IDENTIFY task. We used the FITCOORD task to calculate for transformation of coordinates. The FITCOORD task will determine the user coordinate with the data obtained from the IDENTIFY and REIDENTIY task. Figure 13 shows example about REIDENTIFY task. Figure 14 shows an example of FITCOORD task.

Last, we will use the TRANSFORM task to transform the raw images to user coordinate based on the parameters which were obtained from the FITCOORD task. The images are shifted comparing with the original positions, and the image coordinate transforms from pixel coordinate to wavelength coordinate. Figure 15 shows an example about TRANSFORM task.

After TRANSFORM task, the wavelength calibration and distortion correction are done. The lines images are shifting compare with their origin positions, and the image coordinate transform from pixels to wavelength coordinate. Figure 16 shows sky spectrum of pixel coordinate and wavelength coordinate.

Figure 17 shows the wavelength calibration and distortion correction of the data reduction process.

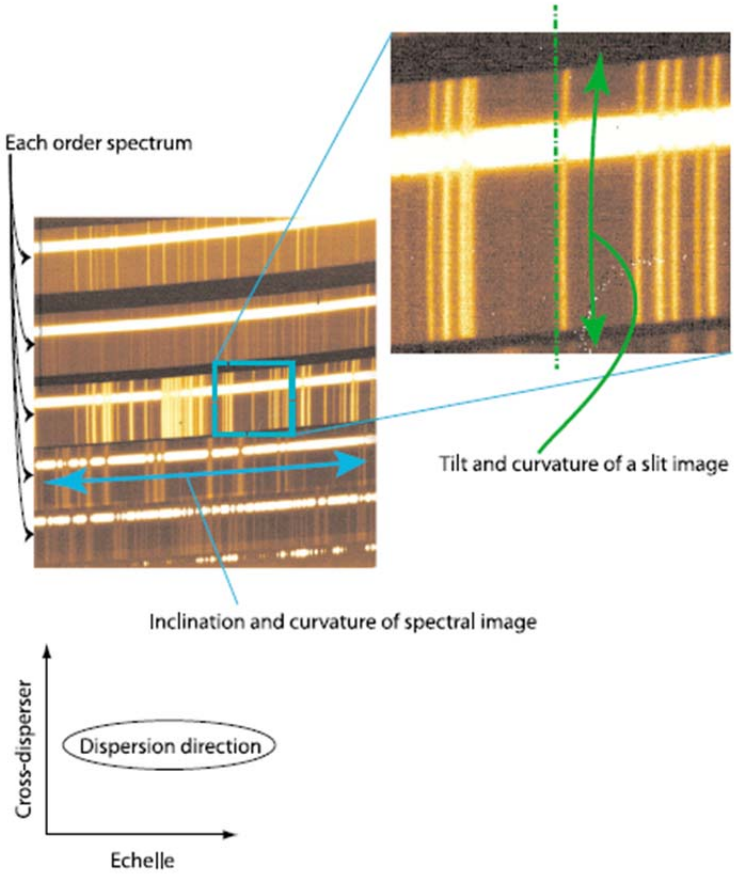

Figure 12. IRCS echellogram (Dr. Pyo dissertation .2002)

```
                            I R A F
                  Image Reduction and Analysis Facility
PACKAGE = longslit
   TASK = reidentify

referenc=    sky.hmg.0001.fits  Reference image
images  =    sky.hmg.0001.fits  Images to be reidentified
(interac=                   no) Interactive fitting?
(section=          middle line) Section to apply to two dimensional images
(newaps =                  yes) Reidentify apertures in images not in reference?
(overrid=                   no) Override previous solutions?
(refit  =                  yes) Refit coordinate function?

(trace  =                  yes) Trace reference image?
(step   =                   10) Step in lines/columns/bands for tracing an image
(nsum   =                   10) Number of lines/columns/bands to sum
(shift  =                   0.) Shift to add to reference features (INDEF to search)
(search =                   0.) Search radius
(nlost  =                    0) Maximum number of features which may be lost

(cradius=                   5.) Centering radius
(thresho=                   0.) Feature threshold for centering
(addfeat=                   no) Add features from a line list?
(coordli= linelists$idhenear.dat) User coordinate list
(match  =                  -3.) Coordinate list matching limit
(maxfeat=                   50) Maximum number of features for automatic identificatio
(minsep =                   2.) Minimum pixel separation

(databas=             database) Database
(logfile=              logfile) List of log files
(plotfil=                     ) Plot file for residuals
(verbose=                  yes) Verbose output?
(graphic=             stdgraph) Graphics output device
(cursor =                     ) Graphics cursor input

answer  =                  yes  Fit dispersion function interactively?
crval   =                       Approximate coordinate (at reference pixel)
cdelt   =                       Approximate dispersion
(aidpars=                     ) Automatic identification algorithm parameters
(mode   =                   ql)


REIDENTIFY: NOAO/IRAF V2.14.1 anh@ircs.khu.ac.kr Wed 00:47:43 20-Oct-2010
  Reference image = sky.hmg.0001.fits, New image = sky.hmg.0001, Refit = yes
         Image Data    Found     Fit Pix Shift  User Shift  Z Shift      RMS
sky.hmg.0001[*,25]     10/10   10/10     0.123       0.123  3.47E-4     203.
sky.hmg.0001[*,15]     10/10   10/10      0.14        0.14  3.32E-4     203.
sky.hmg.0001[*,5]      10/10   10/10     0.193       0.193  5.05E-4     203.
sky.hmg.0001[*,45]     10/10   10/10   -0.0613     -0.0615  -1.7E-4     203.
sky.hmg.0001[*,55]     10/10   10/10    0.0427      0.0425  -4.3E-6     203.
sky.hmg.0001[*,65]     10/10   10/10   -0.0574     -0.0576  -3.6E-4     203.
```

Figure 13. Setting parameters and execution of REIDENTIFY task.

```
                              I R A F
                 Image Reduction and Analysis Facility
PACKAGE = longslit
   TASK = fitcoords

images  =          sky.hmg.0001  Images whose coordinates are to be fit
(fitname=                      ) Name for coordinate fit in the database
(interac=                   yes) Fit coordinates interactively?
(combine=                    no) Combine input coordinates for a single fit?
(databas=              database) Database
(deletio=          deletions.db) Deletion list file (not used if null)
(functio=             chebyshev) Type of fitting function
(xorder =                     6) X order of fitting function
(yorder =                     6) Y order of fitting function
(logfile=        STDOUT,logfile) Log files
(plotfil=              plotfile) Plot log file
(graphic=              stdgraph) Graphics output device
(cursor =                      ) Graphics cursor input
(mode   =                    ql)
```

```
NOAO/IRAF V2.14.1 anh@ircs.khu.ac.kr Wed 10:33:23 20-Oct-2010
  Longslit coordinate fit name is sky.hmg.0001.
  Longslit database is database.
  Features from images:
    sky.hmg.0001
  Map User coordinates for axis 1 using image features:
  Number of feature coordnates = 161
  Mapping function = chebyshev
    X order = 4
    Y order = 3
  Fitted coordinates at the corners of the images:
    (1, 1) = 1.459359  (1024, 1) = 1.495852
    (1, 70) = 1.42477  (1024, 70) = 1.508803
Write coordinate map to the database (yes)? n
```

Figure 14. Setting parameters and execution of FITCOORD task.

```
                          I R A F
           Image Reduction and Analysis Facility
PACKAGE = longslit
   TASK = transform

input   =   sky.hmg.0001.fits  Input images
output  =  sky.hmg.t.0001.fits  Output images
(minput =                     ) Input masks
(moutput=                     ) Output masks
fitnames=         sky.hmg.0001  Names of coordinate fits in the database
(databas=             database) Identify database
(interpt=              spline3) Interpolation type
(x1     =                INDEF) Output starting x coordinate
(x2     =                INDEF) Output ending x coordinate
(dx     =                INDEF) Output X pixel interval
(nx     =                INDEF) Number of output x pixels
(xlog   =                   no) Logarithmic x coordinate?
(y1     =                INDEF) Output starting y coordinate
(y2     =                INDEF) Output ending y coordinate
(dy     =                INDEF) Output Y pixel interval
(ny     =                INDEF) Number of output y pixels
(ylog   =                   no) Logarithmic y coordinate?
(flux   =                  yes) Conserve flux per pixel?
(blank  =                INDEF) Value for out of range pixels
(logfile=      STDOUT,logfile) List of log files
(mode   =                   ql)


NOAO/IRAF V2.14.1 anh@ircs.khu.ac.kr Thu 11:48:44 21-Oct-2010
  Transform sky.hmg.0001.fits to sky.hmg.t.0001.fits.
  Conserve flux per pixel.
  User coordinate transformations:
    sky.hmg.0001
  Interpolation is spline3.
  Using edge extension for out of bounds pixel values.
  Output coordinate parameters are:
    x1 =      1.425, x2 =      1.509, dx =   8.214E-5, nx = 1024, xlog = no
    y1 =         1., y2 =        70., dy =         1., ny =   70, ylog = no
```

Figure 15. Setting parameters and execution of TRANSFORM task.

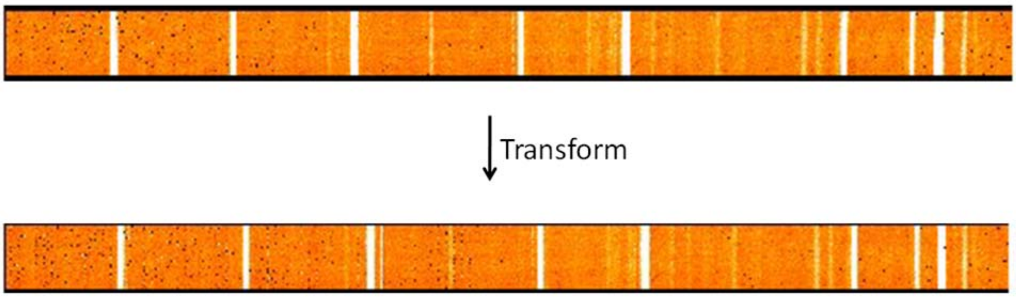

Figure 16. The different position of lines images before and after TRANSFORM task of the data reduction process.

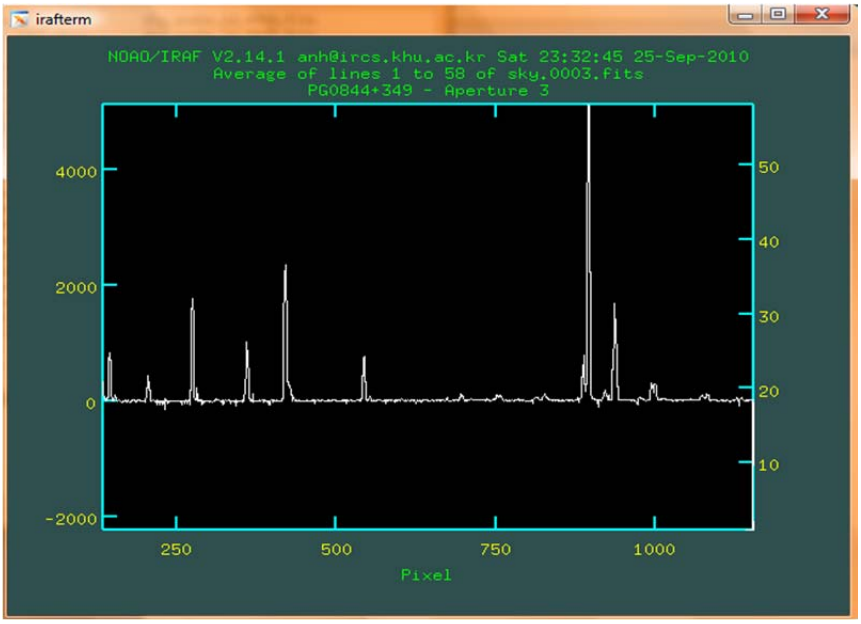

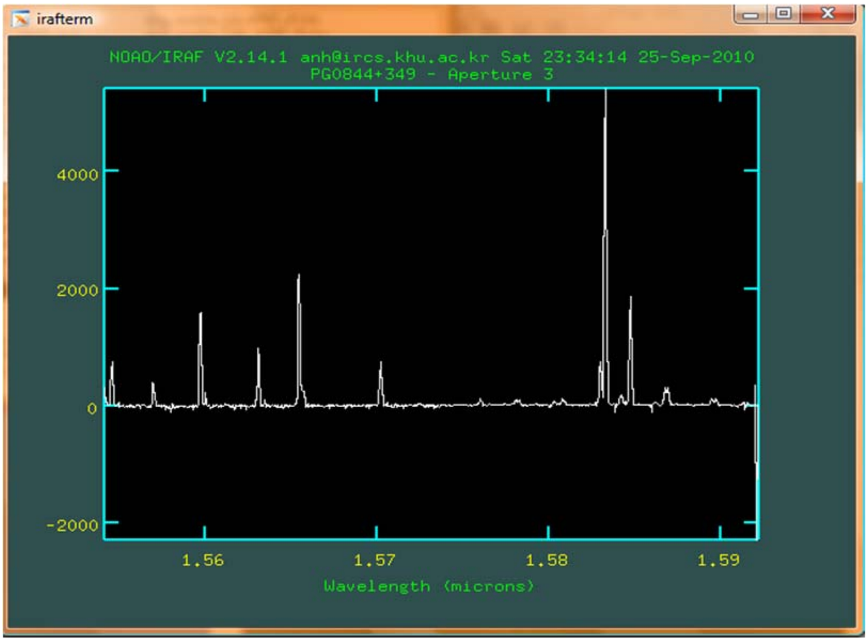

Figure 17. After wavelength calibration, the pixel coordinate becomes to wavelength coordinate. Upper is pixel coordinate, and bottom is wavelength coordinate.

3.3 Standard star

To correcting for the telluric absorption lines in the data spectra, we use standard star spectrum as a referent source. For example, A0V star. By dividing the spectrum data for A0V spectrum, we can correct the telluric absorption lines in the spectrum.

A0V star is taken in *nod-on-slit* mode. The standard star is taken in two positions A and B. In the first exposure, the standard star will be place in one position in the slit (position A), and after that, we move the telescope a little bit along the slit direction compare with position A (position B).

In the data reduction of standard star spectrum, after pre-processing process (correcting cosmic rays, bad pixels, flat correction), we subtract the standard star spectrum of position B from standard star spectrum of position A, and get the final spectrum of standard star. Figure 18 and 19 show the images of standard stars which are taken in position A, position B, and after subtract B from A.

Standard star also used to make spectral distortion correction. From the final combine image of standard star, we use APALL task to extract one dimensional (1d) spectrum for A0V standard star.

From this step, A0V star will be used as a referent source for extract strip spectra for flat spectrum. Figure 20 shows the execution process of extract 1d spectrum for A0V star, and spectrum of interactive process.

From the figure 19, we see the final image of standard star A0V (HD39357) which has eight orders, and each order we call aperture. For this spectrum, we need to use APALL task to extract strip spectra of each aperture with using flat image as a referent source to get two dimensional (2d) spectrum of each aperture. Figure 21 shows one of 2d spectrum of A0V star after using APALL task. After this step, we can use TRANSFORM task to make wavelength calibration for standard star spectrum.

After make wavelength calibration for the spectrum, we need to use APALL task to extract 1d spectrum of each aperture. During the process of making 1d spectrum, if these are residual bad pixels in the images, we also need to use FIXPIX to reduce the bad pixels. Next, we combine all the 1d spectra of each aperture.

The spectrum of standard star needs to be corrected for the stellar lines which are

Bracket lines. To do this step, we fitted the absorption Bracket line by Gaussian fitting, and use SPLOT task in IRAF correcting for the Bracket lines in spectrum. Figure 22 shows the spectrum of A0V star with Bracket lines before and after corrected.

CONTINUUM and GAUSS tasks are used to make the final produce of standard star spectrum. CONTINUUM is used for normalize the intensity of the spectrum, and GAUSS is used to make convolve for the spectrum with higher resolution. Figure 23 shows the spectrum after CONTINUUM and GAUSS process.

Finally, after get the final spectrum of each aperture from IRAF, we need to use Python program to make a combine average spectrum for A0V standard star. In this program, we concatenate all of the apertures ‘spectra to one spectrum in H band, and using an average coding to make average spectrum of H+ and H- band. Figure 24 shows the final spectrum of A0V standard star which wavelength has step of 0.0001μm.

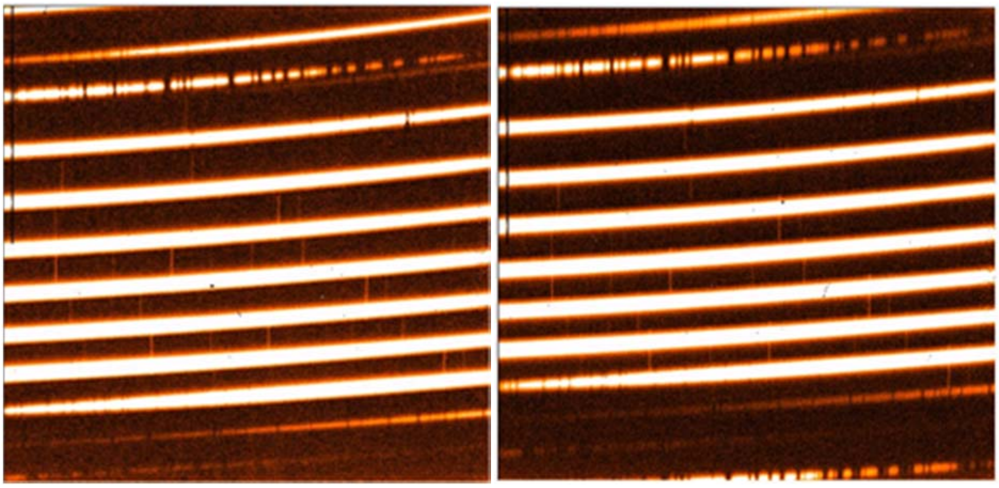

Figure 18. Echellogram A0V standard star image. Left is taken in position A, right is taken in position B.

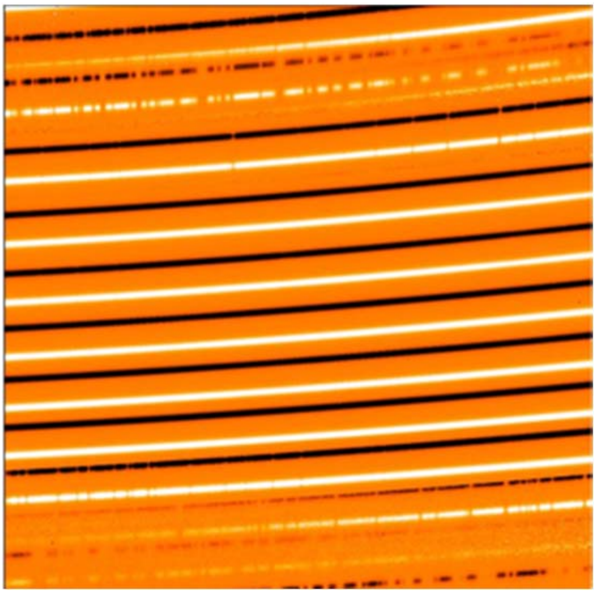

Figure 19. The final combine echellogram image of A0V standard star.

```
PACKAGE = apextract
  TASK = apall

input    =        A0V_A  List of input images
(format =           onedspec) Extracted spectra format
(extras =                 no) Extract sky, sigma, etc.?
(review =                yes) Review extractions?
(line    =               475) Dispersion line ?
(width  =                30.) Profile centering width
(radius  =               15.) Profile centering radius
nfind    =                 8  Number of apertures to be found automatically
(minsep =                70.) Minimum separation between spectra
(maxsep=                130.) Maximum separation between spectra
(bkg     =               yes) Subtract background in automatic width?
(t_funct =          chebyshev) Trace fitting function
(t_order =                 3) Trace fitting function order
```

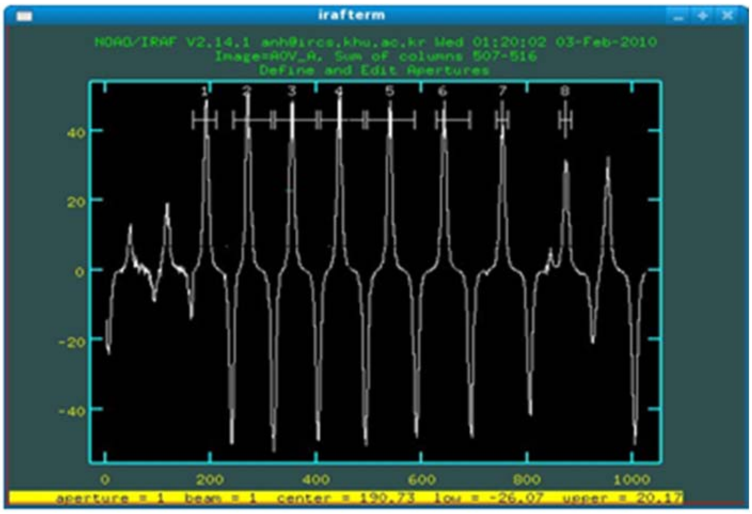

Figure 20. The execution 1d spectrum of A0V star, and the interactive spectrum.

Figure 21. Two dimensional image of A0V star by using APALL task with flat as a referent source.

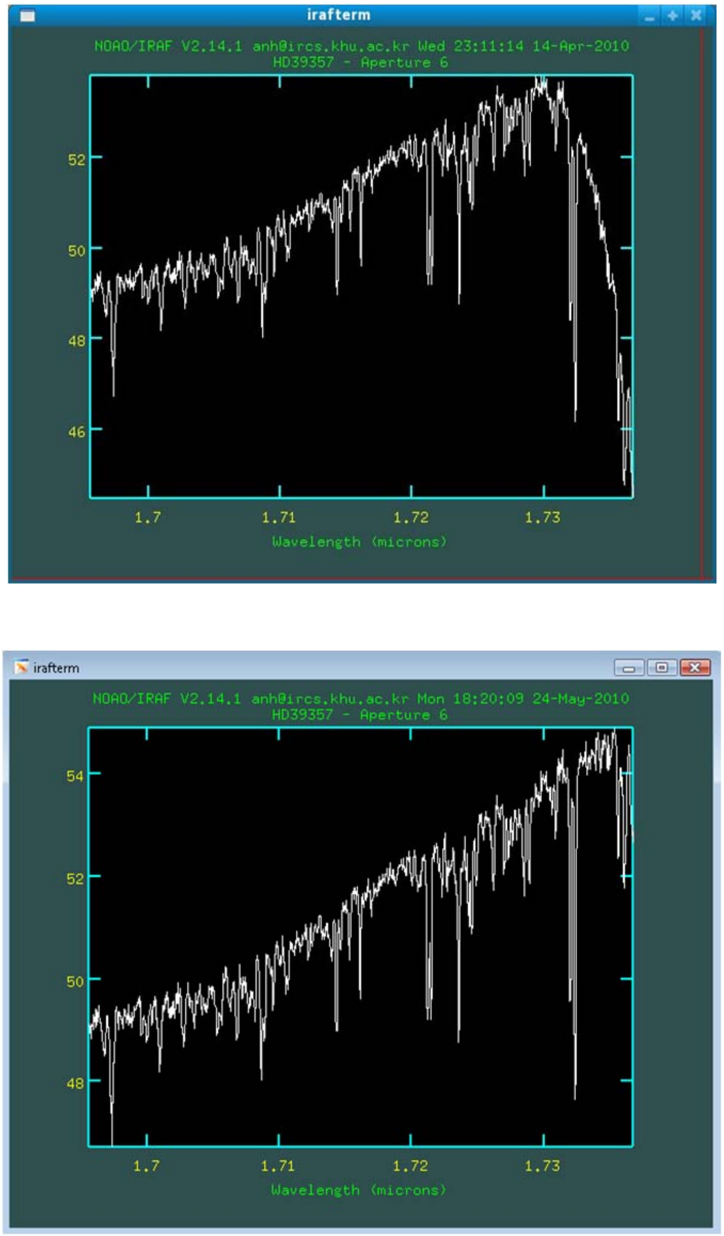

Figure 22. Upper is the A0V standard star spectrum with Bracket line Br10 1.7367 μm, and bottom is the spectrum after corrected for Br10.

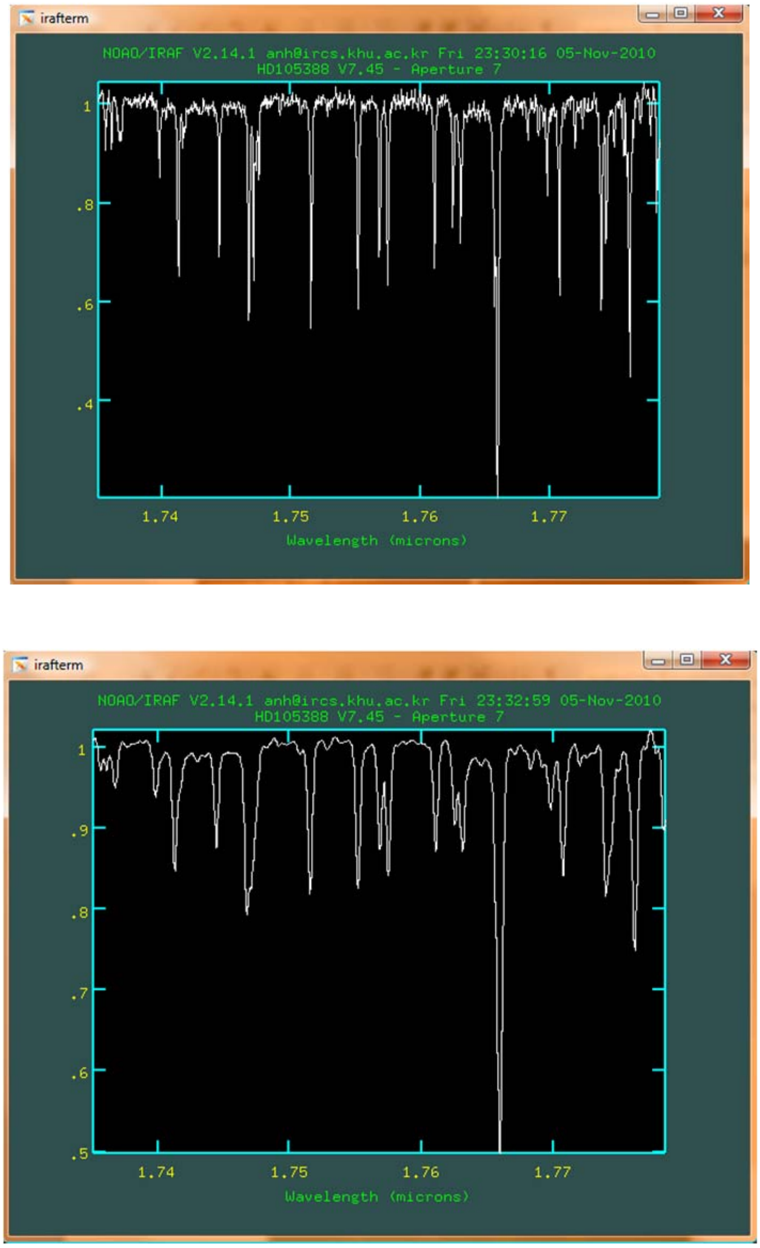

Figure 23. A0V star spectrum aperture 7. Upper is after CONTINUUM task, bottom is after GAUSS process.

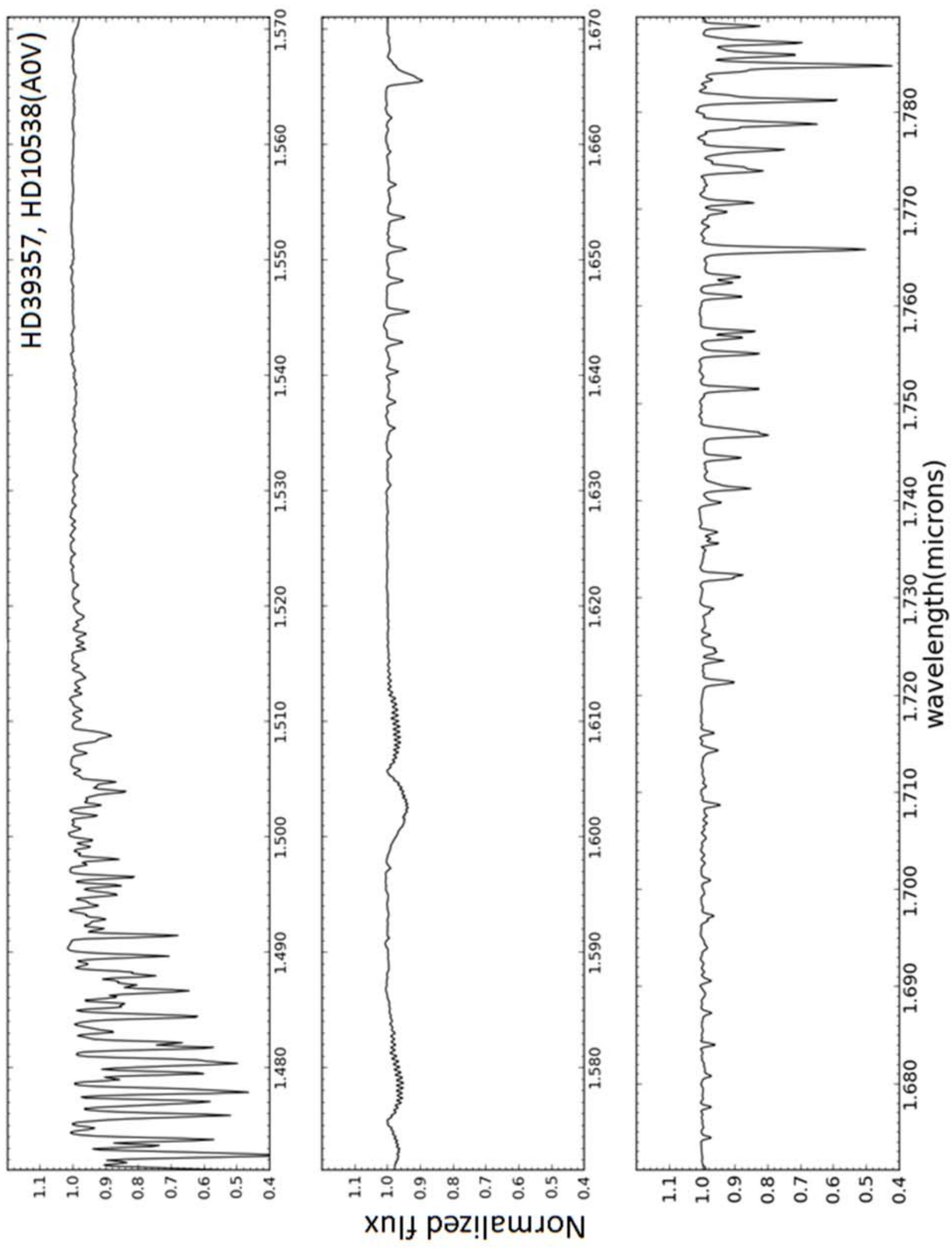

Figure 24. The average combine spectrum of A0V standard star (HD39357 and HD10538).

3.4 Template stars

In data reduction for template stars, after pre-processing processes, we combine all of the spectra in *H*+ and *H*- settings of each star to get the final spectrum. We will use the TRANSFORM task for wavelength calibration, the APALL task to extract strip, and 1D spectrum for the stars as we did in the processes of standard star. After using the IMCOMBINE task to get the final spectrum, we use the GAUSS task for convolution with different resolution. By dividing for the A0V star spectra, we correct the telluric absorption lines in the template star spectra. Finally, we use the CONTINUUM task to normalize the intensity in the spectra. The template star spectra will be used to compare with the spectra of the host galaxy. We make average combine spectra for the template stars with steps of 0.0001μm by Python language.

The final combine average spectrum also corrected for the heliocentric radial velocity. The results of final template star spectra will see in the results part of thesis.

most of the identified features in the template star spectra are overlap, and in this paper, we compare our template star spectra with Arcturus spectrum of Hinkle & Wallace. 1995. We show the identify lines in the spectrum of HD52071(K2III) star which is the most closed to Arcturus star of Hinkle paper. Table 4 shows the identify lines of the spectrum.

Table 4

Identify lines of K2III (HD52071)

Lines[a]	Wavelengths (μm)
CN 1-2	1.50284
CN 1-2	1.50430
Fe	1.52973
Fe	1.53795
Fe	1.56961
Mg	1.58905
Ni	1.59624
Fe	1.60471
Ni	1.60481
Fe	1.63289
Fe	1.65290
Ca	1.65656
Fe	1.66837
OH 4-2	1.67538
Ti	1.69644
C0 7-4	1.69727
Fe	1.69994
OH 2-0	1.71118
C0 5-2	1.72284
C0 11-8	1.73307
Si	1.74717

[a] Identified lines from Hinkle & Wallace. 1995.

3.5 Quasars and Host galaxies

The observations of the nearby quasars were done by *Nod-off-slit* mode. We reduce the sky background, and also the OH night sky emission lines including in the object spectra. Figure 25 and 26 show the sky subtraction background process.

The APALL task is used to extract strip images. Before combine all of the strip spectra, we need to use the IMSHIFT task to do re-center for all of the apertures. Figure 27 shows the re-center process. After combine image, we can make wavelength calibration for the data by TRASFORM task.

We combine all of the columns in the image together. Active galactic nucleus (AGN) is a very compact source including point spread function (PSF) quasar in the center and host galaxy in the wing outer part. In the data reduction processes, to separate the quasar spectra and host galaxy spectra, we use an optical technique to do this step. Figure 28 shows the process of separating between quasar and host galaxy spectra. In this separate method, 00 region is the center part which is quasar, and 01, 02, 03, as well as 04 regions are outer wing parts which are the host galaxy. We make 00 region (-0.15 < r < +0.15 arcsec), 01 region (-0.45 < r < -0.15 arcsec) and +0.15 < r < +0.45 arcsec), 02 region (-0.75 < r < -0.45 arcsec and +0.45 < r < +0.75 arcsec), 03 region (-1.05 < r < -0.45 arcsec and +0.75 < r < +1.05 arcsec), 04 region (-1.35 < r < -1.05 arcsec and +1.05 < r < +1.35 arcsec), and sky background 567 region (r < -1.35 arcsec and r > +1.35 arcsec). We separated the regions in 0.3 arcsec width considering the FWHM of the PSF.

The OH night sky emission lines and sky background still remain in the getting spectra because the subtraction background process cannot reduce all of them. We corrected the residual OH night sky emission lines by subtracting for the scaling the sky images. Because the slit-length used for the observations is only 5 arcsec, so we do not know the reliable sky background. In this case, the real intensity of the spectra in regions of 00, 01, 02, 03, and 04 will add the intensity of 05, 06, and 07 regions in figure 28 as the sky level. Finally, we use the GAUSS task for convolution the spectra. We convolved the spectra to have FWHM of 8 pixels. The corresponding spectra resolution is 55.9 km/s in the 2003 observations, and 58.9 km/s in the 2004 observations. Then, we divide the spectrum for A0V star spectrum to correct the telluric absorption lines.

To make the spectra cleaner, we masked out the high intensity sky lines which are larger than 0.1 ADU, and the deep telluric lines which are deeper than 0.8 ADU. Finally, we used average coding in Python language to make the final combine spectra.

The results of quasars and host galaxies spectrum will be shown in results part of thesis.

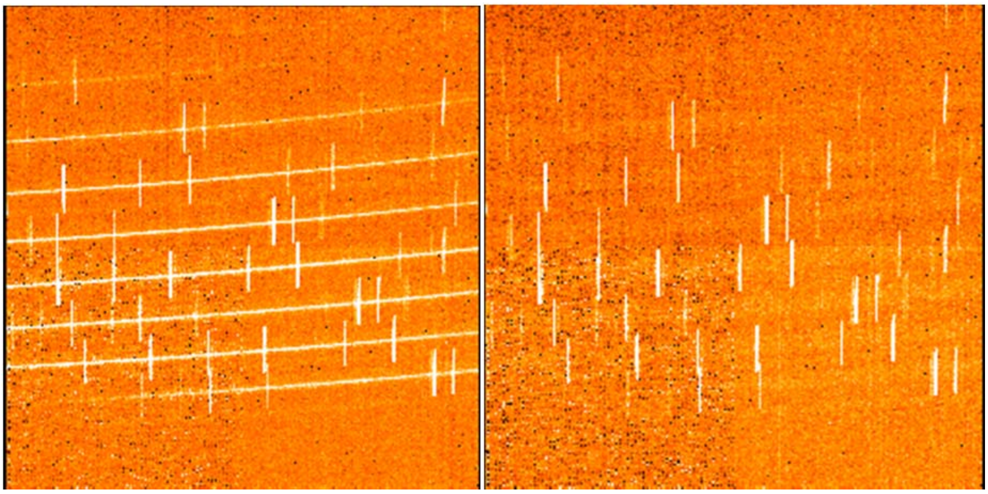

Figure 25. The sky subtraction background process. Left is *object + sky* frame, right is *sky* frame.

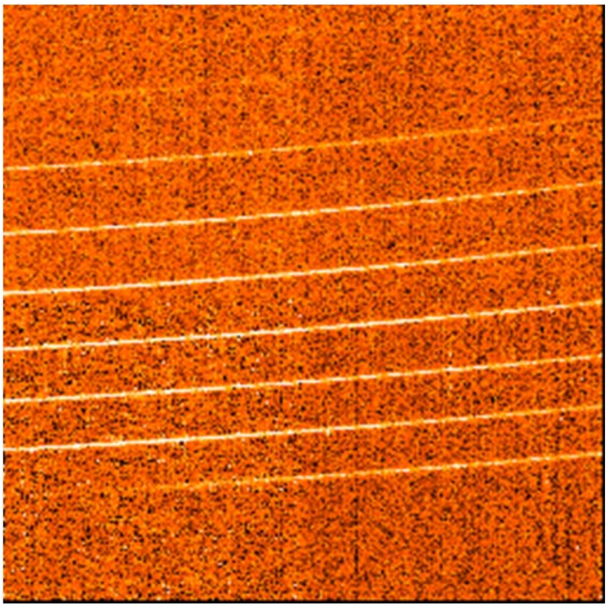

Figure 26. The image of after subtraction sky background process.

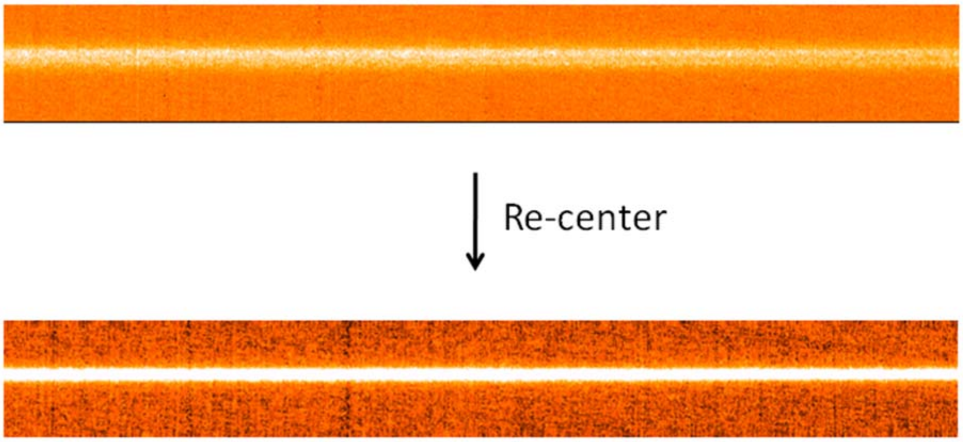

Figure 27. Combine strip images before and after re-center process.

Figure 28. PSF profile and optical technique for separate the center and outer wing parts.

4. RESULTS

From the data reduction processes, we got the results spectra including template star spectra, quasar spectra, and host galaxy spectra.

Figure 29 to figure 36 show the average spectra of template stars which has step of 0.0001 μm. Molecular absorption lines due to CN 1-2 at 1.50 μm, OH 4-2 at 1.68 μm, OH 2-0 at 1.71 μm are strong in the spectra G-K-M type star, and absorption lines due to C0 in the H band at about 1.70 μm, 1.72 μm, 1.73 μm are weaker compare with other molecular absorption lines. The neutral metal absorption features due to Fe at 1.53 μm, Fe at 1.57 μm, Mg at 1.59 μm, Fe at 1.65 μm, Ni at 1.60 μm, and Fe at 1.70 μm are strong dominate in the spectra. Other weaker neutral metal absorption lines are Fe at 1.54 μm, Ni at 1.60 μm, Fe at 1.63 μm, Ca at 1.65 μm, and Si at 1.75 μm.

In the spectra of quasars, we also indentified the features which have in near-infrared band. We show two kinds of spectra which one is spectra with guessed features and other is spectra with error bar of root mean square (RMS) which calculated from the program. Figure 37 to 42 show the quasar spectra.

The average host galaxies spectra including 01, 02, 03, and 04 regions of objects will show from figure 43 to figure 54.

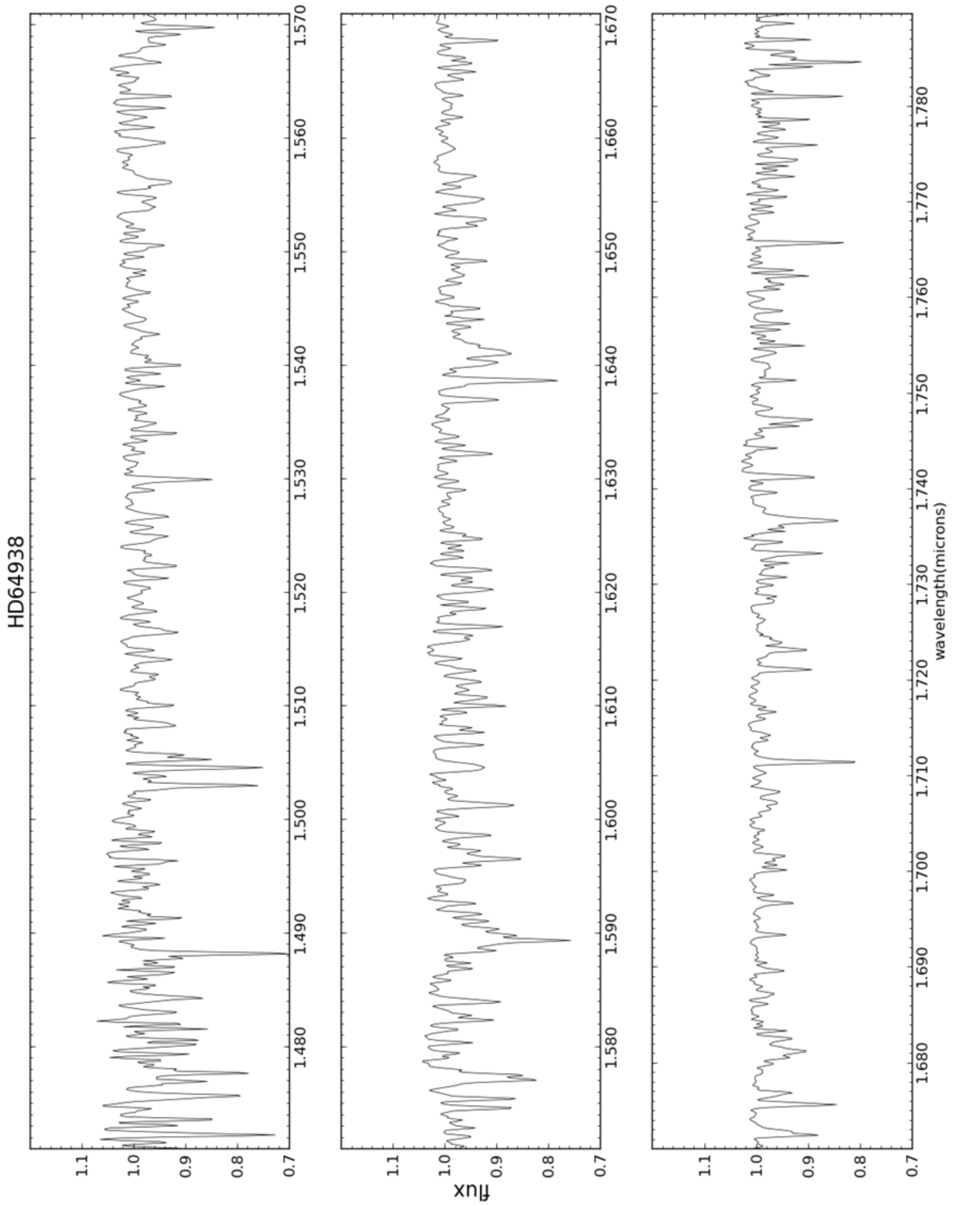

Figure 29. Template star HD64938(G8III)

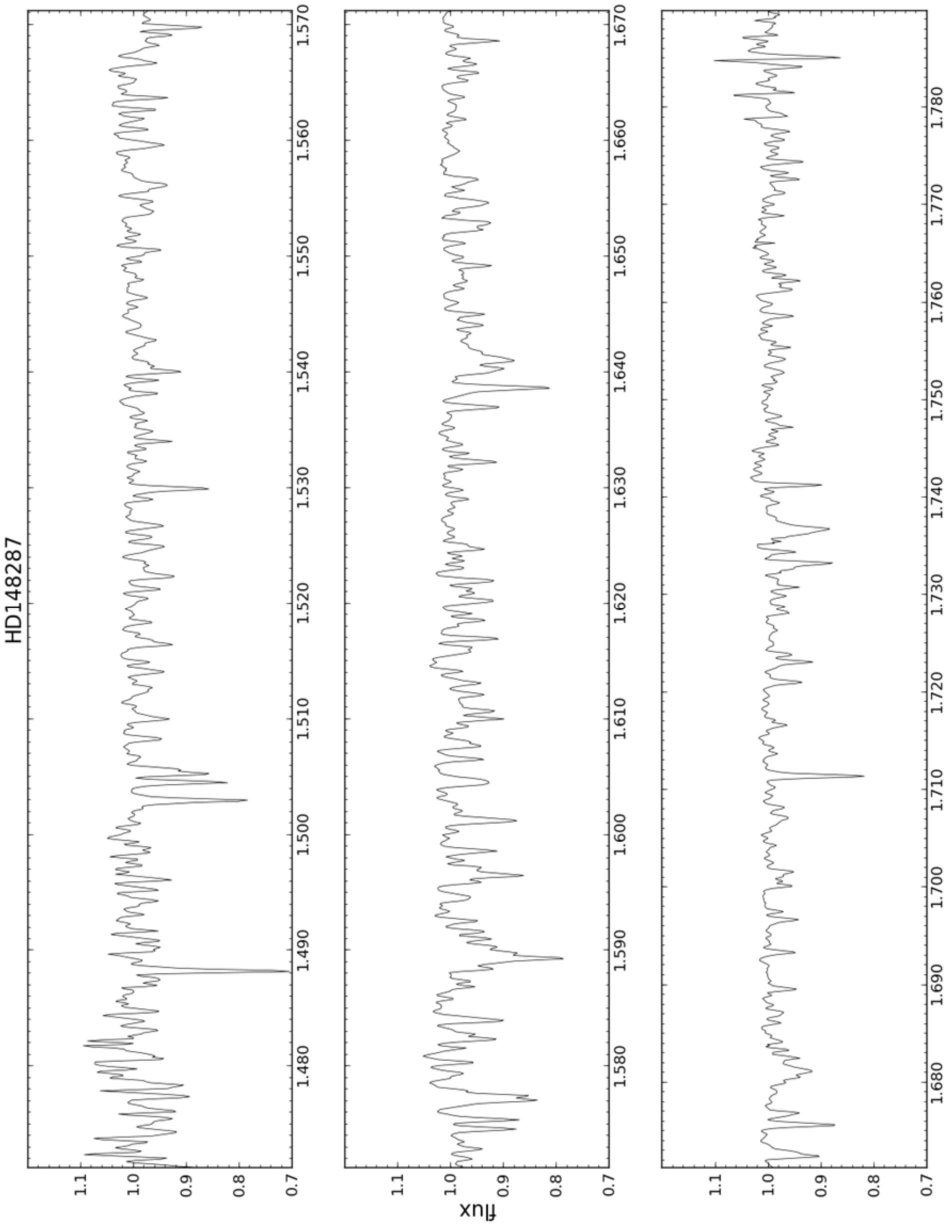

Figure 30. Template star HD14827(G8III)

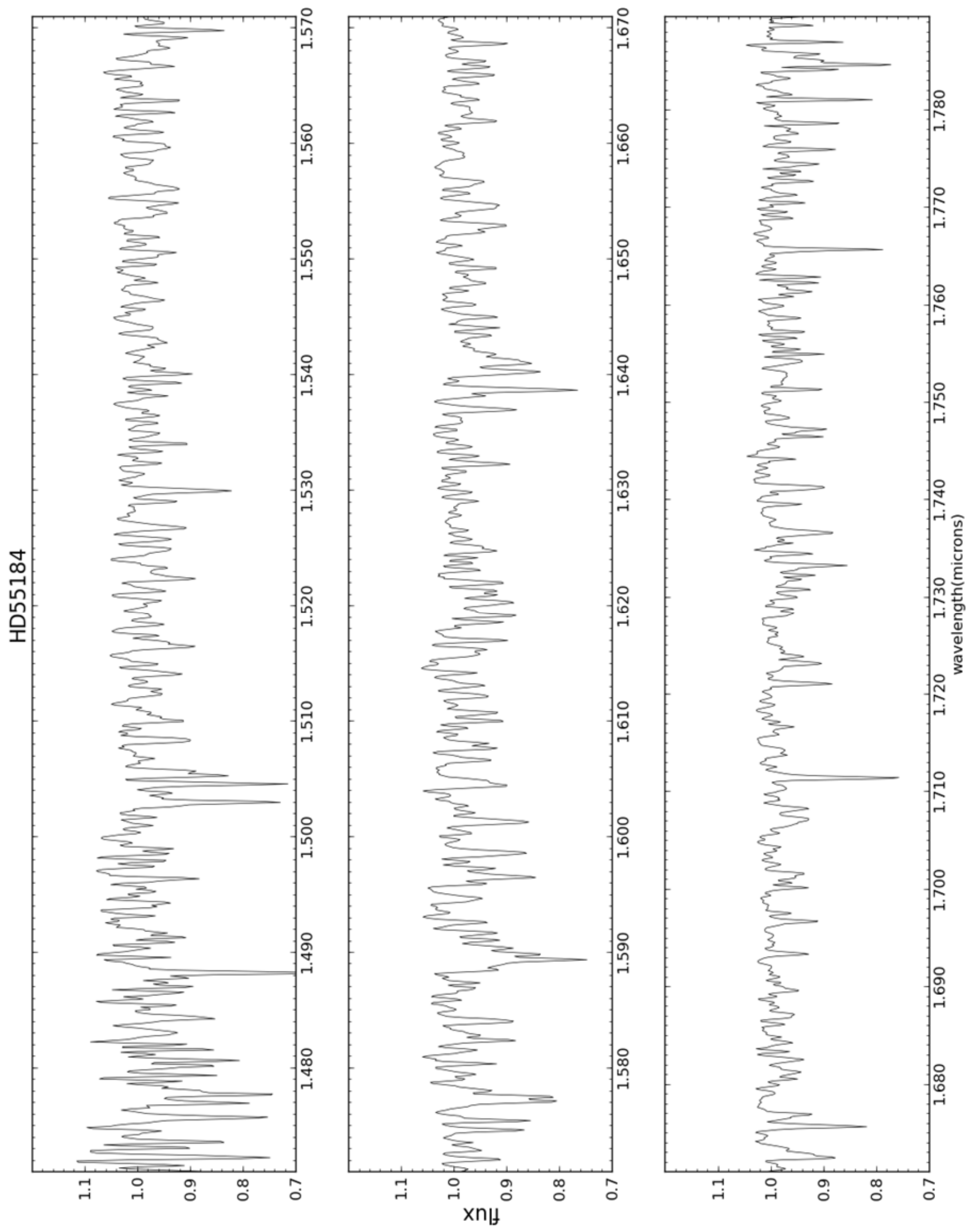

Figure 31. Template star HD55184(K0III)

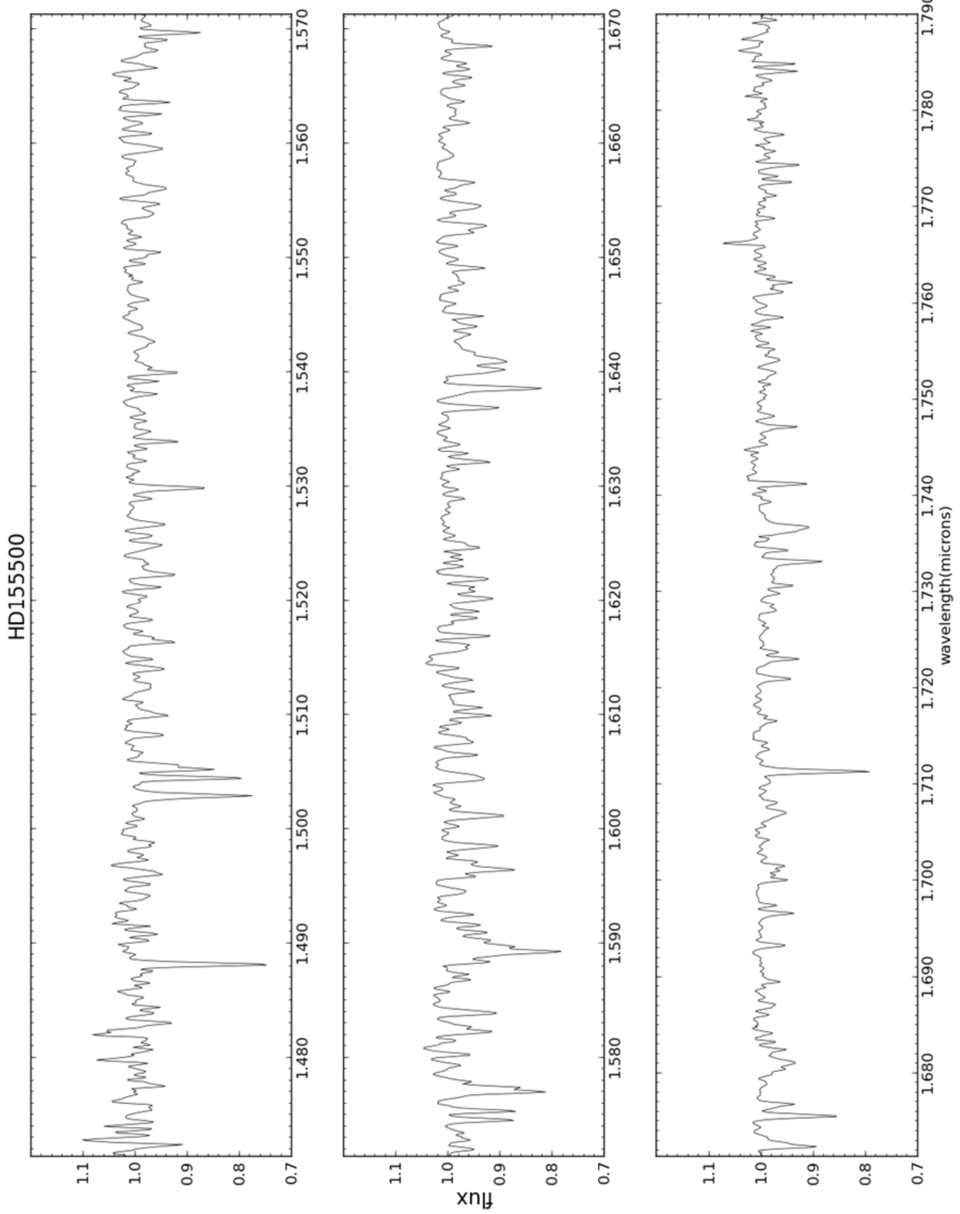

Figure 32. Template star HD155500(K0III)

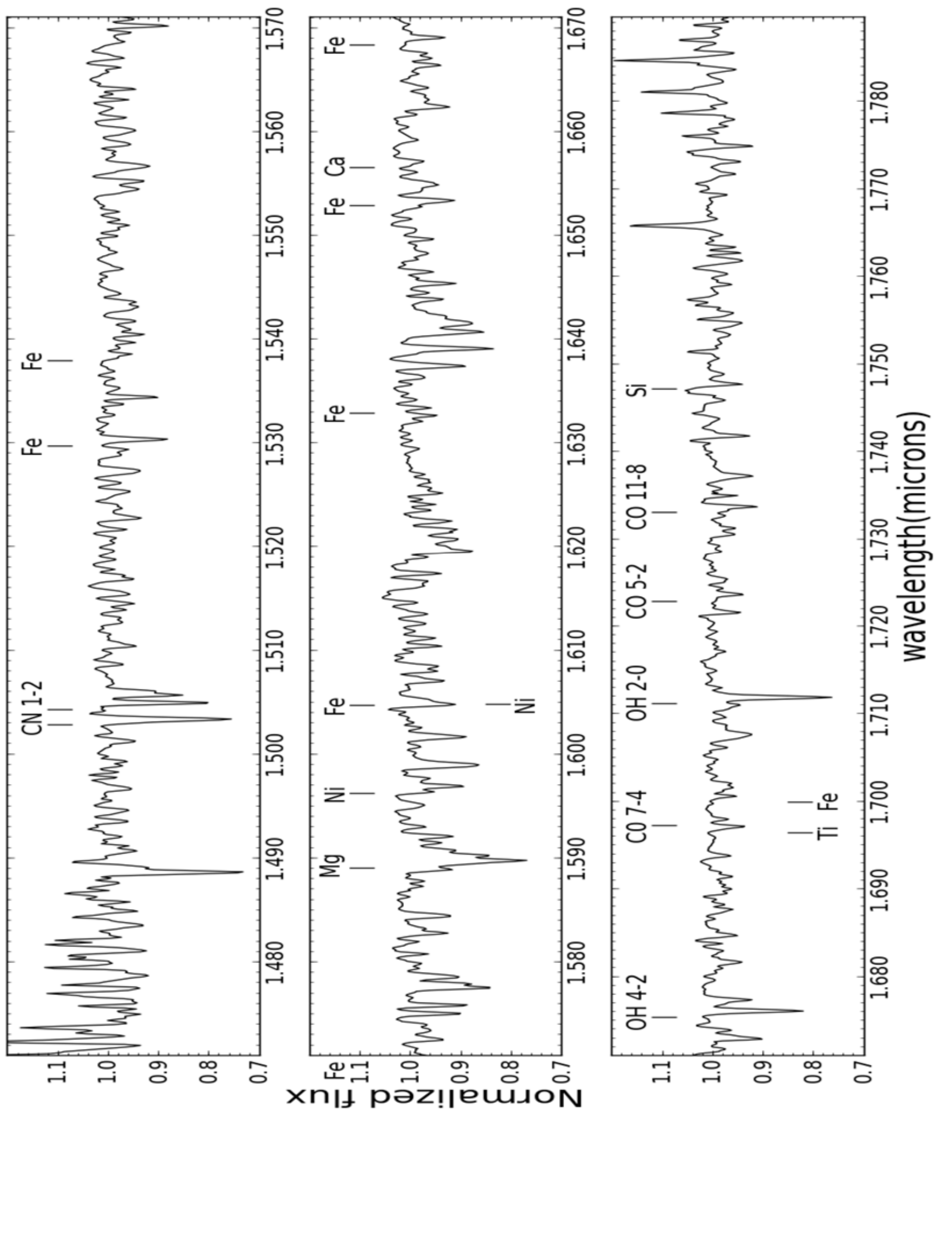

Figure 33. Template star HD52071(K2III)

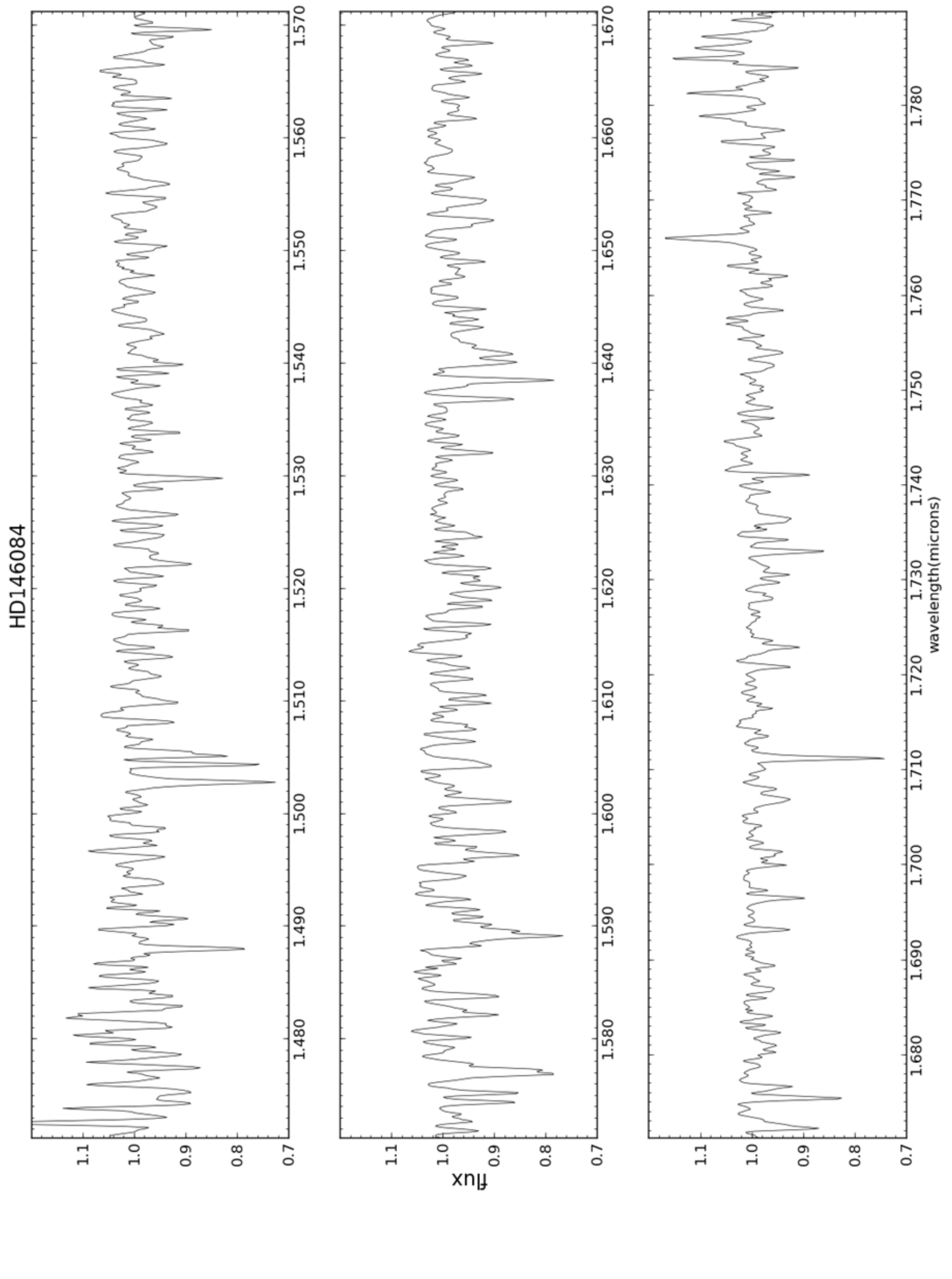

Figure 34. Template star HD146084(K2III)

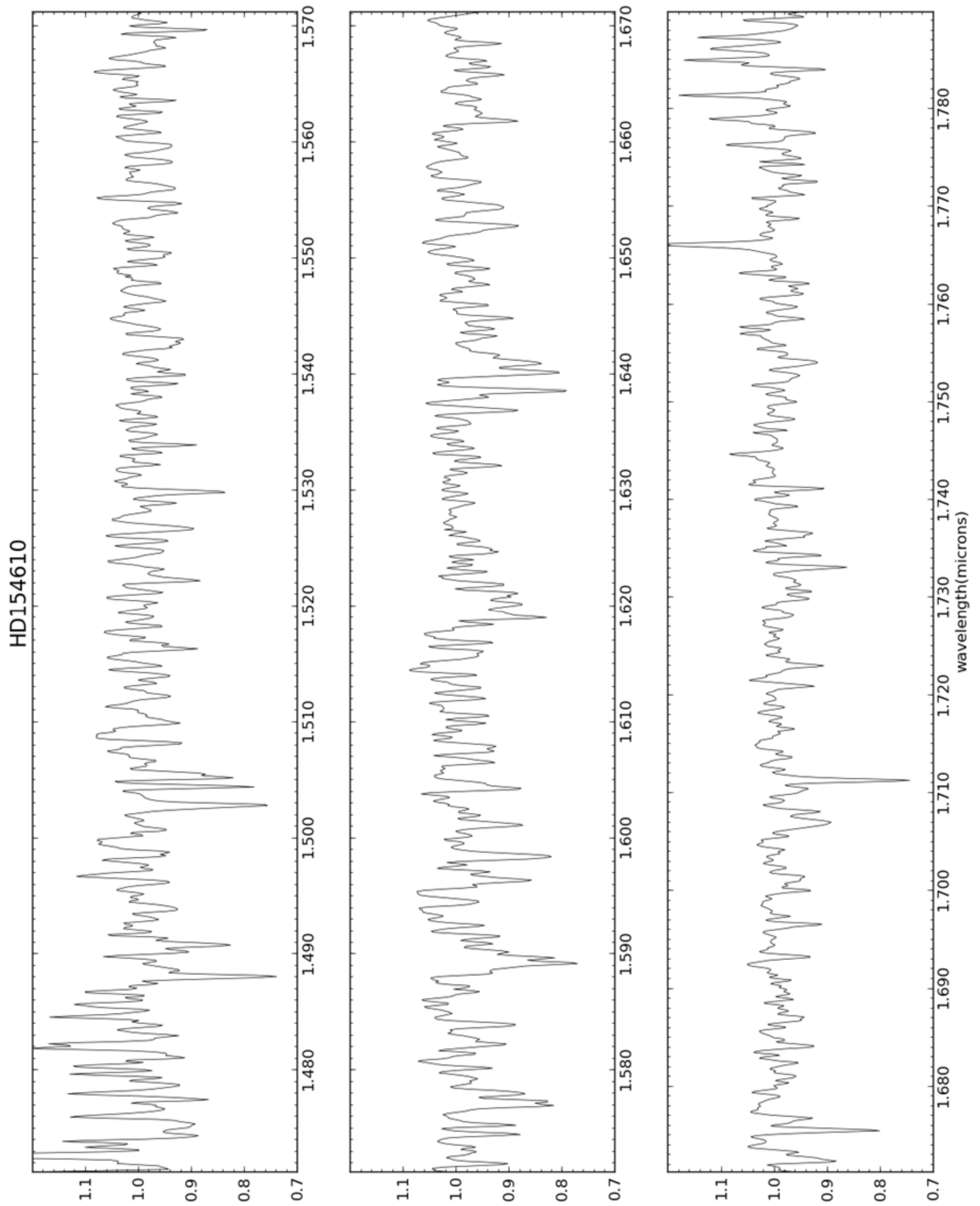

Figure 35. Template star HD154610(K5III)

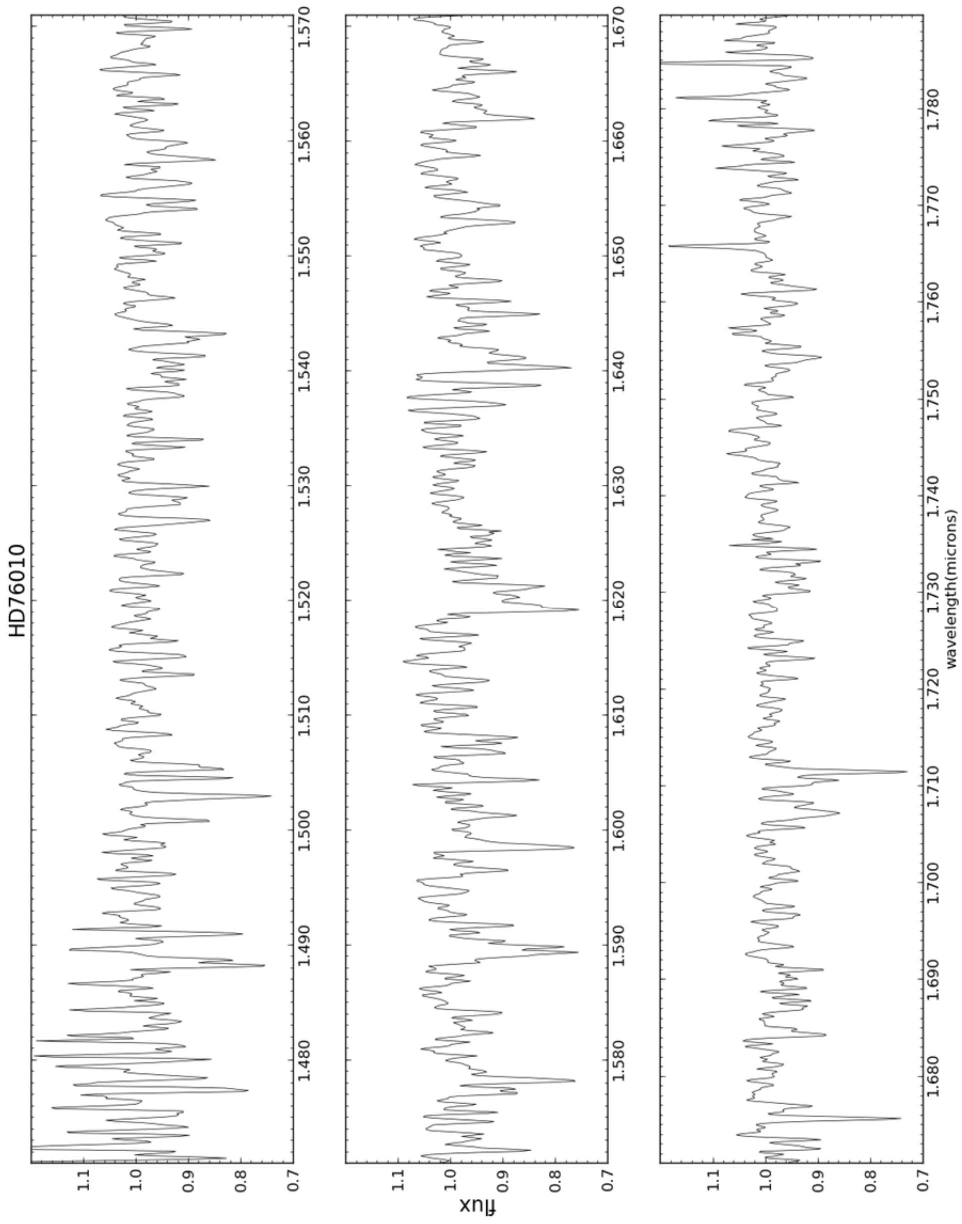

Figure 36. Template star HD76010(M0III)

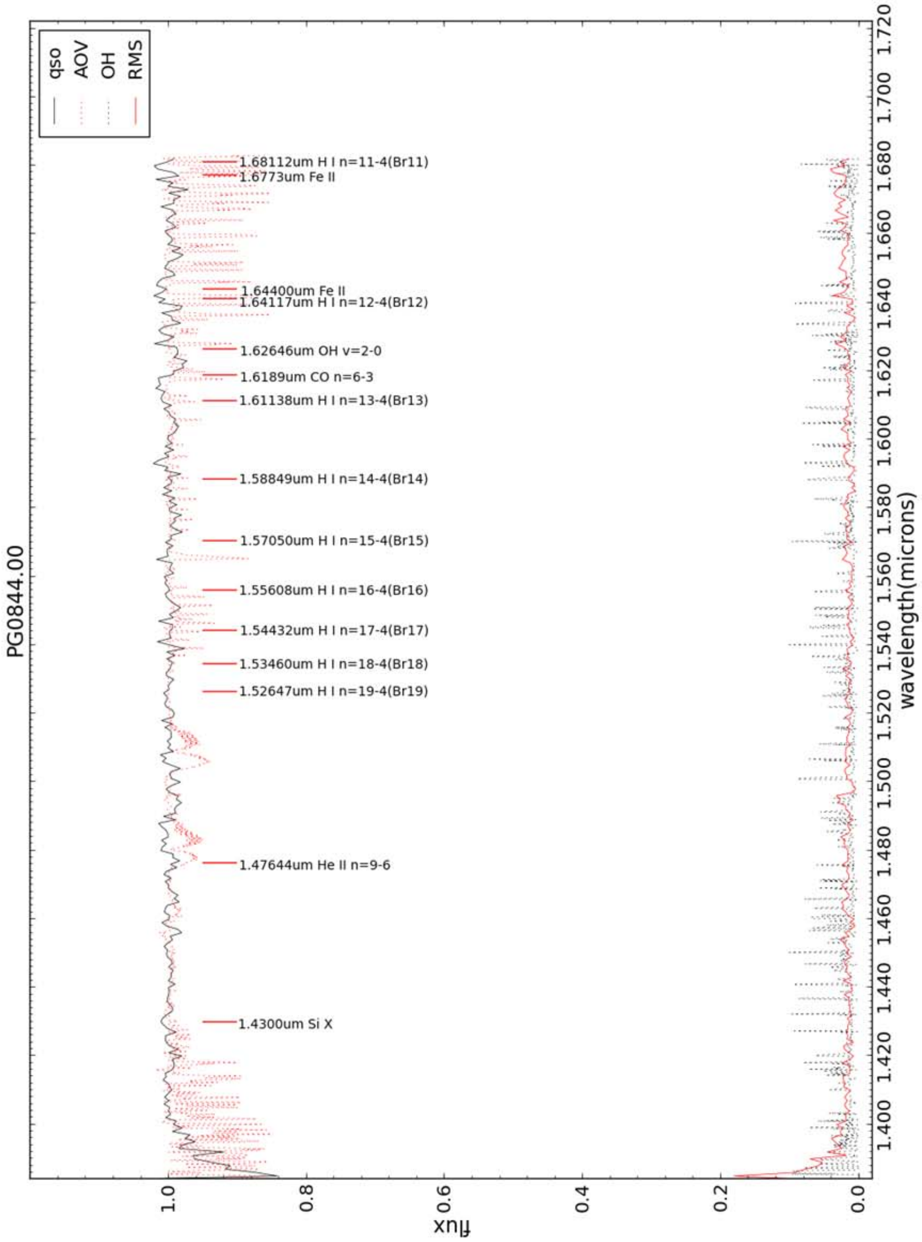

Figure 37. PG0844+349 (00 region)

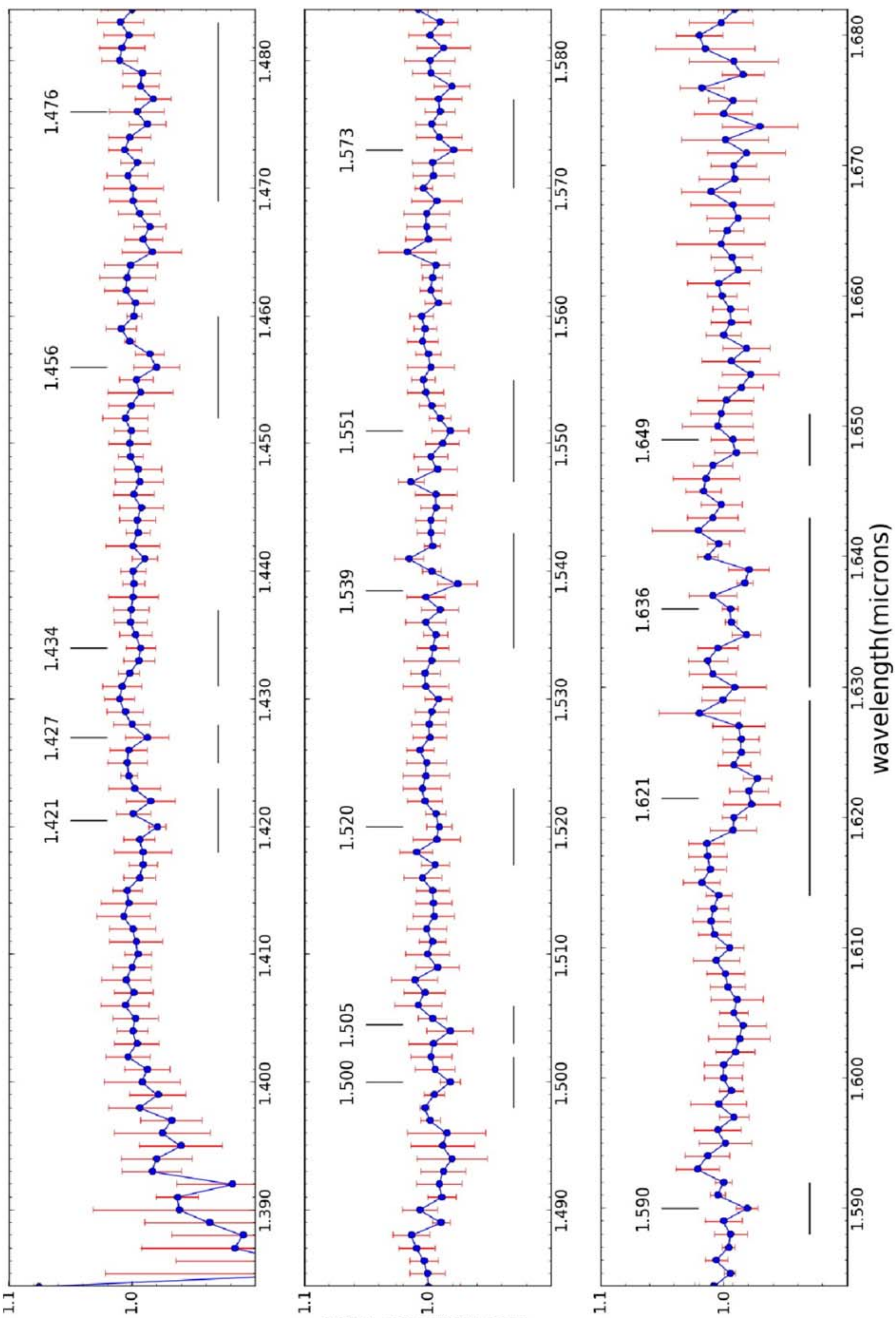

Figure 38. PG0844+349 (00 region)

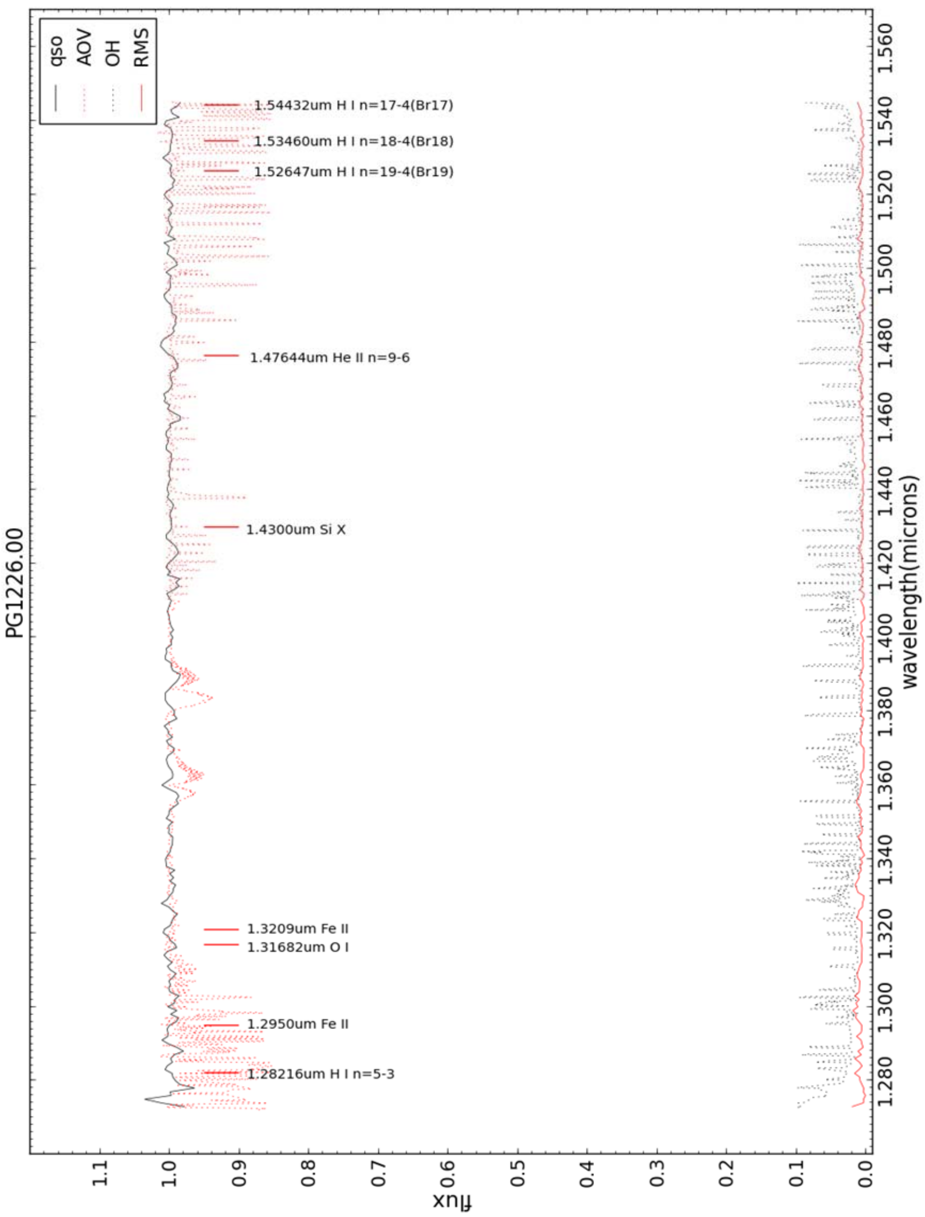

Figure 39. PG1226+023 (00 region)

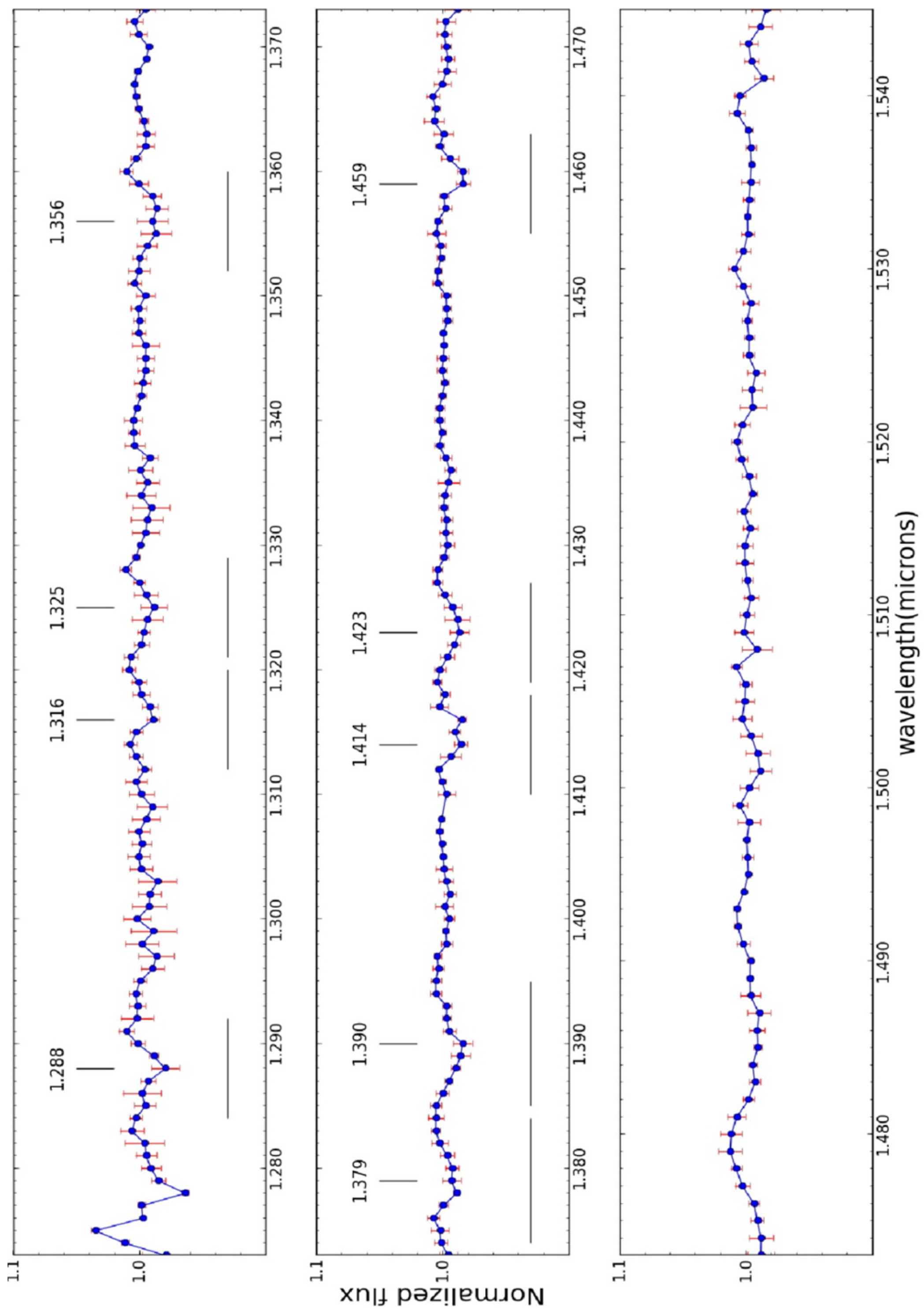

Figure 40. PG1226+023 (00 region)

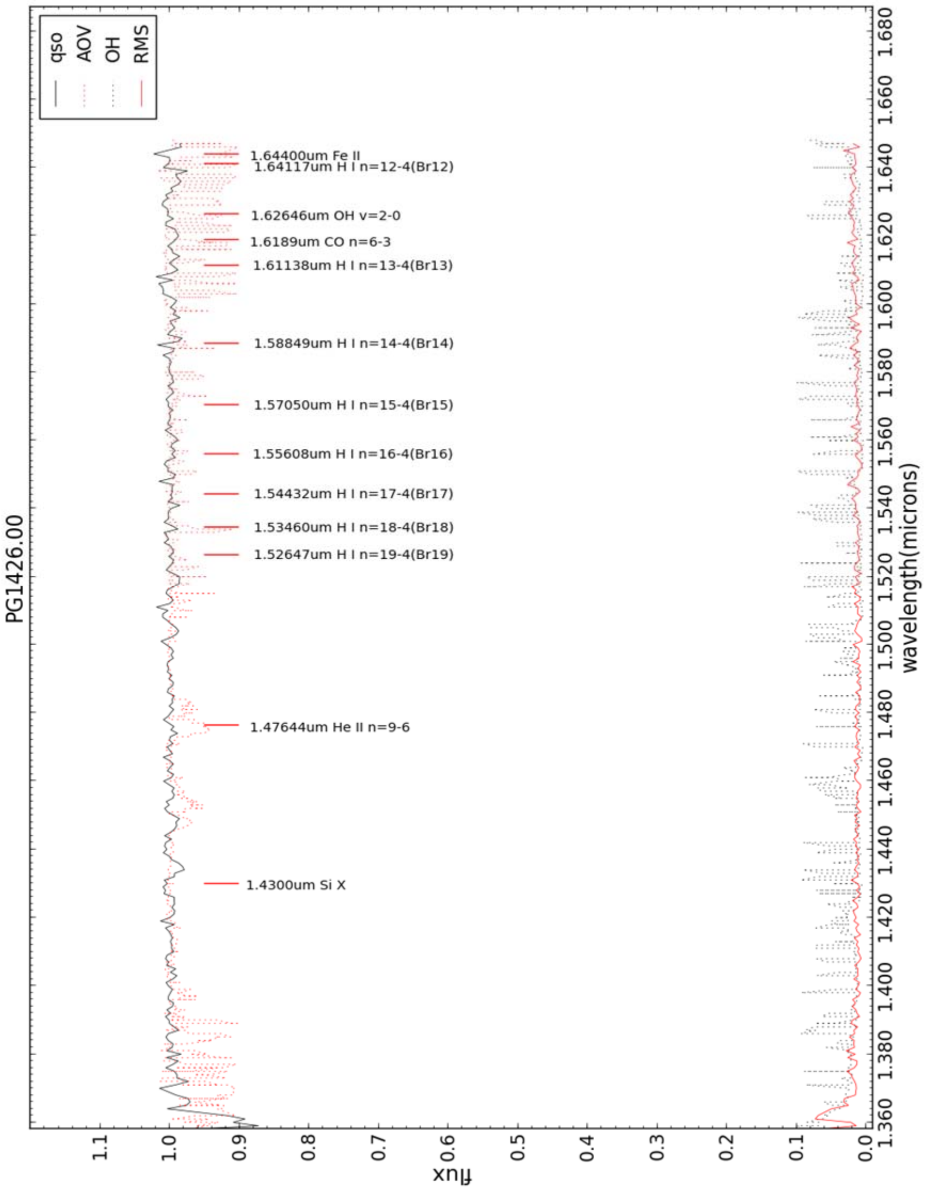

Figure 41. PG1426+015 (00 region)

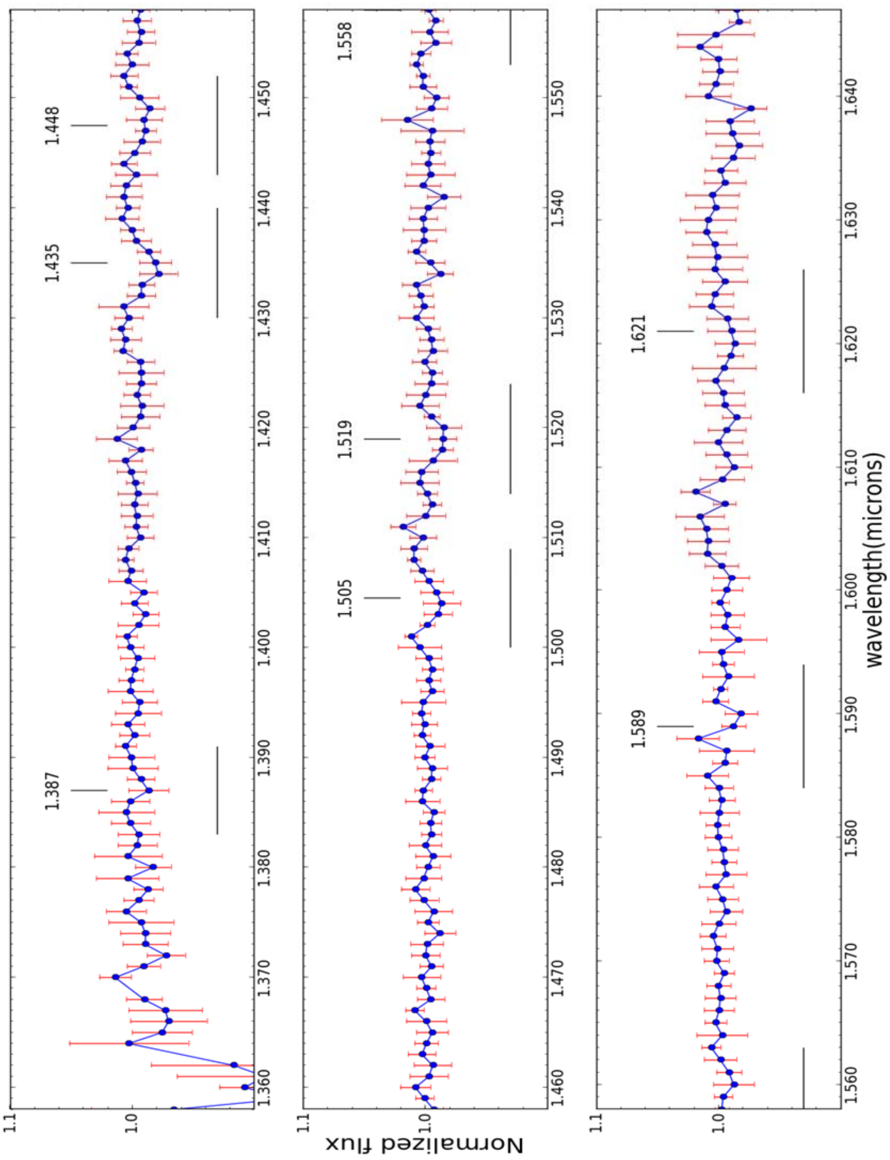

Figure 42. PG1426+015 (00 region)

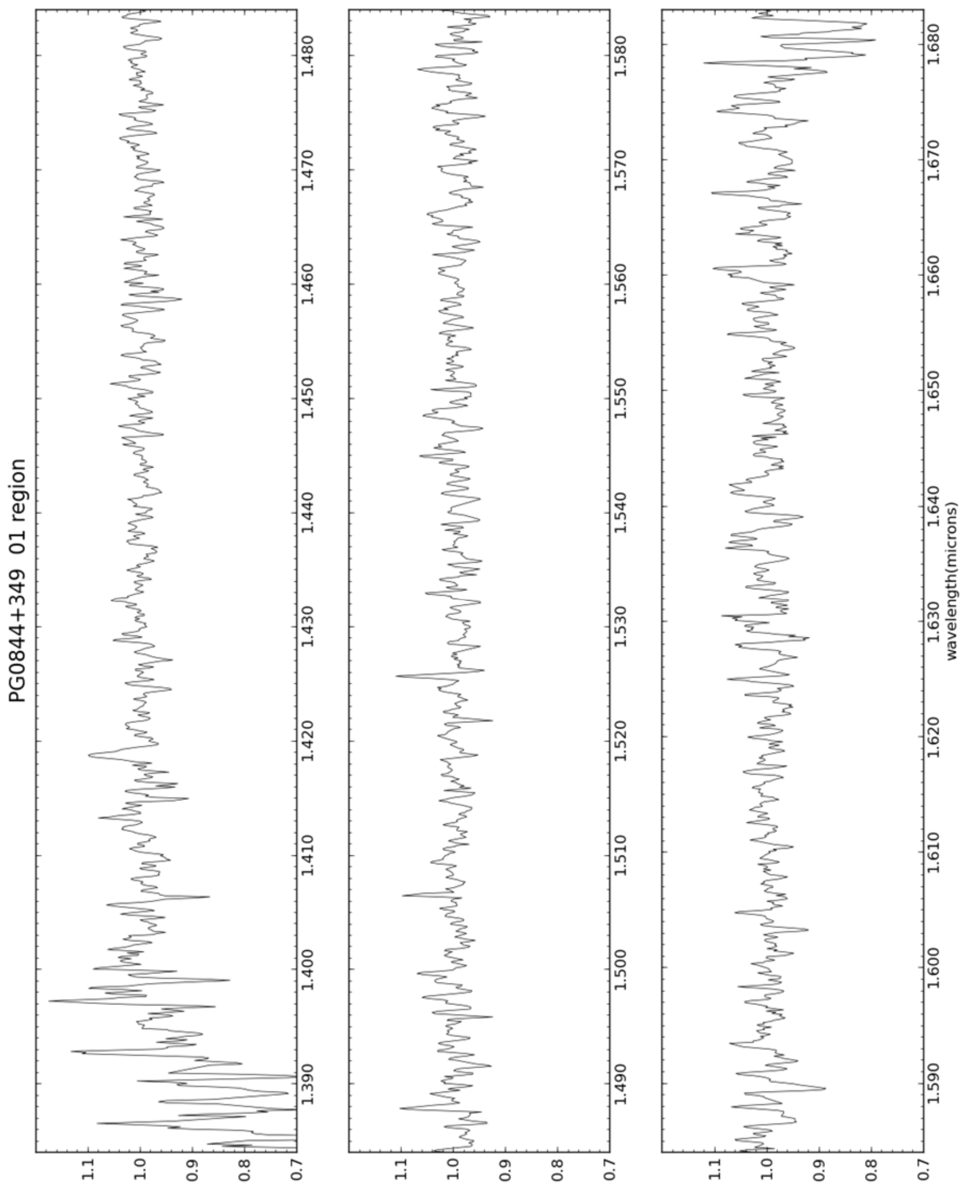

Figure 43. PG0844+349 (01 region)

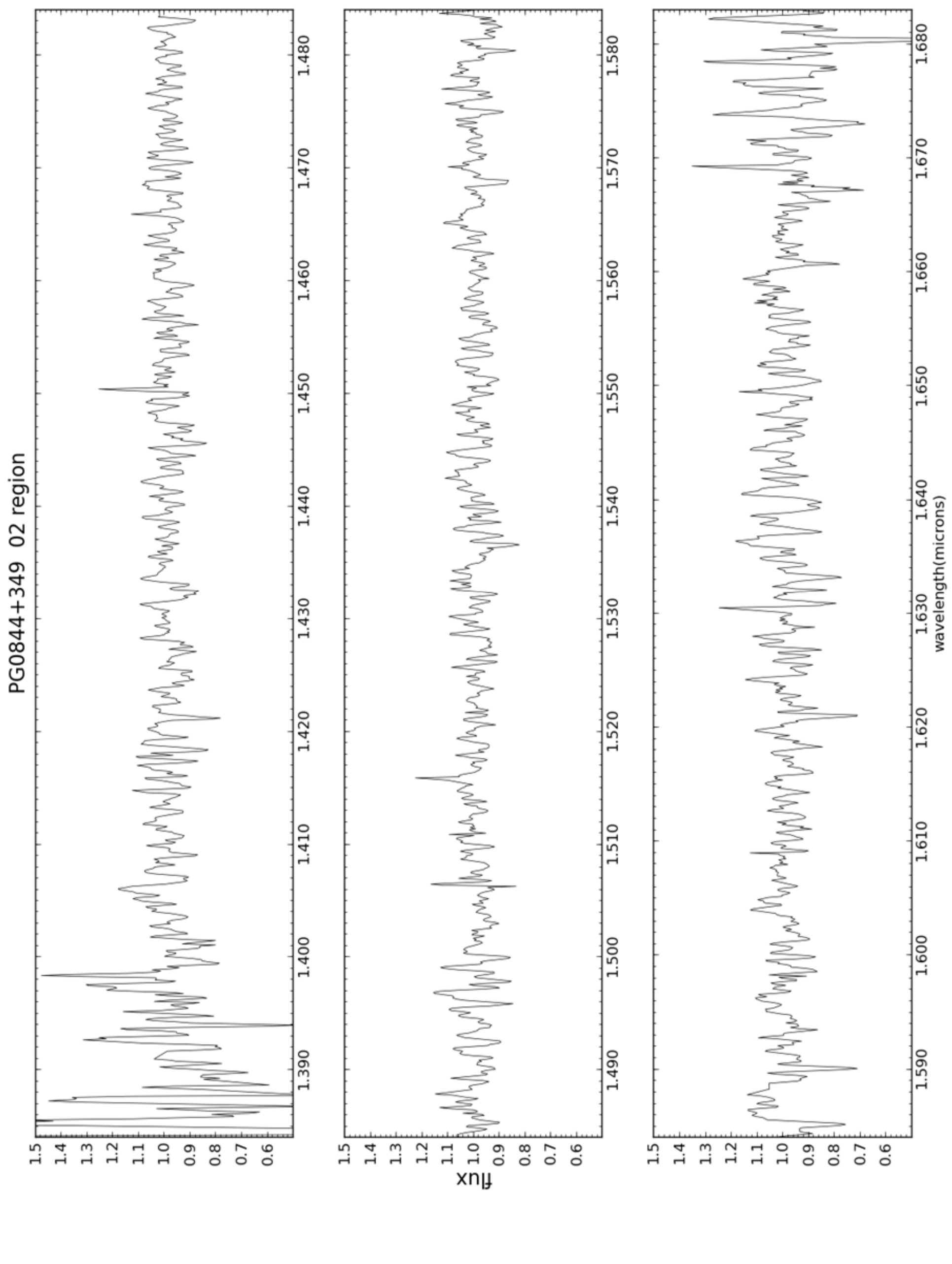

Figure 44. PG0844+349 (02 region)

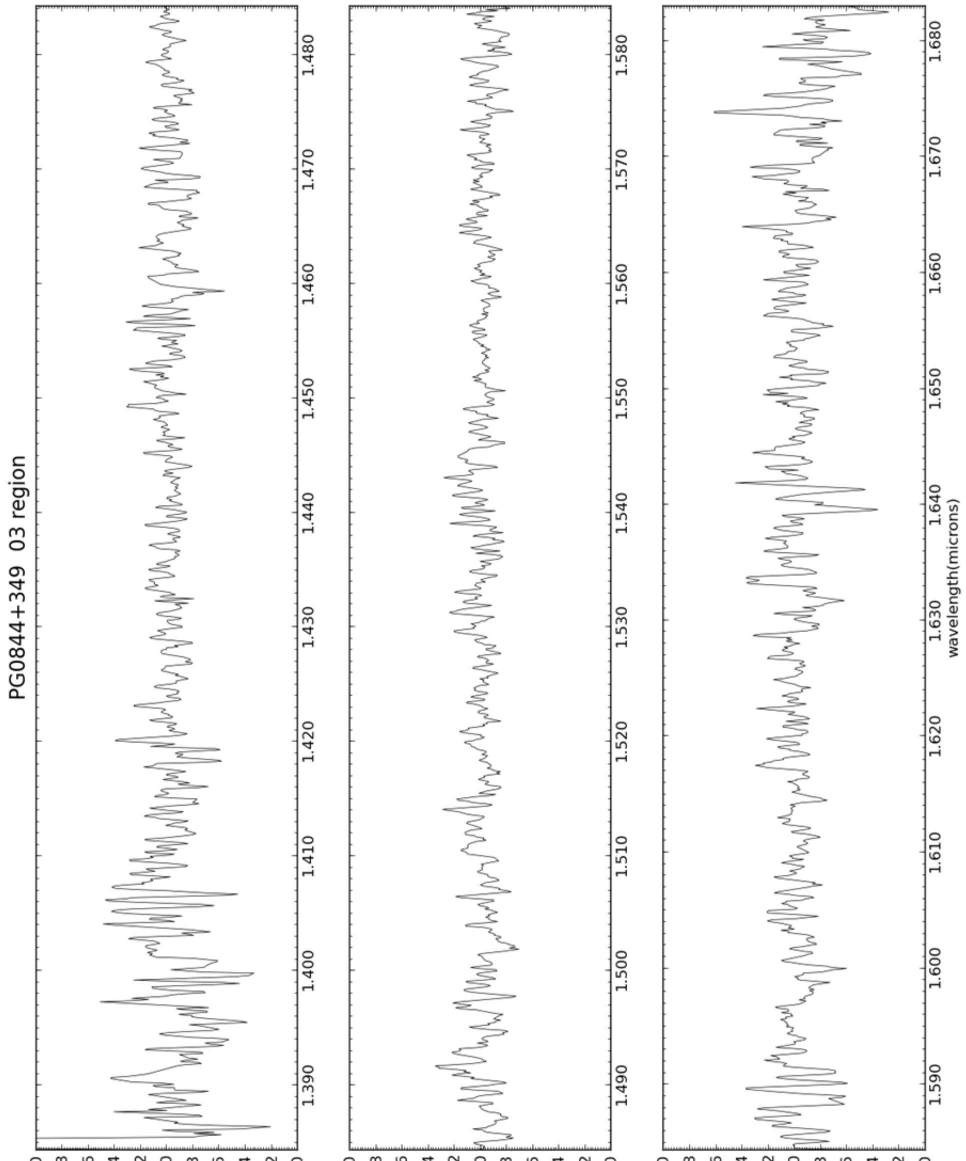

Figure 45. PG0844+349 (03 region)

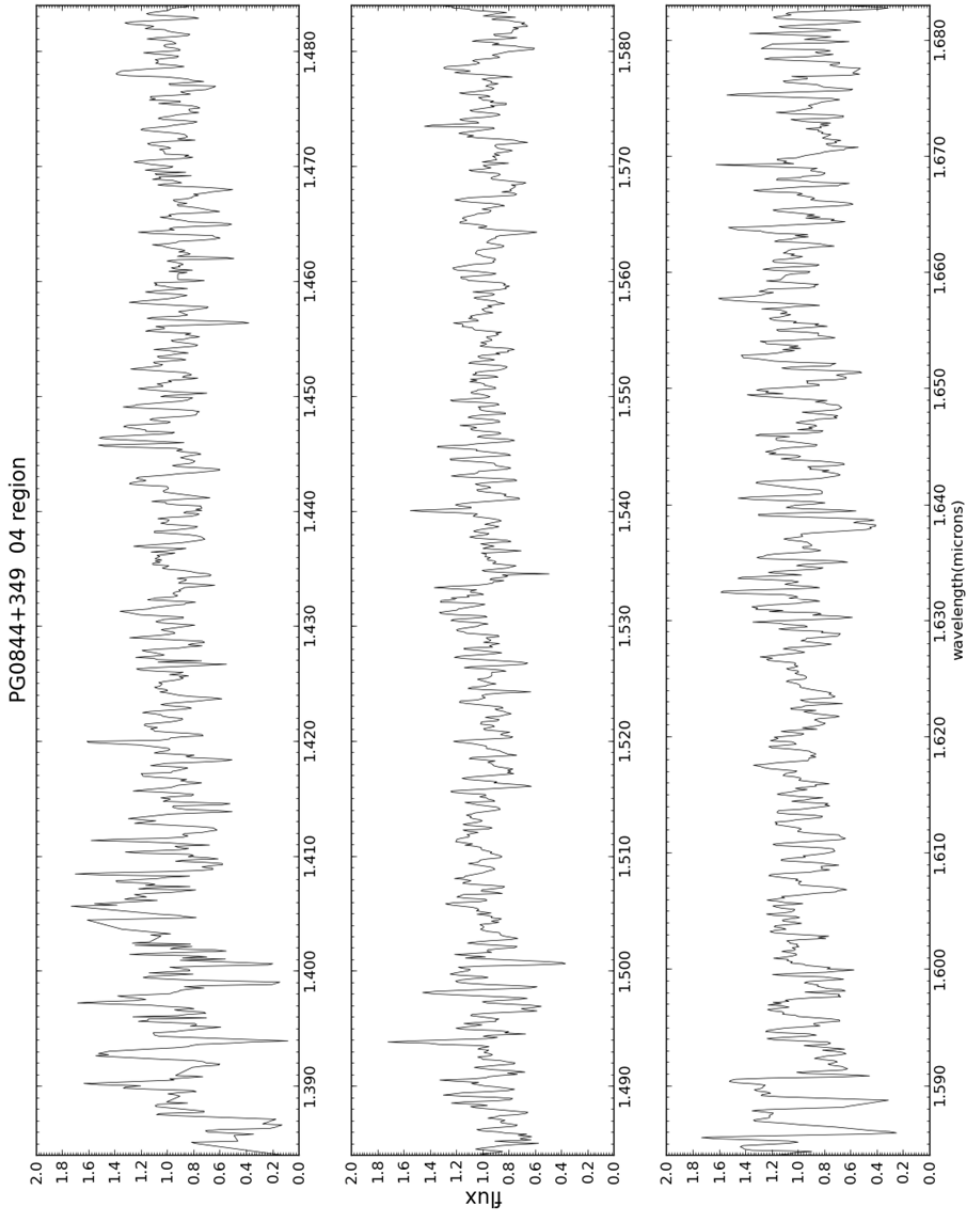

Figure 46. PG0844+349 (04 region)

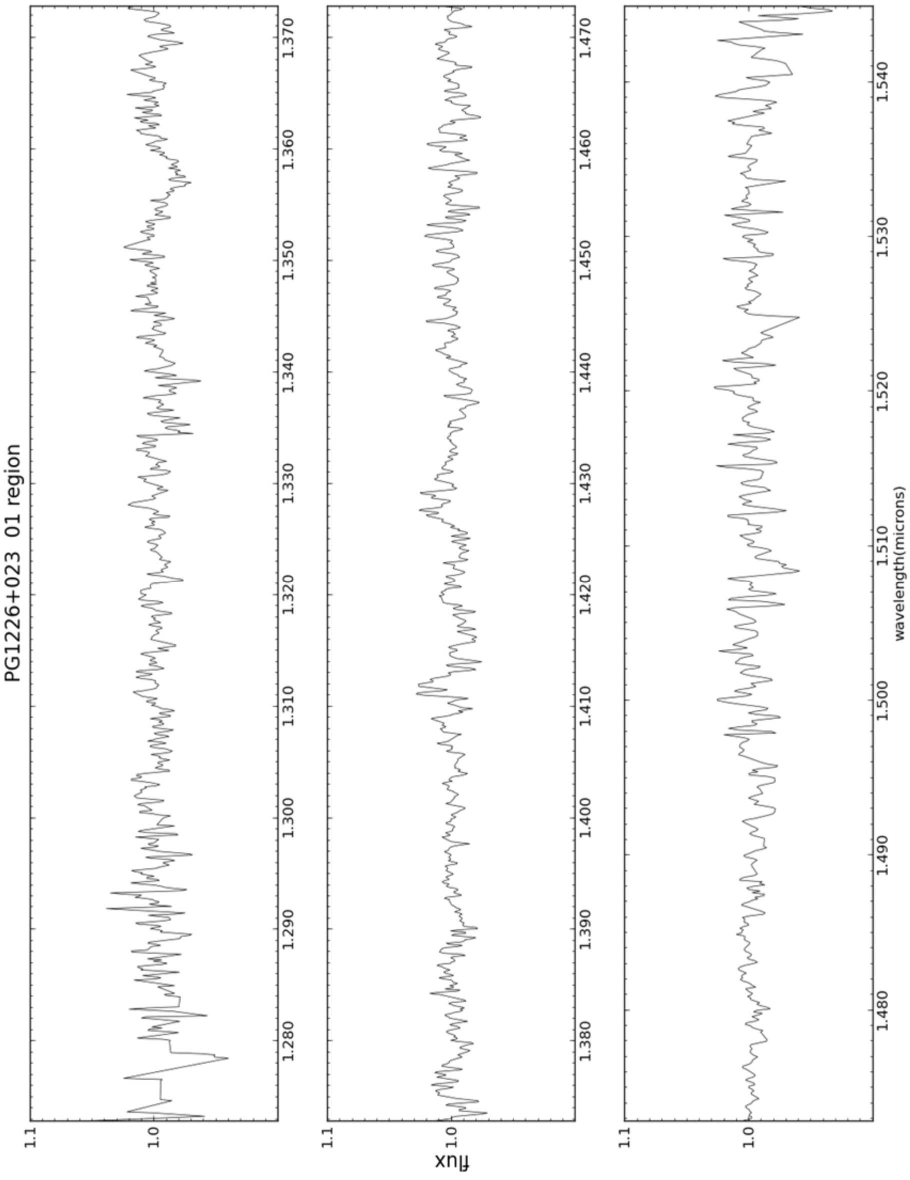

Figure 47. PG1226+026 (01 region)

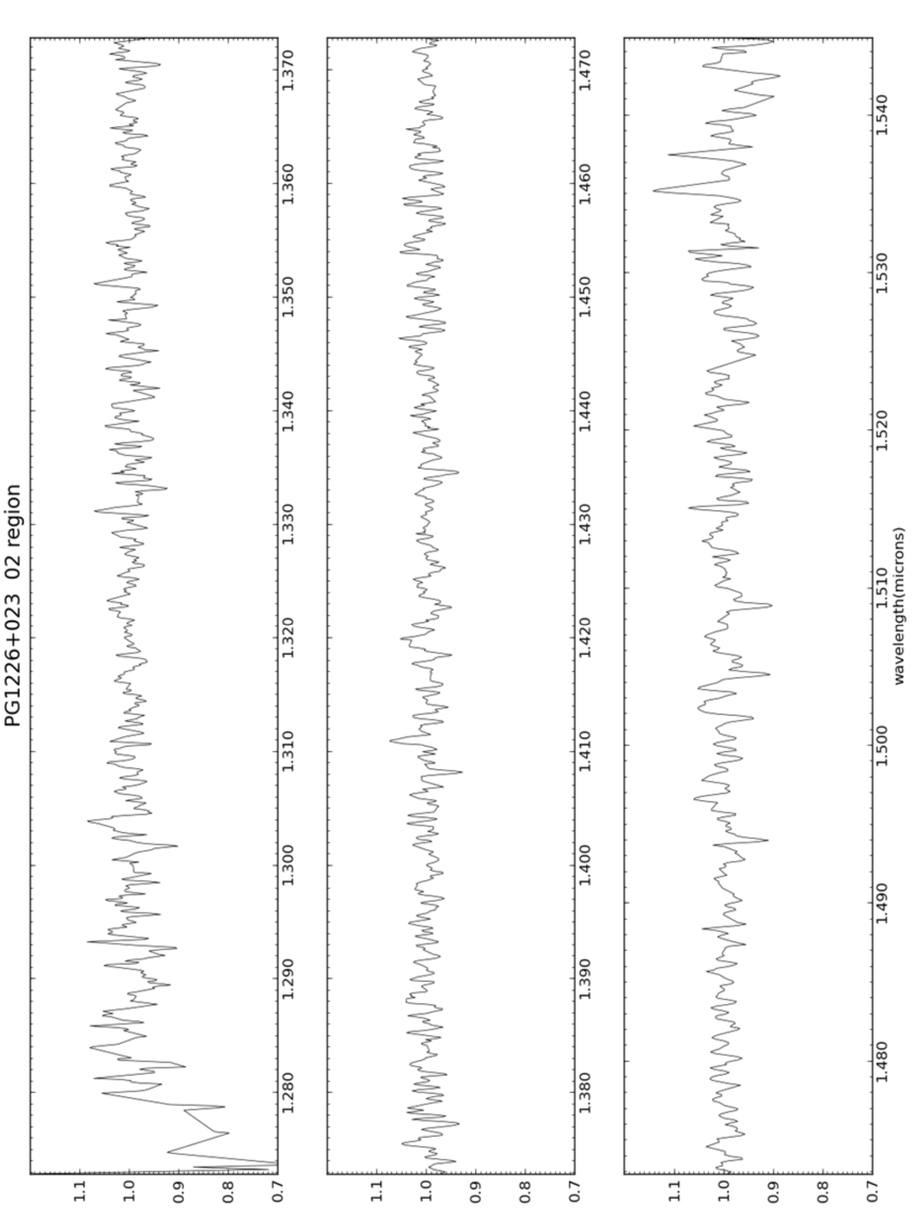

Figure 48. PG1226+026 (02 region)

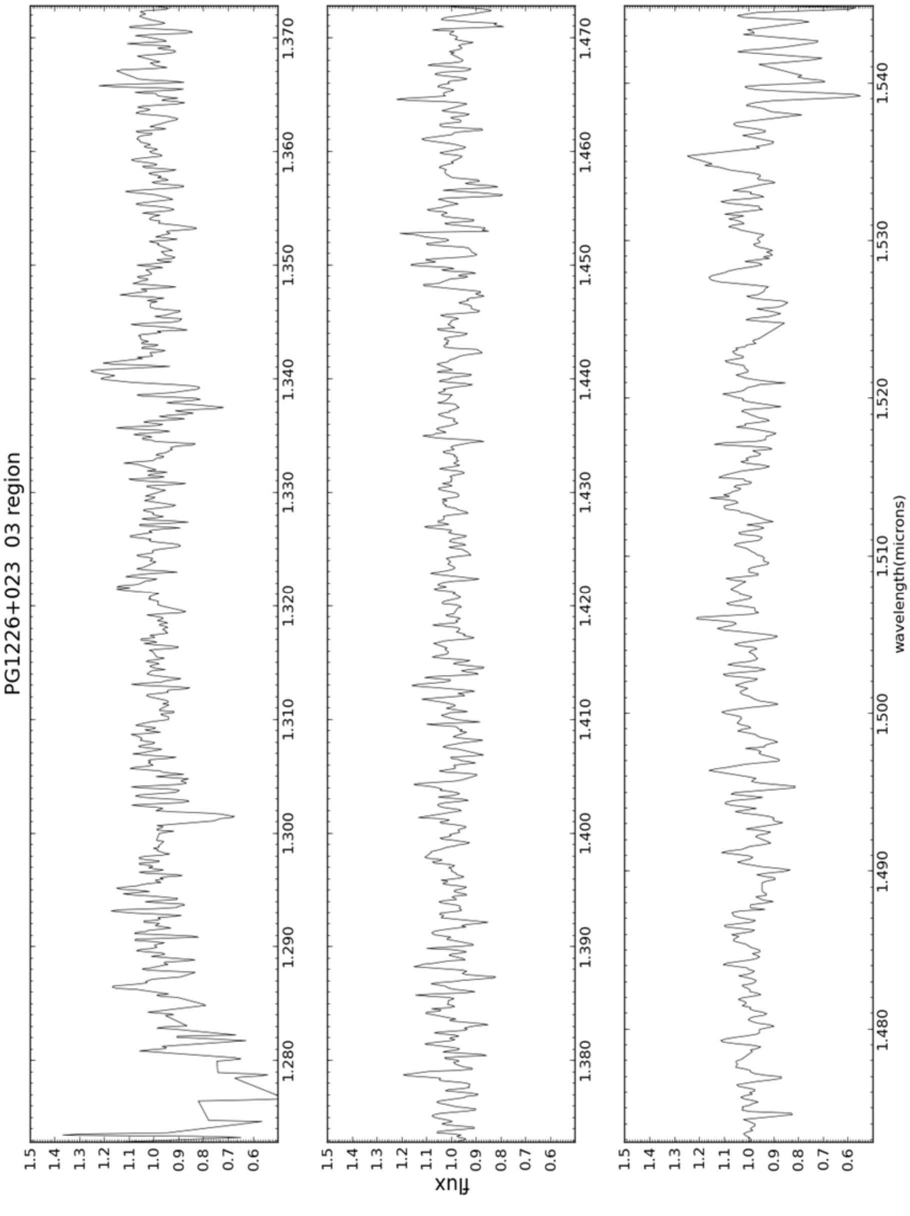

Figure 49. PG1226+026 (03 region)

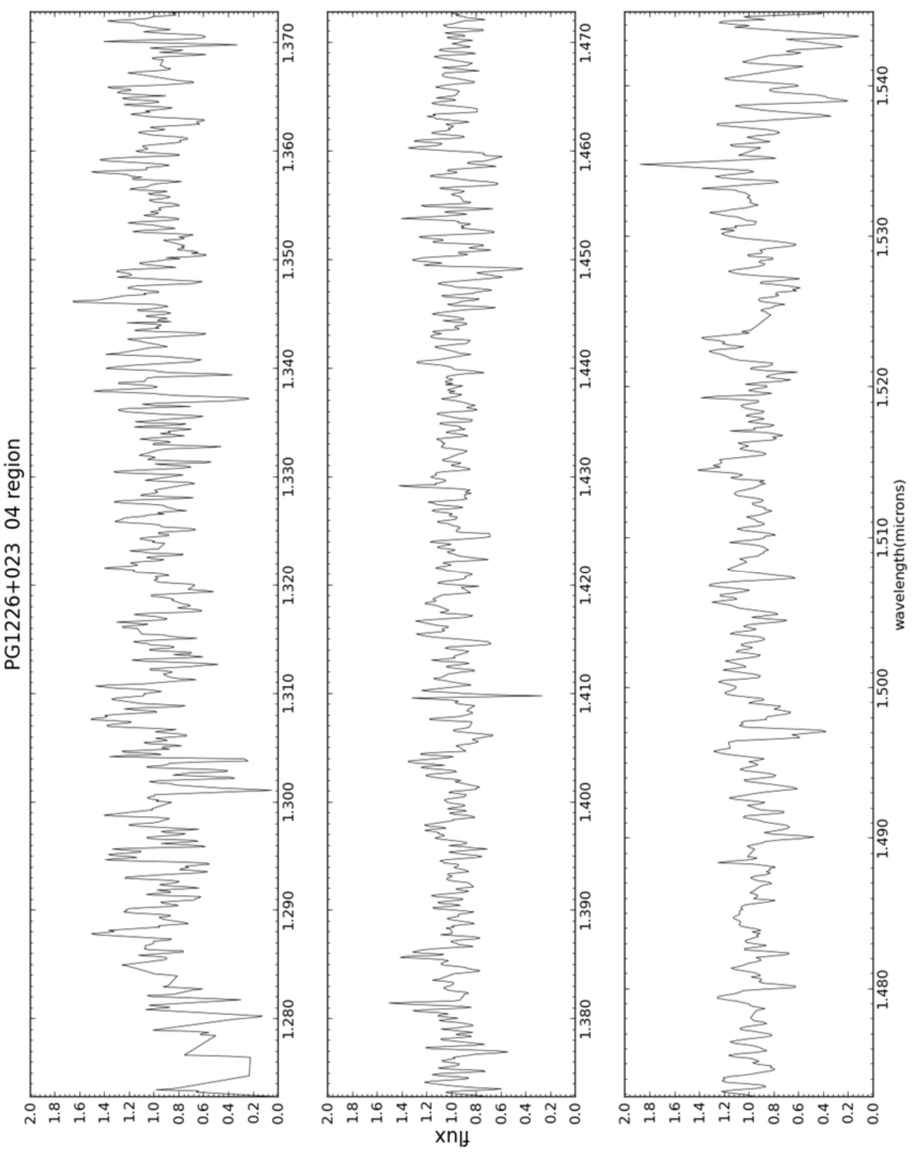

Figure 50. PG1226+026 (04 region)

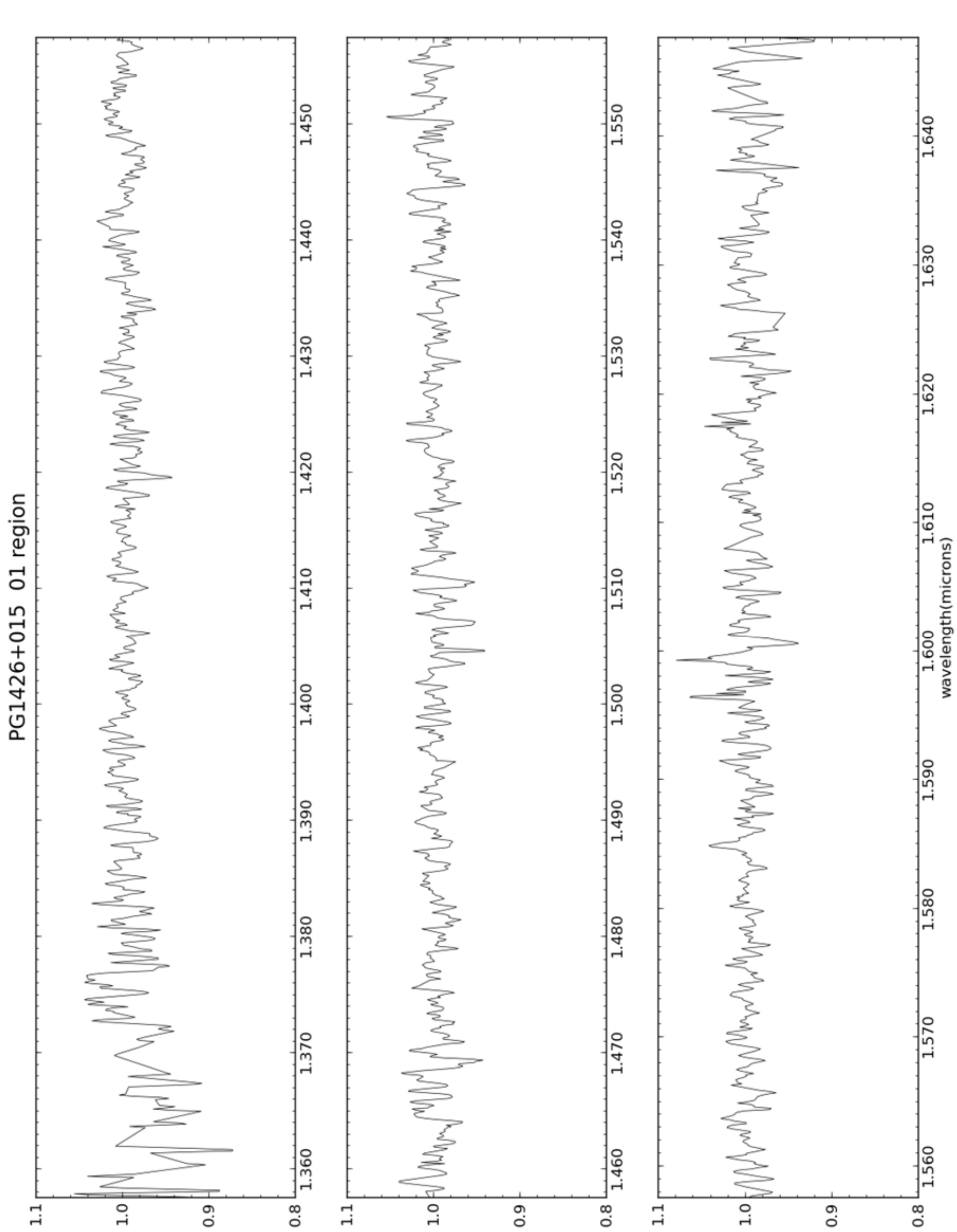

Figure 51. PG1426+015 (01 region)

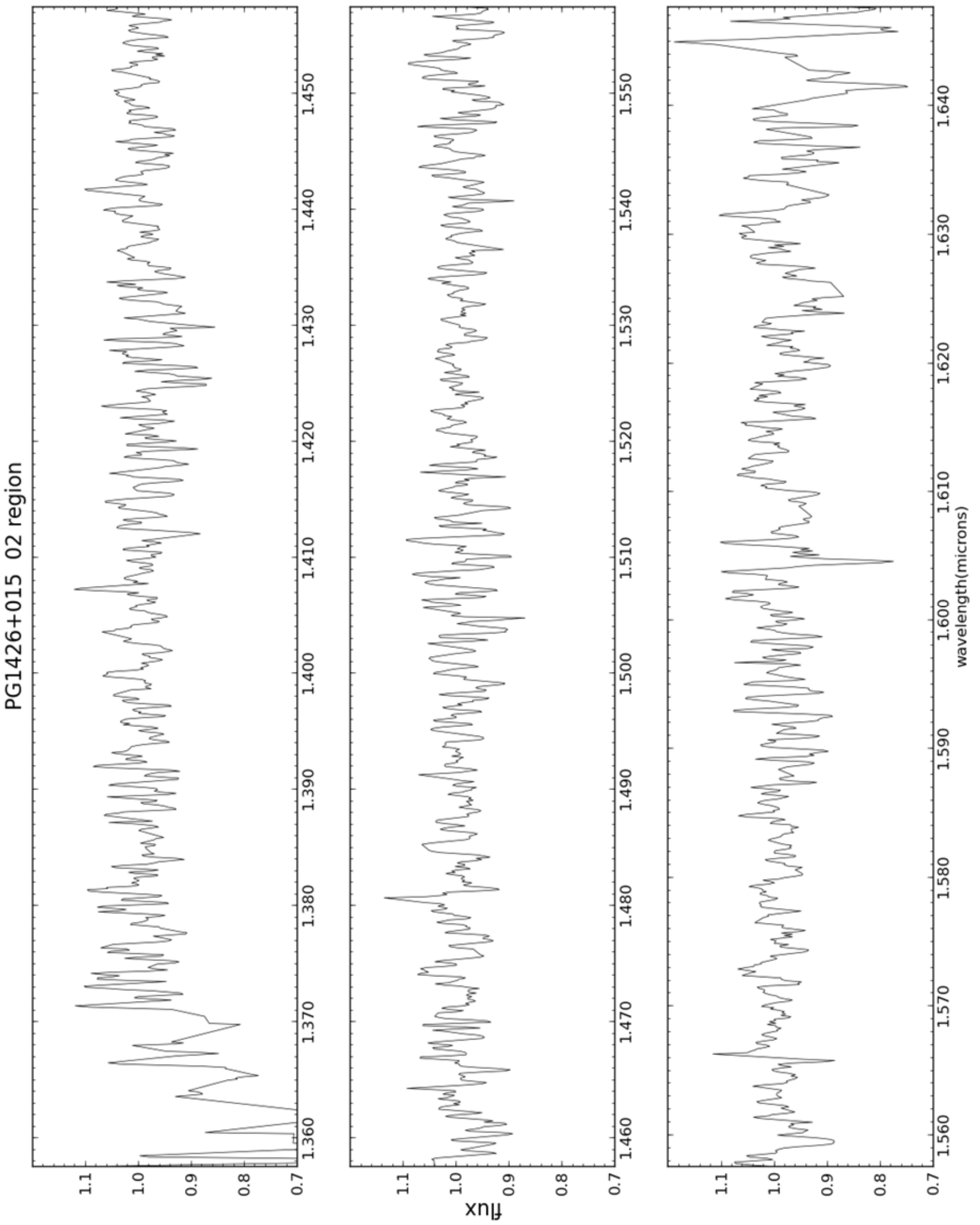

Figure 52. PG1426+015 (02 region)

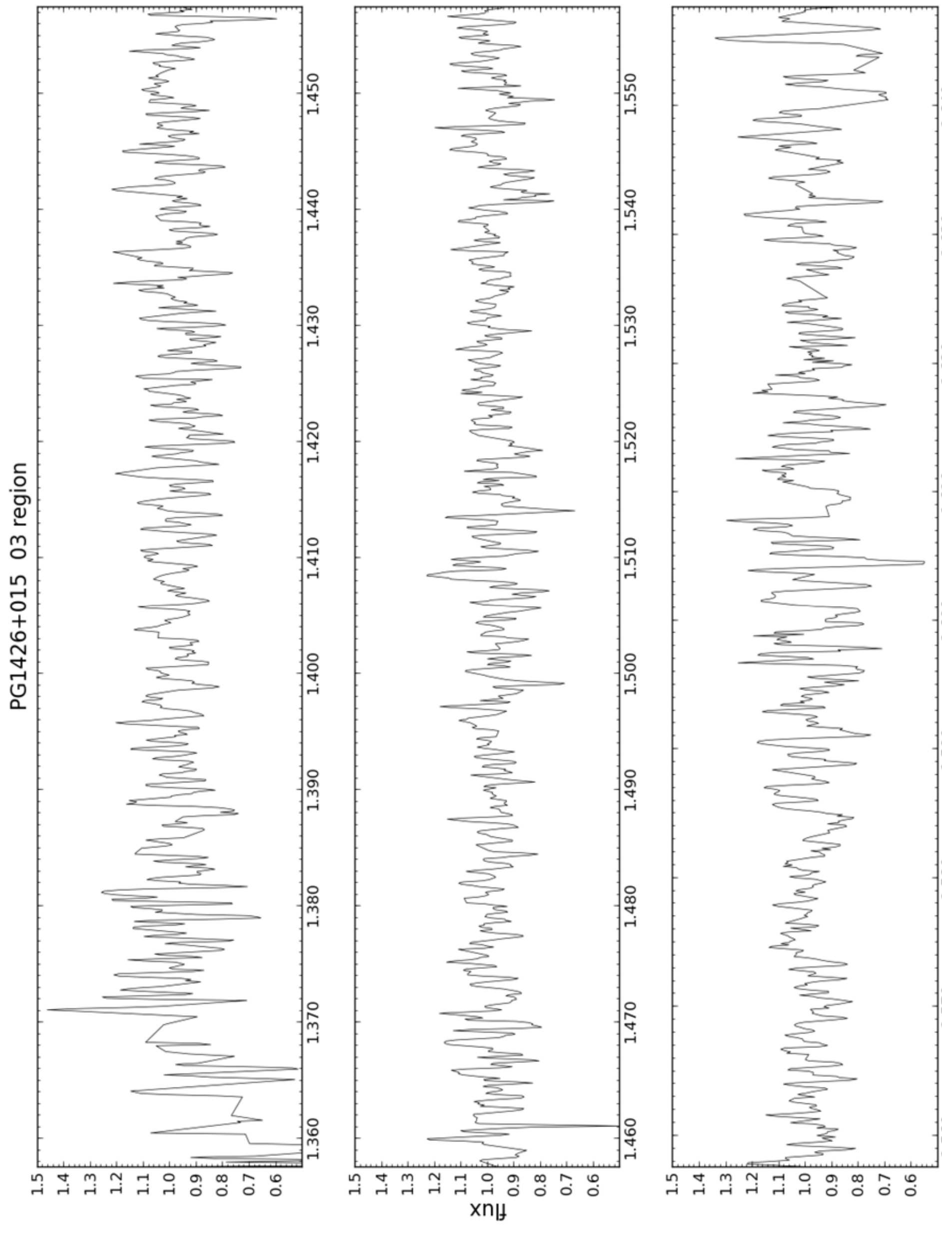

Figure 53. PG1426+015 (03 region)

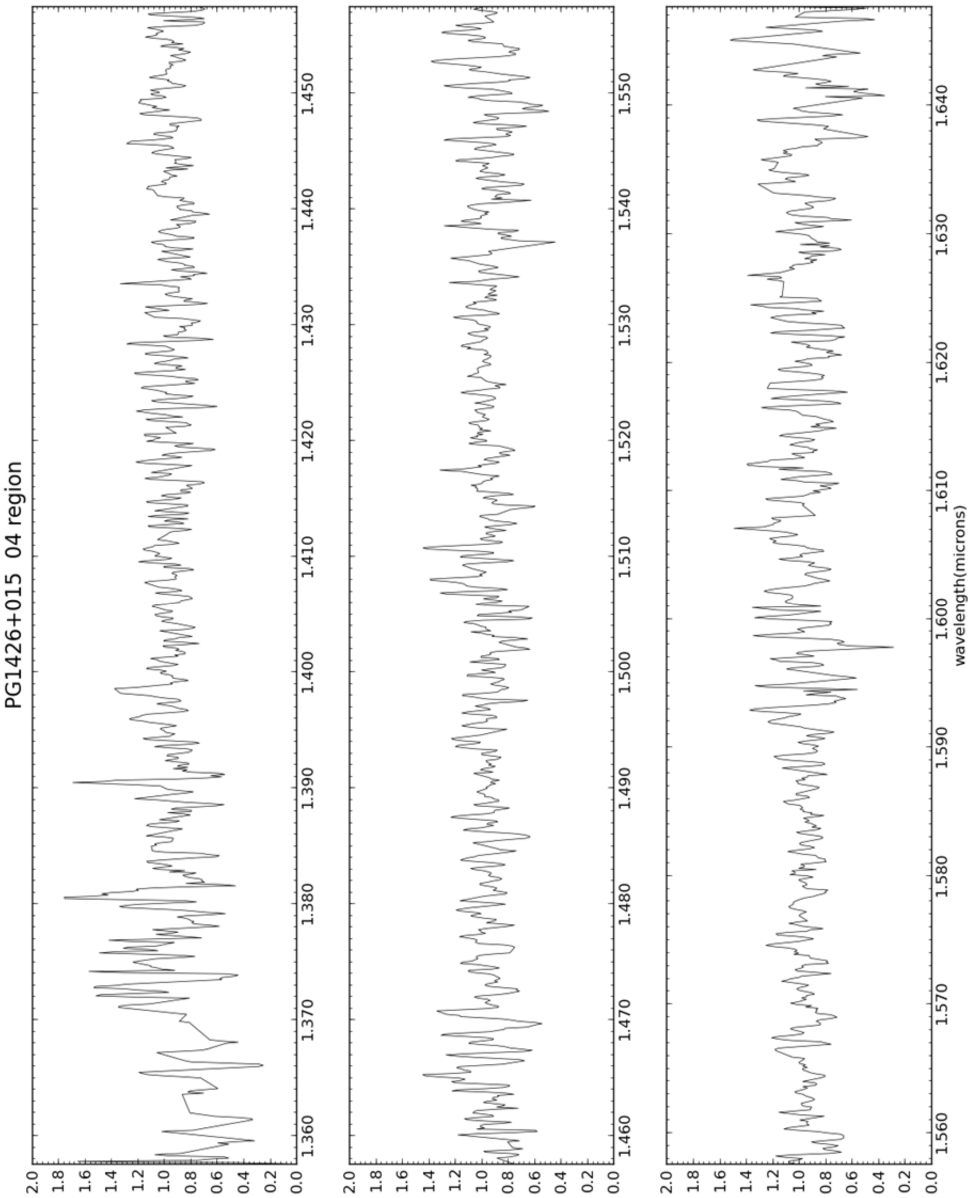

Figure 54. PG1426+015 (04 region)

5. DISCUSSION

5.1 Fitting PSF and host galaxy

Figure 28 shows the PSF profile of target which including the center region quasar, and the wing outer region host galaxy. The way to study the structure components of the galaxy is modeling it by using fitting functions. In this research, we try to fit the structure components of the target PG0844+349 by using Moffat, two Gaussians, exponential, and De Vaucouleurs function (Peng et al. 2011).

5.1.1 Exponential function

We use exponential as a basic function for fitting the wing outer region host galaxy of the target.

$$F = A_0 + A_1 \exp\left[-\left(\frac{|x - A_1|}{A_2}\right)\right]$$

In this, A_2 = Re / 1.678

By using the *optimize.leastsq* routine in Python, we try to fit the outer region of the target to find the best fit number for the outer wing. In the results of fitting, exponential is good for fitting the host galaxy. However, exponential function cannot fit for all the data including host galaxy in the outer region and quasar in the center. Figure 55 and 56 shows the plot of exponential function fitting for the outer wing region host galaxy, and quasar in the center region.

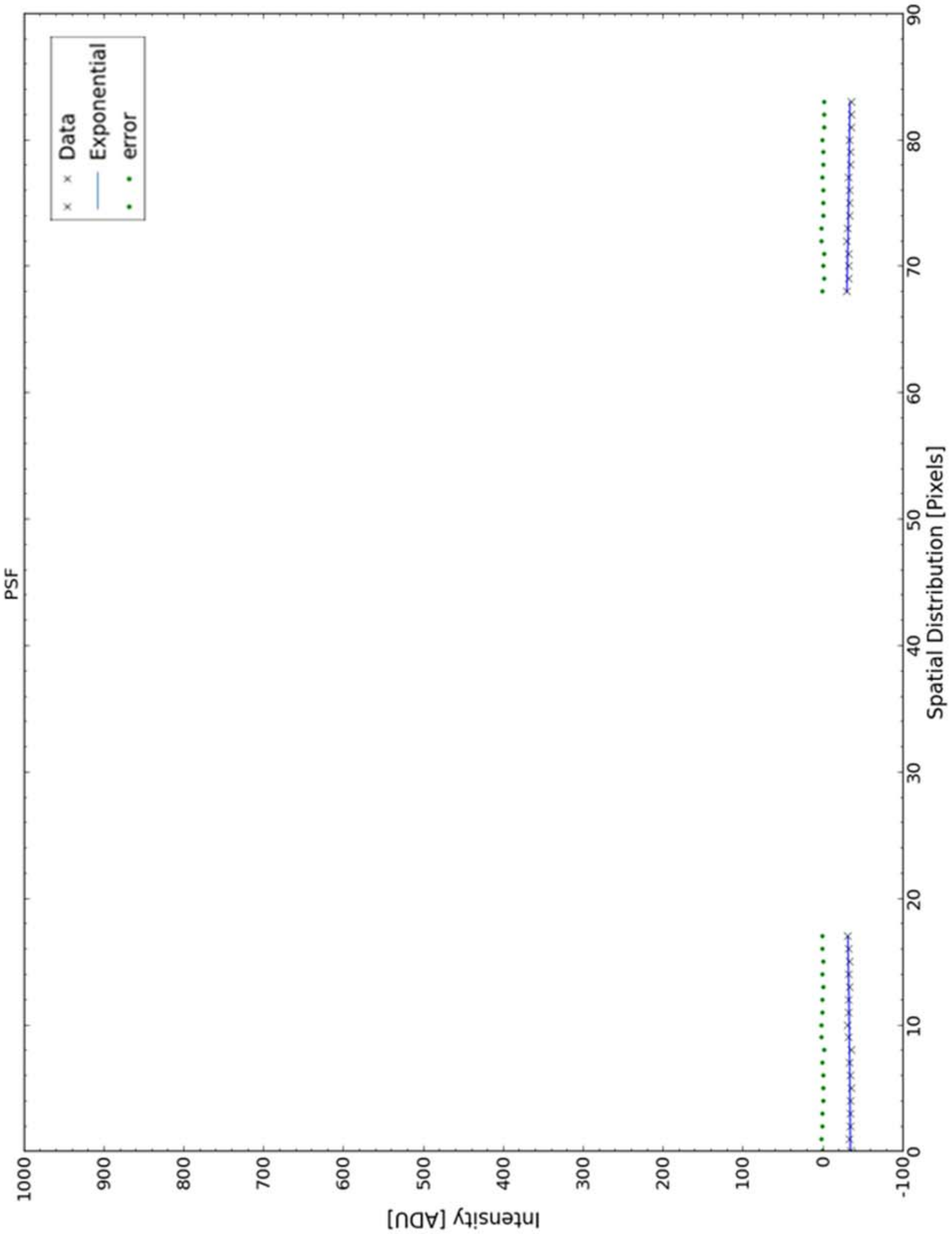

Figure 55. Exponential function fitting for host galaxy region.

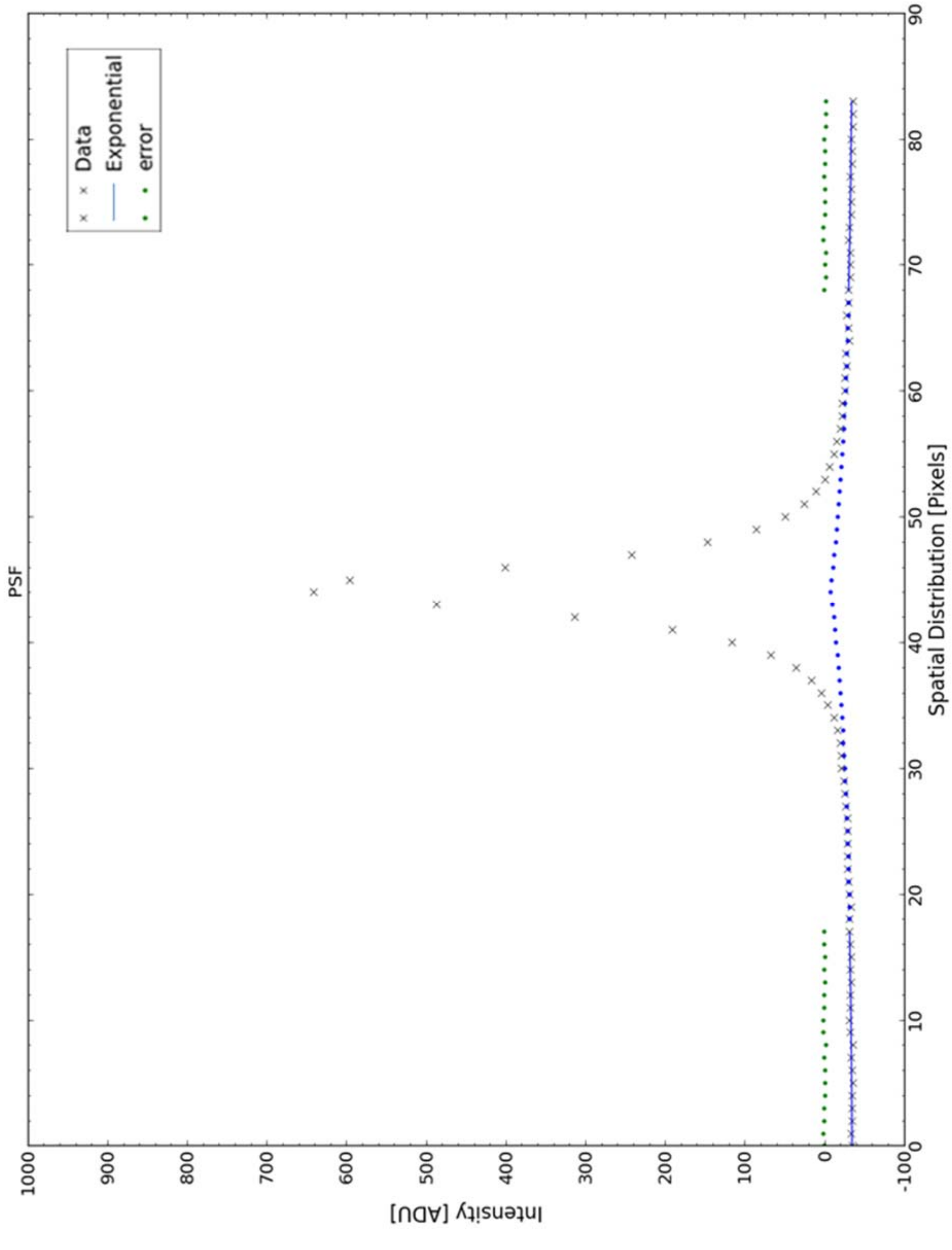

Figure 56. Exponential function fitting for all data.

5.1.2 De Vaucouleurs function

In 1948, De Vaucouleurs was the first person who showed that the light distribution from the elliptical galaxy follows a power law form De Vaucouleurs function

$$\Sigma(r) = \Sigma_e \, exp\left\{-7.67\left[\left(\frac{r}{r_e}\right)^{1/4} - 1\right]\right\}$$

In this formula, $\sum_e$ is the pixel surface brightness at the effective radius r_e

In this research, we use De Vaucouleurs function for fitting the wing outer part host galaxy profile. By using the *optimize.leastsq* routine in Python program, we estimate the fitting function for the host galaxy profile of the target PG0844+349. Figure 57 shows the plot fitting of De Vaucouleurs function for the outer region. In this research, De Vaucouleurs function is very good for fitting the outer region host galaxy, but for all of the regions, the function is cannot fit the data in the center. Figure 58 shows the plot of fitting all the regions of data by De Vaucouleurs function.

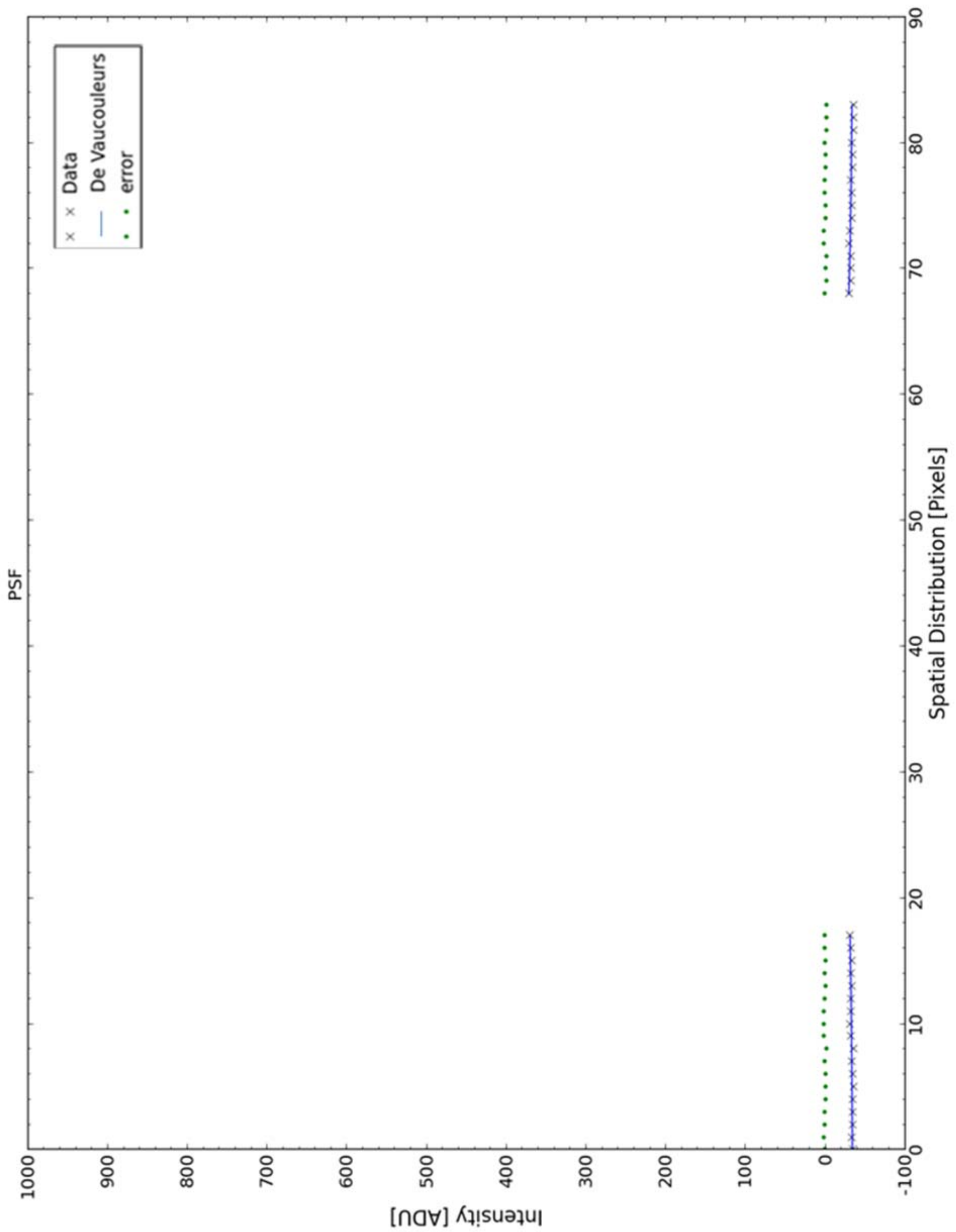

Figure 57. De Vaucouleurs function for host galaxy region.

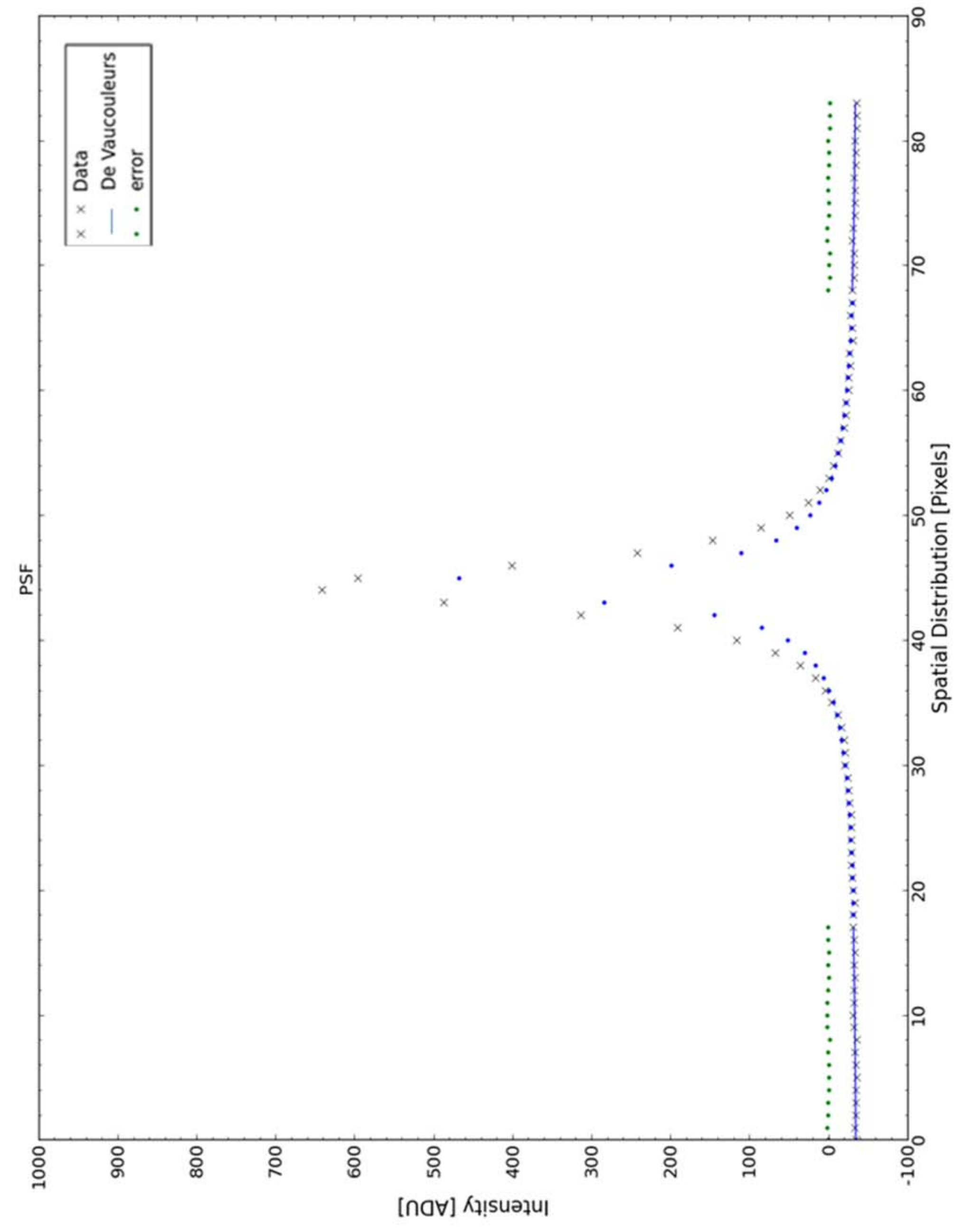

Figure 58. De Vaucouleurs function for all data.

5.1.3 Gaussian function

For fitting the center region of the target, we use a combine function including two Gaussian functions.

$$G = A_0 + A_1 \exp\left[-\frac{1}{2}\left(\frac{x-44.2602}{A_2}\right)^2\right] + A_3 \exp\left[-\frac{1}{2}\left(\frac{x-44.2602}{A_4}\right)^2\right]$$

In the formula,

A_0 is the offset parameter.

A_1 is the brightness papameter.

A_2 and A_4 are the parameters calculated from the effective radius Re.

In the research, for fitting the center region of the target, two Gaussian functions are very good for fitting the profile of quasar in the center region. Moreover, the two Gaussian functions are also very good for fitting all the data of the target including host galaxy and quasar. By using the *optimize.leastsq* routine in Python, we calculate the best fit parameters for fitting the quasar in the center region of the target. Figure 59 and 60 show the plot fitting by using two Gaussian functions.

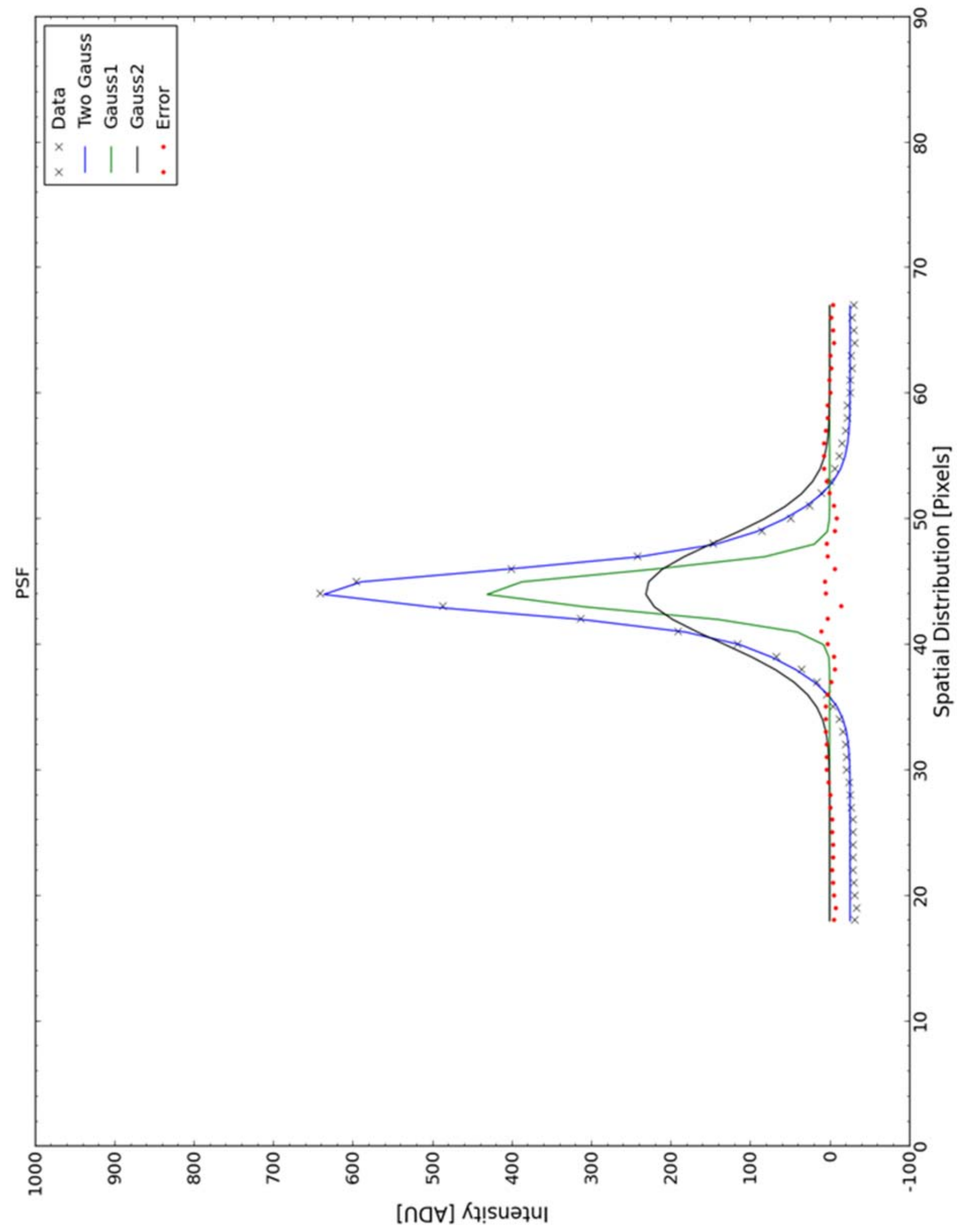

Figure 59. Two Gaussian functions for fitting quasar in the center region.

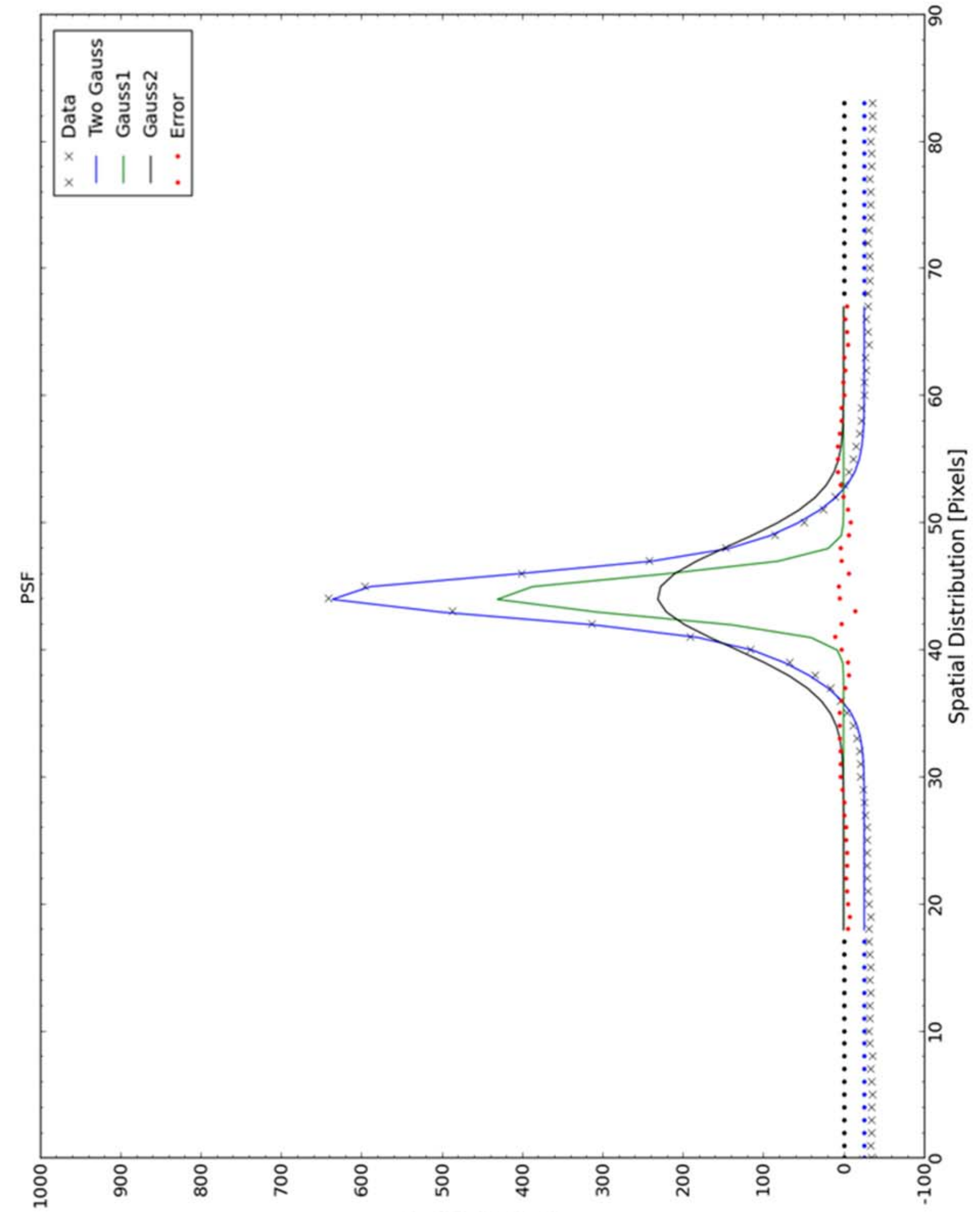

Figure 60. Two Gaussian functions fitting for all data.

5.1.4 Moffat function

In this research, we also try to use Moffat function for fitting the center region quasar of the target.

$$\sum(r) = \frac{\Sigma_0}{\left[1+(r/r_d)^2\right]^n}$$

In this formula, Σ_0 is the pixel surface brightness at the center region.

$$r_d = \frac{FWHM}{2\sqrt{2^{1/n}-1}} \qquad , n \text{ is index}$$

By using *optimize.leastsq* routine in Python, we estimate the function fitting for the center region quasar of the target PG0844+349. Figure 61 shows the plot fitting in the center region. Moreover, the Moffat function also can fit all the structure of the target including center and outer wing region. Figure 62 shows the plot fitting of Moffat function for all the data of target.

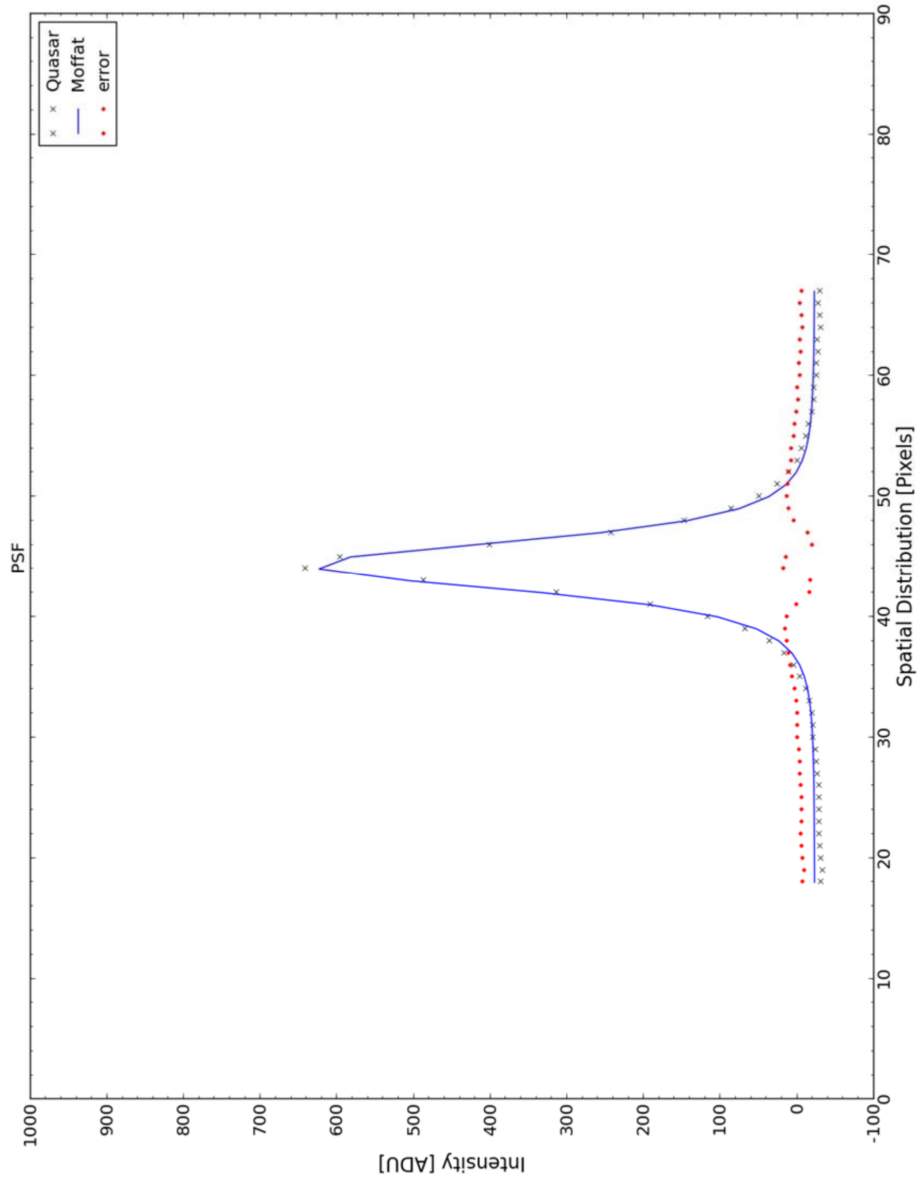

Figure 61. Fitting the center region by Moffat function

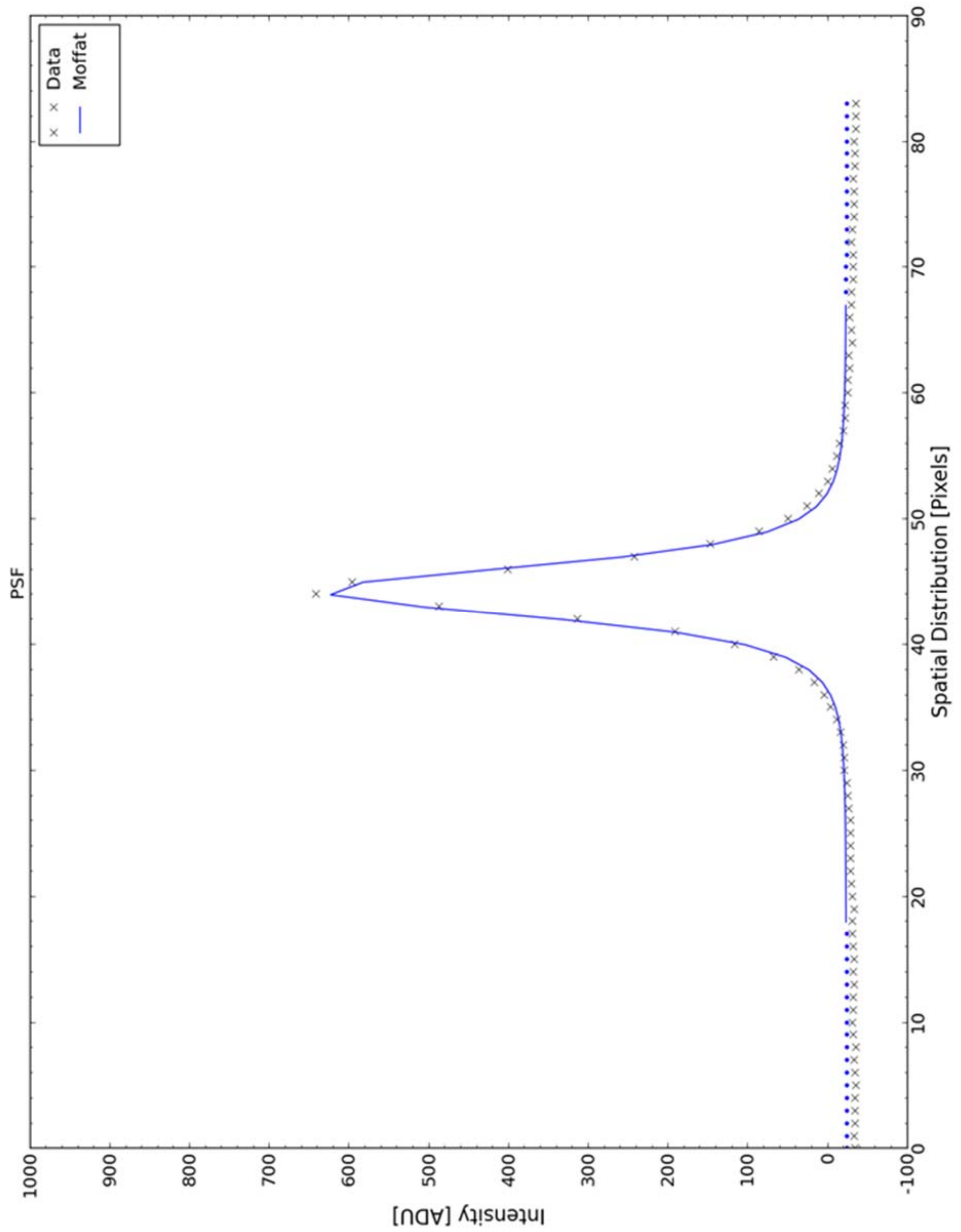

Figure 62. Fitting all the regions by Moffat function.

5.1.5 Summarize and model fitting functions

For estimate the model functions fitting for all components of the targets, we try many basic function for calculate the best fit parameters by using *optimize.leastsq* routine in Python. We use the each function to fitting each region first to calculate the best fit parameters, and then use these parameters to calculate the fitting numbers when we use the functions together for fitting all the data of the target.

The general function which we use to fitting the profile of the target is

$$F = (\text{Offset}) + (\text{Host galaxy}) + (\text{Quasar})$$

Then, we have the general function as follow

$$F = A_0 + \left[\begin{array}{l} \text{Exponential Function} \\ \\ \text{Dev Vaucouleurs Function} \end{array} \right. + \left[\begin{array}{l} \text{Two Gaussian Functions} \\ \\ \text{Moffat Function} \end{array} \right.$$

The detail functions are writing as

$$F = A_0 + \left[\begin{array}{l} A_1 \exp\left[-\left(\dfrac{|x-x_0|}{A_2}\right)\right] \\ \\ A_1 \exp\left[-7.67\left(\left(\dfrac{|x-x_0|}{A_2}\right)^{1/4} - 1\right)\right] \end{array} \right. + \left[\begin{array}{l} A_3 \exp\left[-\dfrac{1}{2}\left(\dfrac{x-x_0}{A_4}\right)^2\right] + A_5 \exp\left[-\dfrac{1}{2}\left(\dfrac{x-x_0}{A_6}\right)^2\right] \\ \\ A_3 \dfrac{1}{\left[1+\left(\dfrac{x-x_0}{A_4}\right)^2\right]^2} \end{array} \right.$$

From the general function, offset A_0 is the background need to be corrected of the target. For the outer wing region, we use Exponential or De Vaucouleurs function for fitting. And, the center region, we try to use two Gaussian functions or Moffat function to fitting. Table 5 shows the table fitting numbers in each case which using each function together (yellow color is constants). Figure 63 to 68 show the plot fitting by using each case of functions in log scale for y axis and arcsec for x axis.

In each case of functions for fitting, the best fitting can be done by the model function of exponential combine with two Gaussian functions. From the model fitting, we can see that the quasar's spectrum is mostly from the quasar in the center region of the target, and the emission from the host galaxy in quasar's spectrum is only about 7.3%.

Table 5. Fitting parameters of using each case functions.

	Function		Offset		Host Galaxy				Quasars							
	Host Galaxies	Quasars	A0		A1		A2		A3		A4		A5		A6	
			Initial	Best fit	Initial	Best fit	Initial	Best fit	Initial	Best fit	Initial	Best fit	Initial	Best fit	Initial	Best fit
1.1	Exponential		-36.00	**-36.35**	15.00	**29.11**	14.80									
1.2	De Vaucouleurs		-36.00	**-36.50**	5.000	**5.694**	24.83									
1.3		Two Gaussians	-30.00	**-25.79**					640.0	**437.5**	2.000	**2.115**	80.00	**231.6**	6.300	**5.658**
1.4		Moffat	-30.00	**-23.99**					675.0	**652.9**	4.200	**3.782**				
2.1	Exponential	Two Gaussians	-36.00	**-38.83**	29.00	**46.55**	14.80		437.5	**376.2**	2.115	**1.949**	231.6	**264.9**	5.658	**4.720**
2.2	Exponential	Moffat	-36.00	**-32.76**	29.11	**189.7**	14.80	**4.464**	675.0	**504.6**	4.200	**3.288**				
3.1	De Vaucouleurs	Two Gaussians	-36.00	**-53.83**	5.693	**0.100**	24.83	**3749**	376.2	**373.0**	1.949	**2.105**	264.5	**226.6**	4.720	**4.993**
3.2.1	De Vaucouleurs	Moffat	-36.50		5.694		24.83		652.9		3.782					
3.2.2	De Vaucouleurs	Moffat	-36.50		5.694		24.83		675.0	**77.45**	4.200	**8.632**				
3.2.3	De Vaucouleurs	Moffat	-36.50	**-46.69**	5.694	**0.173**	24.83	**880.2**	675.0	**564.8**	4.200	**3.722**				

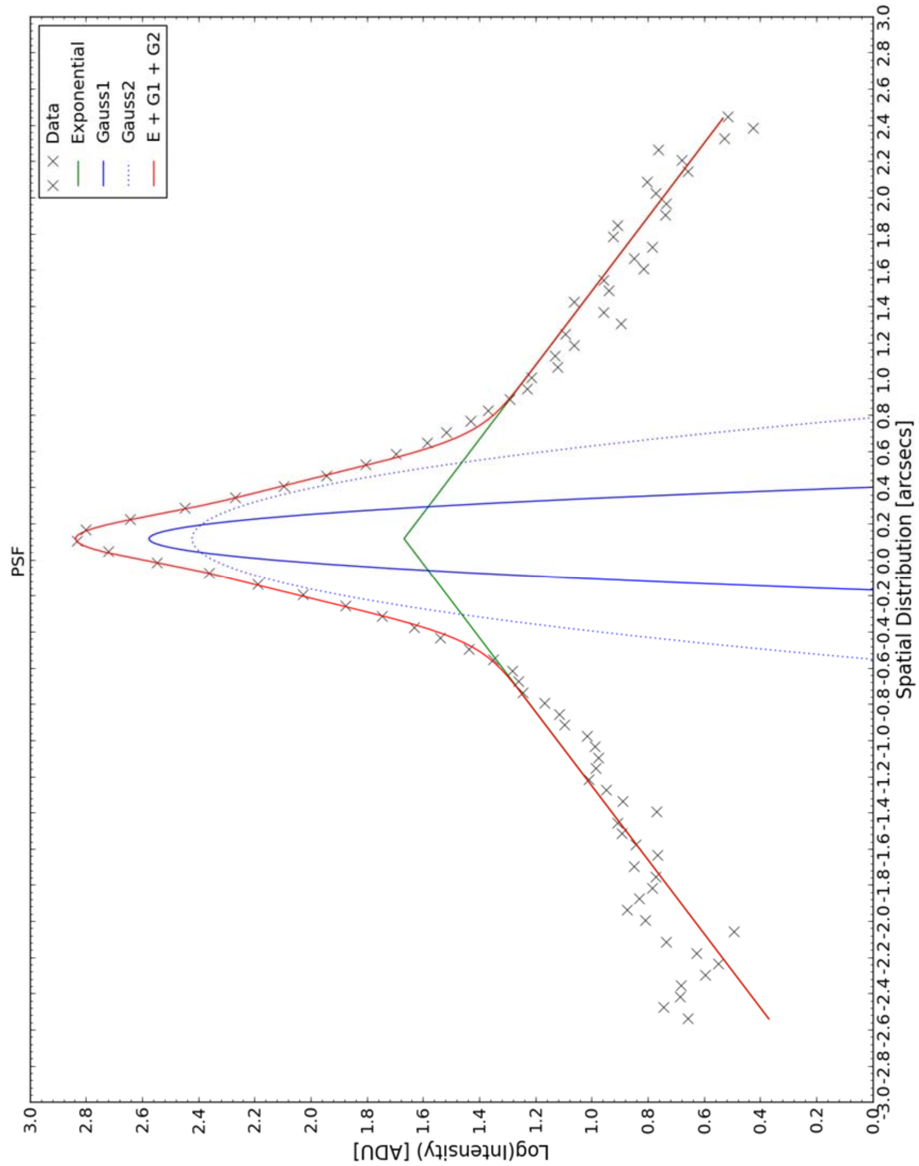

Figure 63. Fitting data with exponential and two Gaussian functions.

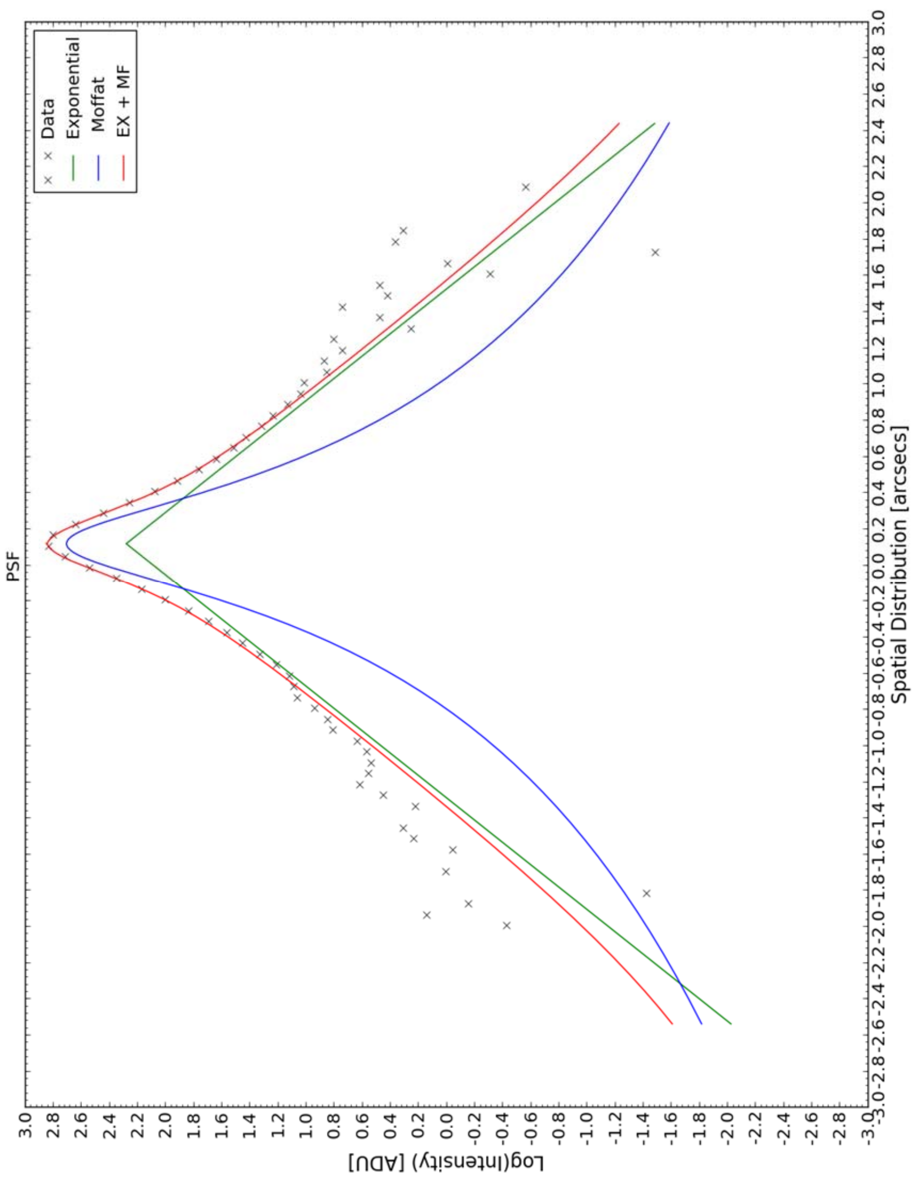

Figure 64. fitting data with exponential and Moffat function.

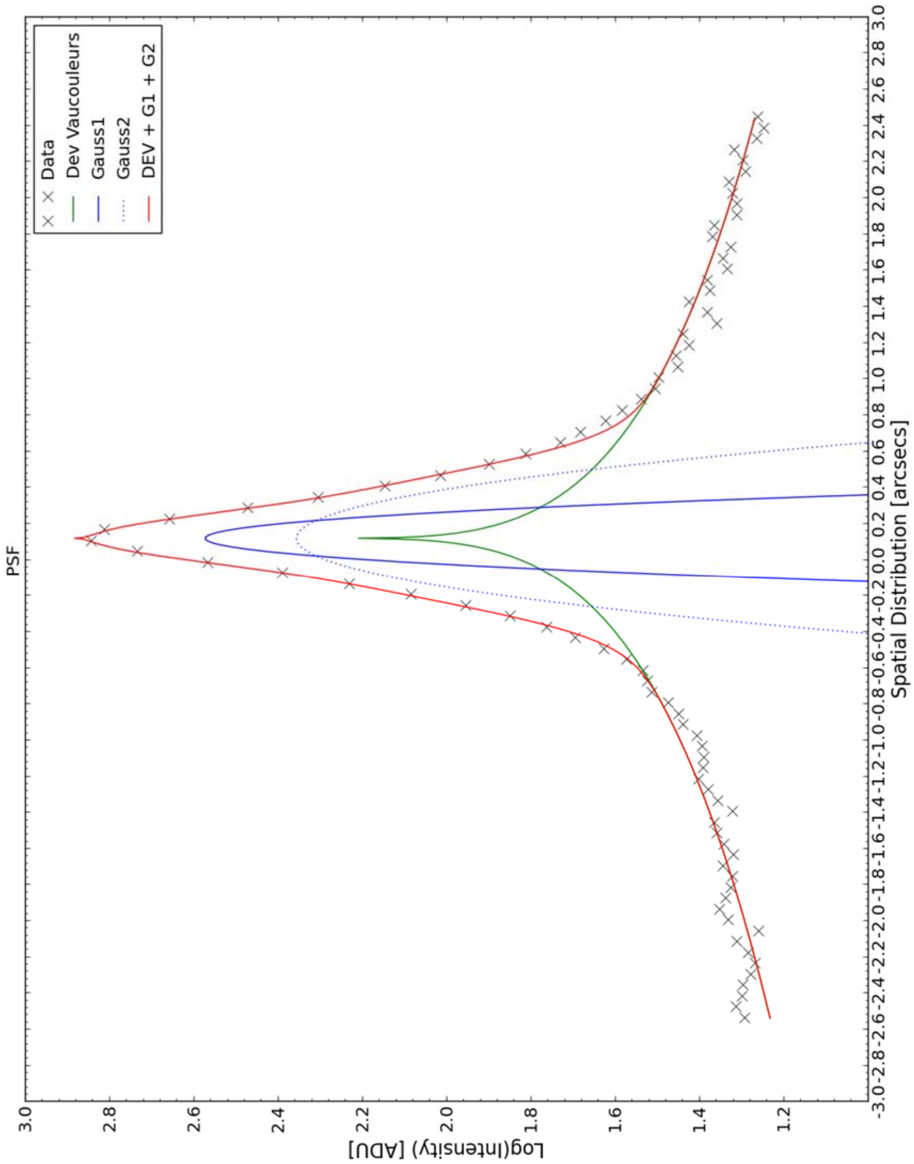

Figure 65. Fitting data with De Vaucouleurs and two Gaussian functions.

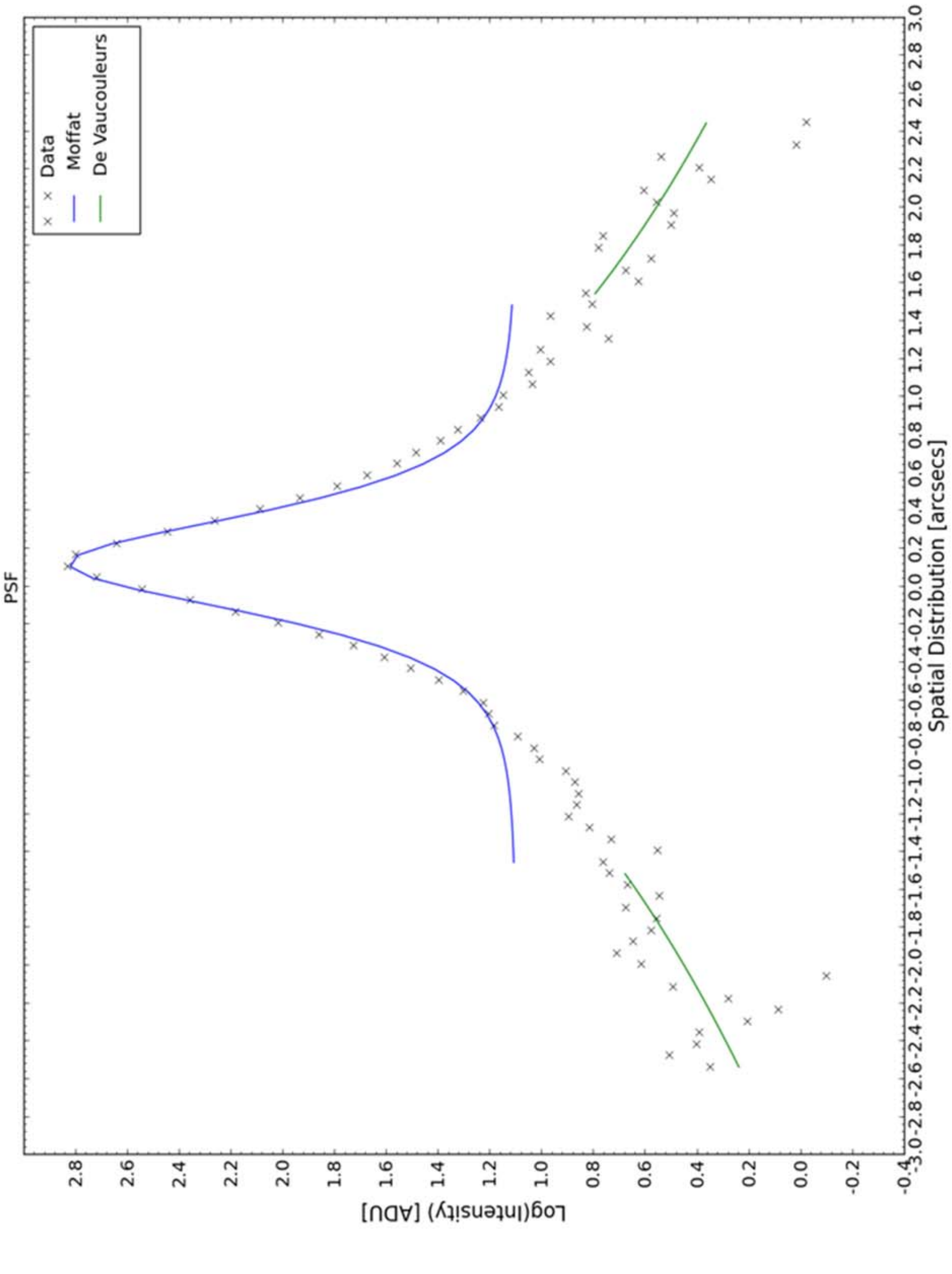

Figure 66. Fitting data with De Vaucouleurs and Moffat function in case of fitting parameter as constants.

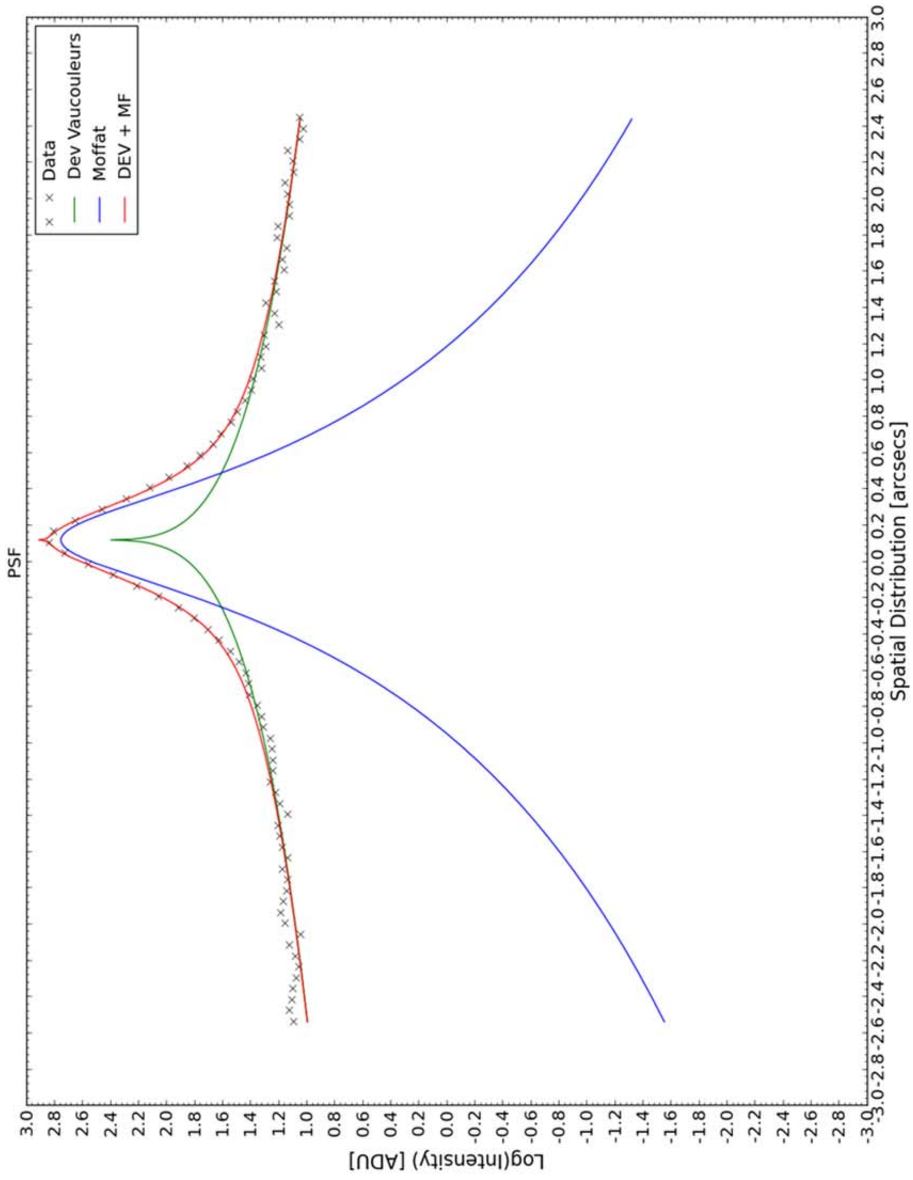

Figure 67. Fitting data with De Vaucouleurs and Moffat for fitting in case of calculate fitting for all parameters.

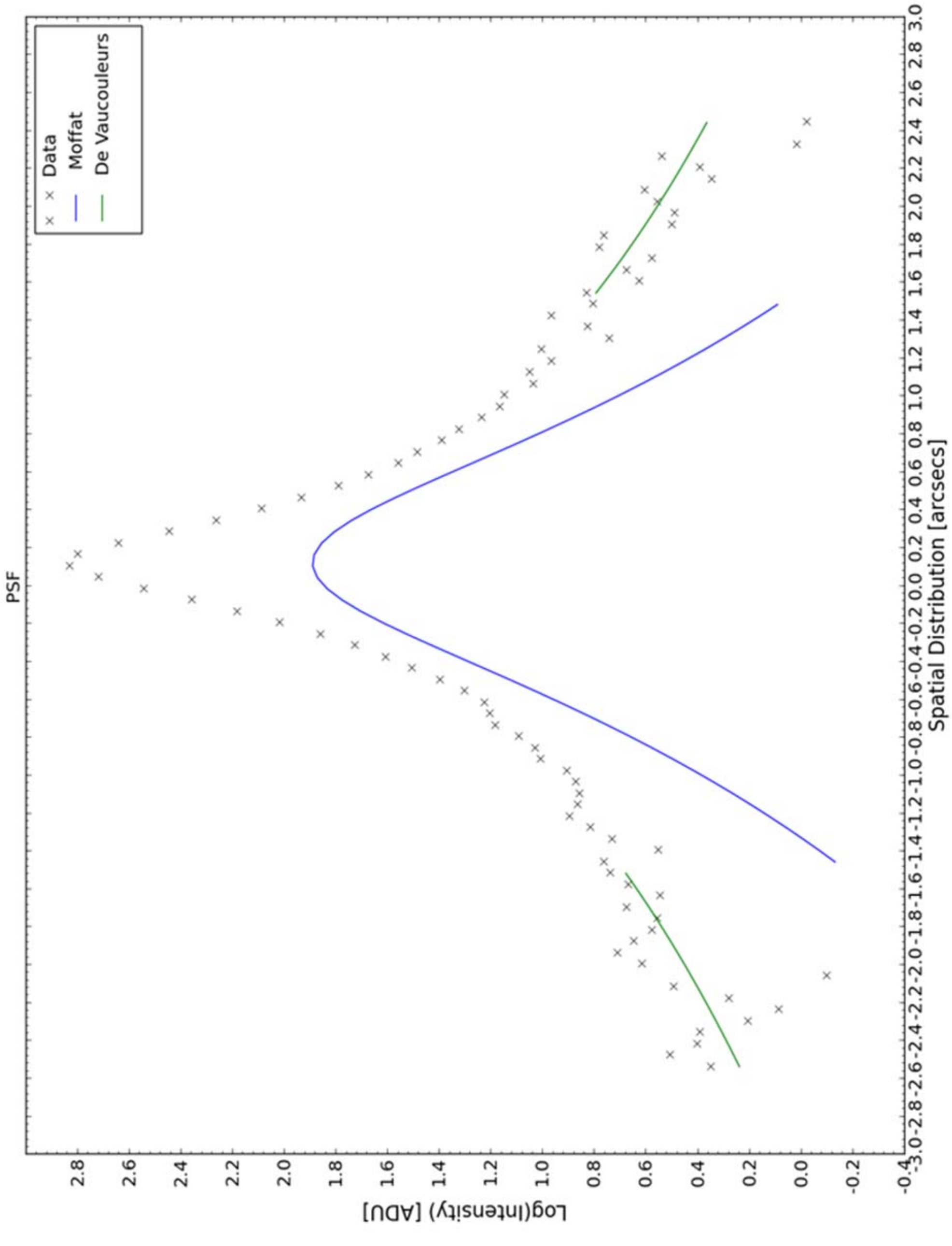

Figure 68. Fitting data with De Vaucouleurs and Moffat function in case of calculate fitting parameter numbers for Moffat function.

5.2 Identify features

From figure 38, 40, and 42, we try to identify the expected features in the spectrum. These are lines that we think these are real lines. We calculate the equivalent width (EW), Noise of EW, signal-to-noise ratio (S/N), and the effective wavelength of the lines.

The formula for calculation EW, Noise of EW, S/N, and effective wavelength (λ_{eff}) are as follow

$$EW = \int_{\lambda_{\min}}^{\lambda_{\max}} d\lambda - \int_{\lambda_{\min}}^{\lambda_{\max}} F(\lambda) d\lambda$$

$$Noise\_EW = \Delta\lambda \times \sum \sqrt{\sigma_i^{\,2}}$$

$$S / N = EW / Noise\_EW$$

$$\lambda_{eff} = \frac{\int_{\lambda_{\min}}^{\lambda_{\max}} \lambda F(\lambda) d\lambda}{\int_{\lambda_{\min}}^{\lambda_{\max}} F(\lambda) d\lambda}$$

We expect the absorption lines in the quasar spectra. In PG0849+349 spectrum, there dominate absorption lines of He (1.47644 μm), Br15 (1.57050 μm), Br14 (1.58849 μm), and CO 6-3 (1.61890 μm). In these absorption lines, Br15 and CO 6-3 have high S/N of 7.7 and 5.5. The spectrum of PG1226+023 may have expected absorption lines of O I (1.31682 μm) with S/N of 0.6. In addition, the PG1426+015 spectrum has expected absorption lines of Br16 (1.55608 μm) and CO 6-3(1.61890 μm), and Br16 has high S/N of 6.6. In comparison to Riffel et al. 2006, we find the absorption lines in our quasars spectra, instead of the emission lines in Riffel quasar spectra. These absorption lines may have origin from the materials of the host galaxies. Table 6, 7, and 8 show the results of unidentified features.

Table 6

Unidentified lines of PG0844+349

Effective wavelength (μm)	λmin (μm)	λmax (μm)	EW (10^{-5}μm)	NOISE_EW (10^{-5}μm)	S/N	Lines (μm)
1.421	1.418	1.423	5.38	2.31	2.3	
1.427	1.425	1.428	5.08	1.63	0.3	
1.434	1.431	1.437	0.39	1.58	0.3	
1.456	1.452	1.460	2.91	1.84	1.6	
1.476	1.498	1.502	1.30	1.92	0.7	He (1.47644)
1.500	1.498	1.502	2.91	0.38	7.6	
1.505	1.503	1.506	1.79	1.86	1.0	
1.520	1.517	1.523	1.27	1.33	1.0	
1.539	1.534	1.543	3.52	1.27	2.8	
1.551	1.547	1.555	3.36	1.04	3.2	
1.573	1.570	1.577	5.67	0.74	7.7	Br15 (1.57050)
1.590	1.588	1.592	1.95	1.32	1.5	Br14 (1.58849)
1.621	1.614	1.629	5.70	1.04	5.5	CO 6-3 (1.61890)
1.636	1.630	1.643	0.31	2.58	0.1	

Table 7

Unidentified lines of PG1226+023

Effective wavelength (μm)	λmin (μm)	λmax (μm)	EW (10^{-5}μm)	NOISE_EW (10^{-5}μm)	S/N	Lines (μm)
1.288	1.284	1.292	2.93	0.49	6.0	
1.316	1.312	1.320	0.33	0.56	0.6	OI (1.32682)
1.325	1.321	1.329	0.65	0.55	1.2	
1.356	1.352	1.360	4.16	0.85	4.9	
1.379	1.374	1.384	0.75	0.52	1.5	
1.390	1.385	1.395	4.18	0.45	9.2	
1.414	1.410	1.418	4.47	0.68	6.6	
1.423	1.419	1.427	3.47	0.34	11.0	
1.459	1.455	1.463	3.12	0.70	4.5	

Table 8

Unidentified lines of PG1426+015

Effective wavelength (μm)	λmin (μm)	λmax (μm)	EW ($10^{-5}\mu$m)	NOISE_EW ($10^{-5}\mu$m)	S/N	Lines (μm)
1.387	1.383	1.391	1.44	1.69	0.9	
1.435	1.430	1.440	5.23	1.25	4.5	
1.448	1.443	1.452	4.03	1.71	2.4	
1.505	1.500	1.509	0.21	1.78	0.1	
1.519	1.514	1.524	5.17	0.79	6.6	
1.558	1.553	1.563	3.58	0.54	6.6	Br16 (1.55608)
1.589	1.584	1.594	3.07	1.16	2.6	
1.621	1.616	1.626	4.30	1.70	2.5	CO 6-3 (1.61890)

6. SUMMARY AND FUTURE WORK

We present the method for data analysis of the near-IR high resolution echelle spectrometer, IRCS, at the SUBARU 8.2 m telescope. From the method, we made three nearby quasars spectra (z < 2) PG0844+349, PG1426+015, and PG1226+023. We try to identify expected features in the spectra, and hoping to find any useful lines which can help us study about the physical mechanisms of quasars.

The method of data reduction we present here is reference for data analysis of IRCS, and also useful for data reduction of similar data.

We also made the template stars spectra of G8 (HD64938 and HD148287), K0 (HD55184 and HD155500), K2 (HD52071 and HD146084), K5 (HD154610), M0 (HD76010). All of the template spectra are similar, so we show only one spectrum of K2 (HD52071) which is most closing type to Arcturus of Hinkle & Wallace. 1995. We found many prominent molecular and neutral metal features in the template star spectra. These lines will be used for the kinematical studies of external galaxies.

To make sure that our quasar spectrum PG0844+349 has mostly light emission from the quasar in the center region. We made the model function for fitting the profile of target PG0844+349. In the best function for fitting the profile is combine of exponential and two Gaussian functions. The exponential is fitting well for the outer wing host galaxy region, and two Gaussian functions are fitting for quasar in the center region of target. The emission from the host galaxy can be model by exponential function.

From the model fitting function, we can conclude that the spectrum of quasar is mostly from the emission of quasar in the center of target, and the emission of host galaxy in the quasar spectrum is only about 7.3%.

REFERENCES

Barvainis, R. 1987, Hot Dust and the Near-Infrared Bump in the Continuum Spectra of Quasars and Ative Galactic Nuclei, ApJ, 320, 357

Boyle, B. J. 1989, A composite QSO spectrum , MNRAS, 243, 231

Brotherton, M. S., Tran, H. D., Becker, R. H., Gregg, M. D. 2000, Composite Spectra from the First Bright Quasar Survey, ApJ, 546, 775

Cristiani, S. & Vio, R. 1990, The Composite Spectrum of Quasars, A & A, 227, 385

Francis, P. J., & Hewett, P. C. 1990, A High Signal-To-Noise Ratio Composite Quasar Spectrum, ApJ, 373, 465

Glikman, E., Helfand, D. J., & White, R. L. 2005, Near-Infrared Spectral Template for Quasars, ApJ, 640, 579

Hinkle, K., & Wallace, L. 1995, Infrared Atlas of the Arcturus Spectrum, 0.9-5.3 microns, PASP, 107, 1042

Kwan, J., Krolik, J. H. 1981, The Formation of Emission Lines in Quasars and Seyfert Nuclei, ApJ, 250, 478

Malkan, M. A., & Sargent W. L. W. 1982, The Ultraviolet Excess of Seyfert 1 Galaxies and Quasars, ApJ, 254, 22

Peterson, B. M. 1997, An Introduction to Active Galactic Nuclei, Cambridge, Cambridge University Press, 8-18

Pyo, T. S. 2002, Near Infrared [Fe II] Spectroscopy of Jets and Winds Emanating from Young Stellar Objects, Ph.D. thesis, Tokyo Univ.

Peng, C. Y., Ho, L. C., Impey, C. D., & Rix, H. W. 2000, Detailed Decomposition of

Galaxy Images. II. Beyond Axisymmetric Models, AJ, submitted

Robson, I. 1996, Active Galatic Nuclei, Chichester, Praxis, 108-189

Rousselot, P., Lidman, C., Moreels, G., & Monnet, G. 2000, Night-sky Spectral Atlas of OH Emission Lines in the Near-Infrared, A & A, 354, 1134

Riffel, R., Rodri'guez-Ardila, A., & Pastoriza, M. G. 2006, A 0.8-2.4 μm Spectral Atlas of Active Galatic Nuclei, A & A, 457, 61

Sparke, L., & Gallagher, J. 2007, Galaxies in the Universe: An Introduction, New York, Cambridge University Press, 241-273

Trump, J. R. et al. 2006, A Catalog of Broad Absorption Line Quasars from the Sloan Digital Sky Survey Third Data Release, ApJS, 165, 1

Zheng, W., Kriss, G. A., Telfer, R. C., Grimes, J. P., & Davidsen, A. F. 1997, A Composite HST Spectrum of Quasars, ApJ, 475, 469